Emergence and Phenomenology in Quantum Gravity

by

Isabeau Prémont-Schwarz

A thesis

presented to the University of Waterloo

in fulfillment of the

thesis requirement for the degree of

Doctor of Philosophy

in

Physics

Waterloo, Ontario, Canada, 2010

Author's Declaration

I hereby declare that I am the sole author of this thesis. This is a true copy of the thesis, including any required final revisions, as accepted by my examiners.

I understand that my thesis may be made electronically available to the public.

AUTHORSHIP STATEMENT

This thesis is based on the following five articles:

- A. Hamma, F. Markopoulou, **I. Prémont-Schwarz** and S. Severini, "Lieb-Robinson bounds and the speed of light from topological order," *Phys. Rev. Lett.* **102** (2009) 017204 [arXiv:0808.2495 [quant-ph]].
- **I. Prémont-Schwarz** ,A. Hamma, I. Klich and F. Markopoulou, "Lieb-Robinson bounds for commutator-bounded operators ," Phys. Rev. A **81**, 040102(R) (2010) .[arXiv:0912.4544 [quant-ph]].
- **I. Prémont-Schwarz** and J. Hnybida, "Lieb-Robinson bounds with dependence on interaction strengths, " [arXiv:1002.4190 [math-ph]].
- L. Modesto and **I. Prémont-Schwarz**, "Self-dual Black Holes in LQG: Theory and Phenomenology," *Phys. Rev. D* **80**, 064041 (2009) [arXiv:0905.3170 [hep-th]].
- S. Hossenfelder, L. Modesto and **I. Prémont-Schwarz**, "A model for non-singular black hole collapse and evaporation ," *Phys. Rev. D* **81**, 044036 (2010) [arXiv:0912.1823 [gr-qc]].

I did the majority of the work in the first article, but the project was initiated by Fotini Markopoulou-Kalamara and Alioscia Hamma and the manuscript was mostly written by Alioscia Hamma. Simone Severini provided a combinatorial calculation.

I did the majority of the work, calculations and writing for the second and third articles and I also initiated the projects. Alioscia Hamma and Israel Klich thought up an applicable example for the second article.

The fourth article was joint work jointly initiated by Leonardo Modesto and myself. I wrote and did the majority of the work for the phenomenology part of the paper. The duality was worked out jointly.

The fifth article was jointly initiated and the work was shared, but most of the writing was done by Sabine Hossenfelder, I only did a small section of the writing.

The Quantum Graphity model is due to prior work by Tomasz Konopka, Fotini Markopoulou-Kalamara, Lee Smolin and Simone Severini. The Loop Quantum Black Hole was derived by Leonardo Modesto in previous work.

ABSTRACT

In this thesis we investigate two approaches to quantum gravity. The first is the emergence of gravity from a discrete fundamental theory, and the second is the direct quantisation of gravity. For the first we develop tools to determine with relatively high accuracy the speed of propagation of information in collective modes which ultimately should give us some information about the emergent causal structure. We found a way of finding the dependence on the relative interaction strengths of the Hamiltonian and we also managed to calculate this speed in the case where the operators in the Hamitonian were not necessarily bounded.

For the second approach, we investigated the phenomenology of Loop Quantum Gravity. We found that ultra light black holes (lighter than the Planck mass) have interesting new properties on top of being non-singular. First their horizon is hidden behind a Planck-sized wormhole, second their specific heat capacity is positive and they are quasi-stable, they take an infinite amount of time evaporate. We investigated the dynamics of their collapse and evaporation explicitly seeing that not only was there no singularity, but there is also no information loss problem. Looking at how primordial black holes were in existence, we found that they might account for a significant portion of dark matter. And if they did, their radiation spectrum is such that the black holes in the dark matter halo of

our galaxy could be the source for the ultra high energy cosmic rays we observe on earth.

ACKNOWLEDGEMENTS

I would like to thank my Ph.D. advisor Fotini Markopoulou-Kalamara for collaborations, guidance and council. Rob Mann for accepting to be my co-supervisor, Lee Smolin, Éric Poisson, Achim Kempf and Seth Major for accepting to be on my committee. I would like to thank everybody I have collaborated with over the course of my Ph.D.: Fotini Markopoulou-Kalamara, Lee Smolin, Alioscia Hamma, Leonardo Modesto, Sabine Hossenfelder, Laurent Freidel, Jeff Hnybida, Simone Severini, Yidun Wan and Jonathan Hackett. I would like to thank Lee also for the wise council throughout my Ph.D.

This work was partially funded by the Natural Sciences and Engineering Research Council of Canada (NSERC). Travel funding to attend conferences, workshops, summer schools, to give talks and to collaborate was graciously provided by my supervisor Fotini Markopoulou-Kalamara, the Perimeter Institute for Theoretical Physics (PI), Nordita, the Institute for Theoretical Physics (Utrecht), UNAM-Morelia, Beijing Normal University, the University of Warsaw and the Jagiellonian University in Krakow, the University of New Brunswick, the Max Planck Institute for Gravitational Physics (Golm), Simone Speziale and the Canadian Association of Physicists.

I am grateful for the friendship and companionship of the great officemates I have had throughout my Ph.D.: Amir Jafari Salim, Camille Boucher-Véronneau, Chanda Prescod-

Weinstein, Jonathan Hackett, Sean Gryb, Jorge (Coco) Escobedo, Francesco (Ciccio) Caravelli, Ryan (Rainbow) Morris, Saurabh Madaan, Åsa Ericsson, Rowan Thomson, Jordan Hovdebo and Matthias Wapler. I would also like to thank all the nice people and friends I met at PI, UW, MIT and at LOOPS conferences and summer schools who are too numerous to name individually here.

I would like to thank LeeAnne Kane and Debbie Guenther for their constant help with administrative issues at PI. I would like to thank Judy McDonnell and Agnes Kolic for helping me navigate through the bureaucratic maze at UW.

I would like to thank Howard Burton, the first director of PI, for his vision of a hierarchy-free research institute, I hope that future directors will embrace his vision. For working so hard to improve the situation of grad students at PI, thank you to all present and pass PI grad student representatives: Chanda Prescod-Weinstein, Jonathan Hackett, Sean Gryb, Sayeh Rajabi, Jorge (Coco) Escobedo.

The format of this thesis is based on the style files that were previously used by Tomáš Liko for his thesis at Memorial University which were in turn based on style files that were given to him by Sanjeev Seahra for his thesis at the University of Waterloo which he in turn obtained from Éric Poisson.

I would like to thank Carolyn Sutherland and the members of the facebook group she administers.

Hvala puno za moju djevojku Miljana Prelić za tvoju veliku podršku tokom pisanja ove teze.

CONTENTS

LIST OF TABLES

LIST OF FIGURES

PART I

INTRODUCTION

Chapter 1

Introduction

1.1 Statement of the problem

It is well known that modern physics is inconsistent. Indeed, the foundations of modern physics rests on two pillars: General Relativity (GR) which is our theory explaining space and time, and Quantum Physics or more precisely, the Standard Model of particle physics (SM) which is our theory of matter. Matter and space-time are, at a fundamental level, intimately linked, and cannot be decoupled. This is because space-time is shaped by matter, and matter can only exist inside the confines of space-time. However, GR and SM form two incompatible languages. This implies that there must exist an overarching theory in which matter and space-time can be described by the same language. In order to have a consistent view of nature, it is of prime importance to discover such an overarching theory. It is the goal of Quantum Gravity (QG) to find a language which can consistently describe both matter and space-time.

There are many proposed theories and models for quantum gravity: Superstring the-

ory, supergravity, twistor theory, asymptotic safety, non-commutative geometry, group field theory, spinfoam models, causal dynamical triangulation, causal sets, loop quantum gravity, quantum graphity and quantum causal histories, are but some of the main proposals. One of the main challenges to date for all but the first four of these models is to obtain, from the fundamental theory, a semi-classical description of space-time. This is absolutely vital in order to predict deviations from General Relativity and make contact with experiments and observations. Bridging the gap between the fundamental theories and models and the semi-classical macroscopic world is not an easy task. The aim of the present thesis is to bring us a step closer to bridging that gap. The thesis is divided into two largely independent sections (Part II and Part III). The first part of the thesis concerns itself with the building of more powerful tools to investigate the possible emergence of gravity in such models as quantum graphity. In the second part, we investigate the symmetry reduction of a theory, Loop Quantum Gravity, to obtain a solvable system and explore the phenomenological ramifications of the theory assuming that not too much is lost through the reductions and simplifications.

1.2 Overview and main results

In chapter 2 we quickly review to approaches to quantum gravity. First Quantum Graphity which is the justification for Part II of this thesis then Loop Quantum Gravity, upon which will be based the black holes we investigate in Part III. The quick review of Loop Quantum Gravity is strongly based on the recent review by Sahlmann [99].

In part II we develop tools to investigate the emergence of gravity in condensed-matter-

like systems, Quantum Graphity in particular. These tools are based on the Lieb-Robinson bound which give a bound on the maximal speed at which information can travel. In chapter 3 we give a brief introduction to the Lieb-Robinson bound as well as general remarks as to how it can be used as a tool to detect the emergence of gravity. In chapter 4 we derive a Lieb-Robinson bound which is sensitive to the relative interaction strengths, this is important in order to understand the functional dependence of the speed or propagation of signals on the different interactions which provides us with tools in investigating quantum phase transitions, the way the universe emerged according to Quantum Graphity, but it is also important in order to give a tighter bound. We also give three examples of the application of the bounds we derived, including one example in which a Minkowski space with $U(1)$-Yang-Mills emerges from a non-relativistic condensed matter system and where we show that the Lieb-Robinson speed we derived is a relatively good approximation to the emerging speed of light. This chapter is largely based on [94]. In chapter 5 we now generalise the Lieb-Robinson bound to a class of systems where the Hamiltonian does not need to be composed of bounded terms. Instead the terms can be commutator bounded, that is the commutator of any two or three of the local operators composing the Hamiltonian must be bounded. In the end we give an application to the XY-Model. This chapter is largely based on [93]. Finally we put our results together in chapter 6 where we provide a bound which is applicable for a Hamiltonian with many interactions and one with commutator-bounded operators.

In Part III we investigate the phenomenology of the Loop Quantum Black Hole and lighter than Planck mass black holes have positive heat capacity and are quasi-stable. All of Part III with the exception of chapter 10 is largely based on [76]. Chapter 10 is largely based

on [53]. We discover that they could be a major constituent of dark matter and find that could be the elusive source behind the ultra high energy cosmic rays (UHECR). In chapter 7 we review the black holes as well as the technique for obtaining them, and we demonstrate the intriguing duality that they exhibit. In chapter 8 we investigate the thermodynamics of the Loop Quantum Black Holes and see how ultra light black holes have positive heat capacity. In chapter 9 we investigate the properties of ultra light black holes more closely and see that their horizons are hidden behind a Planck-sized worm hole and that they take an infinite amount of time to fully evaporate, they are quasi-stable in the low-mass regime. In chapter 10, guided by the Vaidya metric we investigate the collapse and evaporation of a Loop Quantum Black Hole. Chapter 11 investigates the creation of primordial Black Holes and we find that assuming they were created by matter fluctuations in the early universe, it is not unreasonable to think that ultra light Loop Quantum black holes of a typical mass of $10^{-5}m_P$ could constitute a significant part of the dark matter today and in chapter 12 we find that those same black holes, which would constitute dark matter today, would emit ultra high energy cosmic rays to the order of what we observe on earth and so might be the elusive source for those as yet unexplained particles. We summarise our results in chapter 13.

In Part IV we conclude.

Chapter 2

Two Models for Quantum Gravity

2.1 Quantum Graphity

The combination of General Relativity and Quantum Mechanics suggests that there is a UV cut-off at the Planck Energy which corresponds to (via the Fourier transform) a minimum length scale. Heuristically, this is the reason why many[1] theories for quantum gravity involve a discretisation of space and/or space time. However, it turns out that one of the most challenging things to do in those theories is to recover the familiar smooth spacetime manifold of General Relativity. Quantum Graphity, first proposed by Konopka, Markopoulou-Kalamara and Smolin in [64], is a toy model designed to investigate how the continuous manifold-like nature of General Relativity could emerge from a more fundamental theory based on fundamentally discrete space/spacetime. Before pursuing this line of investigation, we should point out here that the discretisation of spacetime need not be taken so literally, it is possible to have a UV cutoff by having a finite information

[1] Example of theories of quantum gravity which predict a discrete space or spacetime structure include: Loop Quantum Gravity, Spinfoam Models, Group Field Theory, Causal Dynamical Triangulations, Causal Sets, Quantum Causal Histories, non-commutative geometry theories, etc.

density in the fields but still having continuous fields [58], having a fundamentally discrete geometry is only one possibility. The goal then of Graphity is to study how a manifold-like structure can emerge from discrete fundamental entities which are not manifestly organised in manifold-like structure. To simplify things (it is a toy model) Graphity makes a split between "space" and time. It is a quantum theory which is evolved by a Hamiltonian H via the unitary transformation $U(t) = e^{iHt}$ where t is called time variable because of the role it plays in the dynamics of the theory, even though it might not correspond to the physical time experienced by internal observers in the low energy limit of the theory.

2.1.1 Kinematics

In what follows we will be considering two different graphs. From experience, we know those two graphs are often confused so we wish here to distinguish them clearly from the outset and so we will give them here two different names by which we will identify them in what follows:

- The Fundamental Graph K_N: the fundamental is the fixed graph K_N that is the complete graph on N vertices.This fundamental graph with $M = \frac{N(N-1)}{2}$ edges, one edge between any two pairs of vertices, is not dynamical, but is used to characterise the Hilbert space of the quantum theory.

- The Space Graph $S(t)$: the space graph is a subgraph of the fundamental graph, K_N. It is dynamical and is evolved by the dynamics. Intuitively, in the low energy limit, $S(t)$ describes the space-like slice of the spacetime manifold at time t.

The Hilbert space of the theory is the following. Let $\mathcal{E}$ be the set of edges of K_N and $\mathcal{V}$ the set of its vertices. Let $\mathcal{H}_e$ and $\mathcal{H}_V$ be two Hilbert spaces (which in the following will be finite dimensional, but the harmonic oscillator would be a natural choice which is not finite dimensional), we interpret $\mathcal{H}_E$ to be the local Hilbert space that sits on each edge of the fundamental graph K_N and $\mathcal{H}_V$ to be the local Hilbert space for each of the vertices. We then have that the total Hilbert space is $\mathcal{H} = \left((\bigotimes_{e\in\mathcal{E}} \mathcal{H}_E^e) \otimes (\bigotimes_{v\in\mathcal{V}} \mathcal{H}_V^v)\right)/\mathcal{R}$, where $\mathcal{H}_E^e$ and $\mathcal{H}_V^v$ are just identical copies of the Hilbert spaces $\mathcal{H}_E$ and $\mathcal{H}_V$ and $\mathcal{R}$ is an equivalence relationship (which can be thought of as being generated by some global symmetry, for example the permutation group of the vertex labels) by which the tensor product of the local Hilbert space is quotiented. In what follows, we take $\mathcal{R}$ to be trivial and so we can ignore it. A final element is needed to finish the description of the kinematics: a distinguished element $\mid 0\rangle \in \mathcal{H}_E$ and the subspace of $\mathcal{H}_E$ orthogonal to it $\mathcal{O}$ so that we have $\mathcal{H}_E = \mid 0\rangle \oplus \mathcal{O}$. If a state $\mid \psi\rangle$ can be written as $\mid \psi\rangle = \mid 0\rangle_e \otimes \mid \psi'\rangle$ we say that edge e is "turned off" meaning that space is absent at this edge. On the other hand, if we can write $\mid \psi\rangle = \mid s\rangle_e \otimes \mid \psi'\rangle$ where $\mid s\rangle_s \in \mathcal{O}^e$, we say that edge e is "turned on" and that space is present at that edge. In the low energy effective limit, the hope is that typical states will be of the form $\mid \psi(t)\rangle = (\bigotimes_{e\in on(t)} \mid s(t)\rangle_e) \otimes (\bigotimes_{e\in off(t)} \mid 0\rangle_e)$, in such a case, the space graph $S(t)$ is the subgraph of K_N whose set of edges is $on(t)$ and whose set of vertices are the vertices at the end of the edges of $on(t)$. The expectation is then that $S(t)$ will be manifold-like. At high energies, the graph $S(t)$ is not well defined in general, but a general state can be decomposed into a superposition of terms which will individually have a well defined space graph (simply by decomposing the states along a basis of $\mid 0\rangle$ and a basis of $\mathcal{O}$). But even then, in general, the space graph of a particular term of a particular state will in

general be a random graph of K_N looking nothing like a smooth spatial manifold, we will call such a space graph (as well as, more generally, the superposition of such graphs) "pre-space". The question is then to probe how space emerges from pre-space. This of course depends on the dynamics. In what follows, we will specialise to the particular model investigated in [64]. We set $\mathcal{H}_V = \mathbb{C}$ and so we can ignore the Hilbert spaces at the vertices, and on the edges we put two spin-$\frac{1}{2}$s: $\mathcal{H}_E = \mathbb{C}^2 \otimes \mathbb{C}^2 =\mid 0,0\rangle \oplus \mid 1,-1\rangle \oplus \mid 1,0\rangle \oplus \mid 1,1\rangle$ and we will interpret the edge as being on if the total spin is one and as being off if the total spin is zero, so $\mid 0\rangle =\mid 0,0\rangle$ and $\mathcal{O} =\mid 1,-1\rangle \oplus \mid 1,0\rangle \oplus \mid 1,1\rangle$ and when the edge is on, there is matter of spin-1 occupying the space.

2.1.2 Dynamics, Thermodynamics and Cosmology

The Hamiltonian is split into five terms:

$$H = H_{links} + H_{vertices} + H_{loops} + H_{hop} + H_{LQG}. \tag{2.1}$$

The links term is a local term acting on edges which are on, the vertices term acts on the space of all edges arriving at one vertex, the loops term creates and destroys loops on "on edges", the hop term permits the interaction of the spin-1 degrees of freedom between adjacent edges and the LQG term allows changes in geometry of the space graph. In [64], the following terms are used:

$$H_{vertices} = V \sum_{a \in \mathcal{V}} \left(v_0 - \sum_{b \in \mathcal{V}} J^2_{<ab>} \right)^2, \tag{2.2}$$

where $< ab > \in \mathcal{E}$ is the edge of the fundamental graph linking vertex a to vertex b and $J^2_{<ab>}$ is total spin squared operator normalised in such a way that it is equal to one when the total spin is one. This operator is non-negative and equal to zero if and only if there are exactly v_0 on edges arriving at vertex a.

$$H_{links} = C \sum_{a\mathcal{V}} \left(\sum_{b \in \mathcal{V}} S^z_{<ab>} \right)^2 + D \sum_{e \in \mathcal{E}} (S^z_e)^2, \tag{2.3}$$

where S^z_e is the spin-z operator acting on $\mathcal{H}^e_E$ The term is again non-negative. In the first line, the C term vanishes if and only if the m values of spins at each vertex add up to zero. The D term is zero if and only if $m = 0$ and will act as a tension term for the loops created by H_{loops}.

$$H_{loops} = - \sum_{\text{minimal loops}} \frac{1}{L!} B(L) \prod_{i=1}^{L} M^{\pm}_i, \tag{2.4}$$

where $M^{\pm} \propto S^x \pm iS^y$ are the raising and lowering operators. The sum is over minimal loops. These are defined to be loops that cannot be factored into the product of two loops of "on" edges that contain some of the same edges. The products are defined over a closed sequence of edges as follows

$$\prod_{i=1}^{L} M^{\pm}_i \; = \; M^{+}_{<ab>} \, M^{-}_{<bc>} \, \ldots \, M^{+}_{<yz>} \, M^{-}_{<za>}. \tag{2.5}$$

a,b,c, $\ldots$, z are the vertices along the minimal loop. L is the length of the loop. The coupling $B(L)$ is assumed to take the form

$$B(L) = B_0 B^L \tag{2.6}$$

where B_0 is a positive coupling constant and B is dimensionless. The separation of B from B_0 is useful because B can be now associated with each instance of M in the loop product (2.5). We note then that the overall coefficient of a loop term is proportional to $B^L/L!$. It is thus small at very low and at very high L, but has a maximum value at some particular L_*,

$$\frac{B^{L_*}}{L_*!} > \frac{B^{L'}}{L'!} \qquad \forall L' \neq L_*. \tag{2.7}$$

We call L_* the preferred loop length.

In comparison with H_{links}, H_{loops} has an overall minus sign. Note also that H_{loops} is identically zero on off edges. Note the competition between the loop term and H_{links} for an edge to have $m = 0$ or $m \neq 0$.

For what follows we disregard the other terms in the Hamiltonian and put them to zero.

Research in [63] leads us to believe that if the loops term is chosen appropriately, in the low energy limit, the space graph will crystalise in a regular lattice, the shape and dimension of which is determined by the loops and vertices term of the Hamiltonian. Thus if we choose V to be large enough and $v_0 = 6$, so that in the low energy limit we are

projected down to the subspace where the space graphs have valence 6, and the loops term is such as to impose the minimal loops to be squares of four edges, then in the low energy limit, we are projected to the subspace where the space graph is the 3D square lattice.

In this phase, the V and C terms in the Hamiltonian are constant and we may ignore them. The non-vanishing terms then consist of the D term and loop operators with exactly four edges,

$$H_{lowT} \sim D \sum_{ab} M_{ab}^2 - \frac{1}{4!} B_0 B^4 \sum_a \prod_{i=1} M_i^{\pm}, \tag{2.8}$$

where we define $M_{ab} = S_{ab}^z$. Since the lattice is regular, the sum over loops can be thought of as a sum over plaquettes. We define a plaquette operator $W_{a'}$ anchored at a point a' as

$$W_{a'} = M^+_{<a'b>} M^-_{<bc>} M^+_{<cd>} M^-_{<da'>}. \tag{2.9}$$

The points $a', \ldots d$ are now fixed by a convention of labelling plaquettes given their base point and an orientation on the lattice, there is no summation over repeated indices. With this operator, the Hamiltonian can be written as

$$H_{lowT} \sim D \sum_{ab} M_{ab}^2 - \frac{1}{3!} B_0 B^4 \sum_{a'} (W_{a'} + h.c.) \tag{2.10}$$

where $h.c.$ stands for the Hermitian conjugate of $W_{a'}$, i.e. a loop operator with M^+ and M^- interchanged on each link. The sum in the second term is over plaquettes.

This is the Kogut-Susskind Hamiltonian [62] for a gauge field on a cubic lattice in three

spatial dimensions and correspond to $U(1)$ gauge theory in axial $A_0 = 0$ gauge. It is very similar to Wen's emerging theory of light[108], the difference being that Wen has quantum rotors on each edge as opposed to spin-1 degrees of freedom. However, in the low energy limit, quantum rotors can be approximated by spins of spin-1.

Thus non-relativistic pre-space condenses into Minkowski space with emergent light!

Cosmologically, the idea of Graphity is that in the early universe, all the energy is in the "geometric" degrees of freedom and thus there is a highly non-trivial pre-space. As the universe evolves, matter degrees of freedom are created and this cools the geometric degrees of freedom, slowly crystalising pre-space into a manifold-like spacetime. This picture solves the horizon problem in cosmology without the need for inflation, because in the pre-space phase, everything was in contact with everything else and interactions were highly non-local. Indeed if the space graph is close to being fully connected, then any pair of edges will meet at a vertex and will be acted upon by a low energy loop term which will propagate information between the two edges.

2.1.3 Lieb-Robinson bound

Of course there are still many issues to be sorted out. It is still not exactly clear how the crystallisation occurs. Also, so far, General Relativity has not been recovered. This is where the Lieb-Robinson bound can be of use. The Lieb-Robinson bound gives a bound on the maximal speed of propagation of signals in quantum systems living on graphs, like Graphity. If we manage to make the bound tight enough so as to have a good idea of the propagation speed of signals with respect to the graph distance in a particular phase of the quantum system, we could deduce the effective light-cone structure and the geometry

induced on the graph by assuming that the signals of maximal speed travel at a constant speed (we will say more on this in section 3.1). Furthermore, if we wish to investigate the phase transition from pre-space to emergent space as a quantum phase transition, we must be able to investigate the effect of varying the relative interaction strengths in the Hamiltonian. Since many collective properties can be probed with the Lieb-Robinson bound, if we had a bound which depended on the relative interaction strengths we would have powerful tools at our disposal to probe this transition. In Part II we will improve the Lieb-Robinson bound by making it dependent on the relative interaction strengths, not only will this be useful for quantum phase transitions, but this will also improve the tightness of the bound, thus give us better accuracy on the maximal speed of signal propagation. Also we will generalise the bound to a class of systems containing unbounded operators allowing for some infinite dimensional local Hilbert spaces.

2.2 Loop Quantum Gravity and Simplified Models

Loop Quantum Gravity is probably the most conservative approach to quantum gravity: it is the direct canonical (non-perturbative) quantisation of General Relativity using the standard procedure prescribed in Dirac's book [29]. Roughly speaking, the technique consists of five steps. First, a kinematical Hilbert space is obtained by naively quantising the classical configuration space variables. Typically one replaces the classical configuration space by square integrable functions over the configuration space and imposes the canonical commutation relations $[q_\alpha, p_\beta] = i\hbar\delta(\alpha, \beta)$ between the configuration space variables and

their canonical conjugate momentum. Second[2], operators corresponding to the constraints are defined in this kinematical representation. Third, one checks to see if the constraints form a closed algebra; if they don't, one adds secondary constraints until they do. Fourth, one forms the physical Hilbert space by projecting down onto the kernel of the constraints. Last, observable quantities are quantised, they should form an algebra and commute with the constraints. The inner product on the physical Hilbert space is in general not the same as the inner product on the Kinematical Hilbert space. So one must find an inner product compatible with the quantised observables, that is, such that the observable operators are Hermitian operators. Depending on the system, these steps can be easy, or very hard. In the case for gravity it is very difficult because there are only Hamiltonian constraints and there is no "absolute" or "external" time. This absence is one way to formulate the "problem of time". The following short review of Loop Quantum Gravity is strongly inspired by a review by Sahlmann [99].

2.2.1 Quantisation

Loop quantum gravity starts with the following action, called the Holst-Action:

$$S[e,\omega] = \int \epsilon^{IJKL} e_I \wedge e_J \wedge F_{IJ}(\omega) + \frac{1}{\gamma} e^I \wedge e^J \wedge F_{IJ}(\omega), \tag{2.11}$$

where ω is an $\mathfrak{sl}(2,\mathbb{C})$connection (i.e. a Lorentz group connection as $SL(2,\mathbb{C})$is the double cover of the Lorentz group) and F its curvature, e is a tetrad and γ is the Immirzi parameter. The indices I, J, K, L label a basis of $\mathfrak{sl}(2,\mathbb{C})$and a raise and lowered with the

[2]The first and second step are sometimes interchanged, depending on what is easier to do with the given theory at hand. However, these two steps need not commute and so interchanging them might result in a different quantum theory altogether.

Minkowski metric η_{IJ}. Taking $\gamma = -i$ yields the self-dual Ashtekar canonical formalism for ω, while a real γ leads ω to be the $SU(2)$ Barbero connection. The first term in the action is simply the Palatini action of General Relativity. The second term, called the Holst term, vanishes identically on shell and thus is of no physical consequence classically[3]. Varying this action with respect to e gives Einstein's equations of motion: $F^I_\mu = F^{IJ}_{\mu\nu} e^\nu_J = 0$ where F^I_μ is the Ricci tensor due to the equation of motion for ω which imposes that ω is the spin connection for e ($\nabla_\mu e^I_\nu = \frac{\partial e^I_\nu}{\partial x^\mu} + \omega^I_{J\mu} e^J_\nu = 0$). Thus, the Holst action is classically equivalent to the more common Hilbert-Einstein action $S[g_{\mu\nu}] = \int d^4x \sqrt{-\det g_{\mu\nu}} R$ where R is the Ricci scalar.

In order to canonically quantise, we need to go over to the Hamiltonian picture. Assuming the spacetime to be globally hyperbolic we may fix a foliation of spacetime of the form $M = \mathbb{R} \times \Sigma$ where M is the 4D spacetime, Σ is the manifold of spacelike slices and $\mathbb{R}$ is the time direction. For a fixed foliation, we can split the field into spatial and temporal components. After a partial gauge fixing to get rid of second class constraints, we obtain a canonical pair consisting of an $SU(2)$ connection A^I_a and a conjugate canonical momentum E^b_J,

$$\{A^I_a(x), E^b_J(y)\} = 8\pi G\gamma\, \delta^b_a \delta^I_J \delta(x,y). \tag{2.12}$$

These fields take values on the spatial slices Σ of the manifold of the chosen foliation.

[3] Actually this not exactly true, in the case where we could be considering fermion fields in addition to pure gravity, the second term would not vanish classically. It is the Nieh-Yang term, instead of the Holst term that should be added if we wanted the statement to be entirely true. We thank Andy Randono for giving a talk on this issue and explaining this subtlety at the Perimeter Institute.

E^b_J is interpreted physically as densitised triad on the spacial slices:

$$\det qq^{ab} = E^a_I E^b_J \delta^{IJ}, \tag{2.13}$$

where q is the induced 3-metric on the spacial slices and A^I_a is interpreted as

$$A^I_a = \Gamma^I_a + \gamma K^I_a, \tag{2.14}$$

where Γ^I_a is the spin connection related to E^b_J and K^I_a is the extrinsic curvature of Σ in M so that we have the extrinsic curvature K as a function of phase space variables A and E.

There are several constraints on these variables. As previously mentioned, due to diffeomorphism invariance the Hamiltonian is itself just a linear combination of constraints. The constraints are the following:

$$G_I = D_a E^a_I \tag{2.15}$$

$$C_a = E^b_I F^I_{ab} \tag{2.16}$$

$$H = \frac{1}{2}\epsilon^{IJ}{}_K \frac{E^a_I E^b_J}{\sqrt{\det E}} F^K_{ab} - (1+\gamma^2)\frac{E^a_I E^b_J}{\sqrt{\det E}} K^I_{[a} K^J_{b]} \tag{2.17}$$

where D is the covariant derivative induced by A, F is its curvature of A and K is the extrinsic curvature of Σ in M. The constraints each have their own geometric interpretation: G_I, the Gauss constraint, generates gauge transformations on the phase space. C_a, the diffeomorphism constraint, generates the transformations induced in phase space under diffeomorphisms of Σ. H, the Hamiltonian constraint, generates the transformations

induced in phase space under deformations of (the embedding of) the hypersurface Σ in a timelike direction in space-time, in other words one can see it as generating "translations in time" hence the term "Hamiltonian" for it as it "evolves" the spacial slices. The quotation marks in the last sentence are there because seeing as it is a constraint, it is not a Hamiltonian in the true sense of the word and evolution in this case has a more complicated interpretation.

We now wish to quantise this theory. Our configuration space is the space of $SU(2)$ connections A on Σ. The typical quantisation scheme then tells us to look at "square integrable" functionals of A, $f : A \mapsto \mathbb{C}$. However, we know that in step four of our quantisation scheme we will need to project down on the kernel of the constraints, so it would be to our advantage right now to construct functionals which are invariant under as many of the constraints as possible. Given a connection, in the end we need to associate to it a complex number. We can obtain complex numbers from the connection by integrating the connection, in a representation of $SU(2)$ over certain paths in Σ. However, if we wish the Gauss constraint to vanish on our functionals of A, they must be gauge invariant. One way to do this is to integrate the connection over a closed loop and then take the trace.

$$f[A] = Trh_\alpha[A] = Tr\mathcal{P}\exp\int_\alpha A, \tag{2.18}$$

Initially, this was what was done in Loop Quantum Gravity and this is where Loop Quantum Gravity got its name. However, more generally one can integrate along edges of an embedded closed graph in Σ, each edge with its own representation of $SU(2)$ as long as at the vertices we contract together all the indices of the group elements representing

parallel transportation along different paths and in different representations in an $SU(2)$-invariant way [97]. The objects we use to this end are called intertwiners, they project a tensor product of spins into a spin-0 subspace. Alternatively, one can view intertwiners as being $SU(2)$ homomorphisms mapping the tensor product of the spins on the incoming edges to the tensor product of the spins on the outgoing edges (the previous definition corresponding to the special care when all the edges are seen incoming):

$$I_v : \bigotimes_{e \text{ incoming}} \pi_{j(e)} \longrightarrow \bigotimes_{e \text{ outgoing}} \pi_{j(e)}, \qquad I_v \pi_{\text{ incoming}}(g) = \pi_{\text{ outgoing}}(g) I_v. \tag{2.19}$$

To recap, we can represent a gauge-invariant functional of the connection A as an embedded graph in Σ where each edge is labelled by an irreducible $SU(2)$ representation (a number j such that $2j \in \mathbb{N}$) and the vertices are labelled by $SU(2)$ intertwiners (in the case of a trivalent vertex, there is only one intertwiner so we need not worry about the label). A functional so represented then prescribes that given a connection A, we should integrate it along every edge e in the representation j_e which labels the edge and then contract the group elements obtain at the vertices using the intertwiner labelling the vertex.

With such a prescription we have functionals, or states in the kernel of G^I however these states are still not in the kernel of C_a or H. We can "easily" project them in the kernel of the C_a by smearing them over spatial diffeomorphisms of Σ. After we have done this, the spin-and-intertwiner-labelled-graph becomes independent of the particular embedding in Σ, and were it not for the possibility of topologically distinct embeddings, it would be an abstract labelled graph called a spin-network. Thus we have projected down to the kernel of both G and C and the only constraint we have not imposed is the

Hamiltonian constraint, which we use to evolve the states in time. The spin-networks or the functions they represent, which we call cylindrical functions, are then the basis states of Loop Quantum Gravity.

The connection was a 1-form so we had to integrate it along a path to get a number out of it, its conjugate momentum,E, which will act as a derivative on A is a 2-form, so we must integrate it over a surface:

$$E[S,f] = \int_S *E_I f^I \tag{2.20}$$

where f is a function taking values in $\mathfrak{su}(2)^*$ and *E is the two-form $E^a \epsilon_{abc} \mathrm{d}x^b \wedge \mathrm{d}x^c$.

Using this, we get the following algebraic relations on a Hilbert space:

$$\begin{aligned} f_1 \cdot f_2[A] &= f_1[A] f_2[A] \\ [f, E_{S,r}] &= 8\pi\gamma l_P^2 X_{S,r}[f] \\ [f,[E_{S_1,r_1}, E_{S_2,r_2}]] &= (8\pi\gamma l_P^2)^2 [X_{S_1,r_1}, X_{S_2,r_2}][f] \\ &\dots \\ (E_{S,r})^* = E_{S,\overline{r}}, &\qquad (f[A])^* = \overline{f}[A], \end{aligned} \tag{2.21}$$

where X is a derivative operator on the space of cylindrical functions which takes the functional derivative of cylindrical function with respect the the connection at the point where the graph of the cylindrical function intersects the surface of the smeared E in the direction that the E field takes at that point. So for a surface S that is intersected transversely by a path e, splitting it into a part e_1 incoming to, and a part e_2 outgoing from the surface we

get

$$X_{S,r}\pi(h_e)_j = \sum_i r_i(p)\pi_j(h_{e_1}\tau_i h_{e_2}). \tag{2.22}$$

2.2.2 Kinematics

Now that we have done all this work, it would be nice to understand the physical meaning of the quantum states we have derived.

The canonical momentum E has a direct geometric interpretation: It encodes the spatial geometry:

$$|\det q| q^{ab} = E^a_I E^b_J \delta^{IJ} \tag{2.23}$$

where q_{ab} is the metric induced on Σ by the space-time metric on M. Thus E is a densitised triad field for q. The interpretation of A is a combination of the spin connection and the exterior curvature:

$$A^I_a = \Gamma^I_a + \gamma K^I_a \tag{2.24}$$

where Γ is the spin connection related to E.

Armed with this knowledge, let us try to calculate the area of a surface S in Σ. When the field E is pulled back to Σ one obtains a vector valued two-form. The norm of this two-form is directly related to the area [96]:

$$A_S = \int_S |E(\sigma)| = \int_S d^2\sigma \sqrt{E^a_I E^b_J \delta^{IJ} n_a(\sigma) n_b(\sigma)}, \tag{2.25}$$

where $n_a(\sigma) = \epsilon_{abc}\frac{dX^b}{d\sigma^1}\frac{dX^c}{d\sigma^2}$ is the normal to the surface. Regularising in terms of fluxes in the form of (2.20), substituting operators, and taking the regulator away leads to a well defined, simple operator $\widehat{A}_S$. Its action on states with just a single edge is especially simple: If edge and surface do not intersect, the state is annihilated. If they do intersect once, one obtains

$$\widehat{A}_S \,\mathrm{Tr}[\pi_j(h_\alpha[A])] = 8\pi\gamma l_P^2\sqrt{j(j+1)}\,\mathrm{Tr}[\pi_j(h_\alpha[A])]. \tag{2.26}$$

Thus these states are eigenstates of area, with the eigenvalue given as the square root of the eigenvalue of the $SU(2)$-Casimir in the representation given on the edge.

Similarly (though much more complicated), one finds that quanta of volume are located at vertices with valence greater than or equal to four[96]. The spectrum of the volume however, is much more complex.

We can thus visualise states of Loop Quantum Gravity as spin-networks with each edge labelled by j representing a quanta of area $\propto jl_P^2$ and each vertex representing a quanta of (possibly zero) volume.

2.2.3 Dynamics

Since we have already projected into the kernel of the other constraints, all the only remaining dynamics are left in the Hamiltonian constraint:

$$H = \underbrace{\frac{1}{2}\epsilon^{IJK}\frac{E^a_I E^b_J}{\sqrt{\det E}}F_{abK}}_{H_E} - (1+\gamma^2)\frac{E^a_I E^b_J}{\sqrt{\det E}}K^I_{[a}K^J_{b]}. \tag{2.27}$$

The Hamiltonian constraint evolves the spin networks by changing the graph and its labels [97]. In the most well known version of the Hamiltonian constraint, the graph is evolved by creating a new edge linking to old edges which meet at a vertex. The dynamics however are still relatively poorly understood.

2.2.4 Simplifications

Because the full theory of Loop Quantum gravity is so difficult to solve in full, we will attempt to make some simplifications to it in order to try to extract from it some meaningful phenomenology. One way to simplify the theory is instead of considering all graphs of spin-networks, one considers only one graph, a highly symmetric lattice (which allows us to do dimensional reduction at the same time). Then we evolve the theory classically using Poisson brackets instead of commutators. This technique has already been used quite successfully in order to obtain Loop Quantum Cosmology, a Loop Quantum Gravity inspired cosmology (see for example [6] for an overview and introduction to Loop Quantum Cosmology), and in part III of this thesis we will use it to obtain black hole solutions.

Part II

Emergence

Chapter 3

Introduction to the Lieb-Robinson Bound

3.1 General Remarks

The principle of locality is at the heart of the foundations of all modern physics. In quantum field theory, the principle of causality is enforced by an exact light cone. Whenever two (bosonic) observables are space-like separated they have to commute, so that neither can have any causal influence on the other. On the other hand, in ordinary quantum mechanics, it is, in principle, possible to signal between arbitrarily far apart points in an arbitrarily short time.

Nevertheless, a simple perturbation analysis shows that such an influence must decay exponentially with the distance between the observables. The seminal work by Lieb and Robinson [68] made the above statement rigourous for non relativistic spin systems. In essence, it states that a quantum system whose Hilbert space is composed of a tensor product of local, finite dimensional, Hilbert spaces and whose Hamiltonian is the sum of local operators will have an approximately maximum speed of signals. Here local just

means that every operator has as a support the tensor product of only a few "nearby" local Hilbert spaces. The approximation consists in the fact that outside the effective light cone, the amount of information that can be sent is exponentially suppressed. For some systems like quantum random walks, the maximal speed of signal has been calculated exactly [59], here we will expose a framework for getting a good approximation of that speed in general circumstances.

This discovery provides a mechanism for models of quantum gravity, like Quantum Graphity, which at the fundamental level have a preferred time slicing exhibit the emergence of local Lorentz symmetry in the infrared limit like is the case for the well-tested theory of General Relativity. Heuristically[1], the argument for the previous statement goes as follows.

As will be explained latter in section 3.2, in the continuum limit, the Lieb-Robinson bound becomes sharp and no signals, even suppressed, can travel faster than the finite speed given by the bound. Because special relativity is implied by isotropy, homogeneity and "the First Postulate" [35], speeds in a homogeneous and isotropic system must transform either according to Galilean transformation or Lorentz transformations. The First Postulate can be stated as that the transformation rules for speed depend only on the relative speeds and that they are consistent, where by consistent we mean that the speed of a particle X with respect to a reference frame R is inferred to have the same magnitude by observers in any two other reference frames R' and R''. If we start with a quantum system living on a homogeneous and isotropic flat[2] lattice which is evolved by a homogeneous

[1] A more detailed version will come out in a future article [95].

[2] By flat we mean that if we assign the length value a to each edge of the graph and embed the graph in $\mathbb{R}^n$ (for n sufficiently large) such that each edge is mapped to a straight segment of length a and take the limit $a \to 0$, the resulting submanifold of $\mathbb{R}^n$ has vanishing intrinsic curvature.

and isotropic Hamiltonian such that some excitations propagate with a constant speed with respect to the underlying graph distance (providing inertial reference frames), then, if distances in all reference frames are defined to be the graph distance, the system satisfies the three conditions of isotropy, homogeneity and First Postulate. The transformation rules of speeds will be Galilean, a special case of Special Relativity when the parameter of the transformations, c (usually identified with the speed of light), is infinite. Now suppose that we are in such a system but that the conditions for the existence of a Lieb-Robinson Bound are satisfied. Then there will be a constant (due to homogeneity and isotropy) maximum speed of propagation of information v_{max}. In such a system, we can, if we so desire, continue to use the graph distance as the metric in all reference frames, in which case speeds will continue to transform according to Galilean transformations (Lorentz transformations with $c = \infty$) but the maximum speed at which one can send signals will be reference frame and direction dependent. Alternatively, in the infrared limit when the lattice is no longer detectable, one should define a different metric, operationally defined with what is accessible at that energy scale. Due to homogeneity and isotropy, we have that speeds must transform according to Lorentzian transformations with speed of light c (where the transformation is Galilean if $c = \infty$). In the lattice reference frame, the maximum speed observed is v_{max}, so to ensure that we can pass from the original lattice reference frame to the reference from of any signal we must have $c \in [v_{mac}, \infty]$. Because we do not have access to the lattice and thus to the preferred lattice reference frame and the metric that comes with it, any choice of $c \geq v_{max}$ is acceptable, however the choice $c = v_{max}$ is clearly favoured since it is the only choice for which physics is identical in all reference frames (other choices will see different maximal speeds for different reference frames and differ-

ent directions). This choice, however, implies that in reference frames other then the lattice reference frame, we are now using a different metric than the lattice distance; in fact, since we do not see the lattice, we are using the metric obtained operationally assuming v_{max} to equal c in all reference frames and then using "light" clocks (probably more appropriately name maximal speed signal clocks) to measure time and bouncing maximal speed signals between objects to determine distances. Absent an observable lattice, it is the only way we can measure distances anyway. Thus special relativity is recovered[3]. Such a situation occurs in Wen's string net condensate model of emergent light[108] which we discuss in section 4.1.6. If we define distances using the maximal speed of signals, we will always have at least local isotropy. Thus if homogeneity is lost, global Lorentz transformations are substituted for local Lorentz transformations and we can view the system (in the continuous limit) as relativistic quantum fields on a manifold $\mathbb{R} \times S$ where S corresponds to the static spacial slices with static metrics. If we then allow for the graph to be dynamic, as in Loop Quantum Gravity and Quantum Graphity, or if we allow the Hamiltonian to be time dependent (which will change the maximum speeds with respect to the graph, and thus the distances as calculated using the maximal speed of signals which is assumed constant) we obtain a quantum field theory on curved spacetime with a dynamical metric. It is then possible to recover General Relativity if the correct relationships are imposed between local energy densities and the dynamical metric. This last part, however, is far from

[3]One potential problem that can arise at this level when there are many excitation types is if, in the reference frame of the graph, the limiting speed v_L for one type of excitation is less than v_{max}. In such situation, a frame with speed $v > v_L$ would see these excitations as being unable to propagate in some directions, this implies a preferred reference frame. We thank Niayesh Afshordi for pointing this out. This is an important problem which will not be dealt with here. Let us however indicate briefly a possible solution. So that they can be seen, it must be possible for the slow excitations to interact with the fast ones, this means that in the infrared limit, they might be dressed-up in clouds of virtual fast excitations which would allow them to go much faster. Afshordi suggests a different resolution: the fast excitations might not be stable in the infrared limit, they might emit Cherenkov radiation in the form of the slow excitations

straightforward.

It is important to note here that for all the calculations to be performed in this thesis, we only consider the graph-distance metric and the speed as defined in this metric. This is because we are working with the "fundamental" theories/models and at the "fundamental scale" calculations are most easily performed in the preferred rest frame at rest with respect to the graph.

Lieb-Robinson bounds (LRB) however have mostly been used in the fields of theoretical condensed matter and quantum information theory [24, 28, 27, 60, 84, 45, 32, 101, 33, 92, 82, 85, 86, 83]. In particular, the LRB has been used to prove that a non-vanishing spectral gap implies an exponential clustering in the ground state [45, 84, 101]. Further developments can be found in [82], where the LRB is used also to argue about the existence of dynamics. The LRB has also been instrumental in the recent extension of the Lieb-Schultz-Mattis theorem to higher dimensions [43, 85]. In [32], it has been shown how the Lieb-Robinson bounds can be exploited to find general scaling laws for entanglement. In [24] these techniques have been exploited to characterise the creation of topological order. The locality of dynamics has important consequences on the simulability of quantum spin systems. In [88, 89] it has been shown that one dimensional gapped spin systems can be efficiently simulated. A review of some of the most relevant aspects of the locality of dynamics for quantum spins systems can be found in [86]. Other developments of significant interest include [33, 92] which show that it is possible to entangle macroscopically separated nano-electromechanical oscillators of oscillator chain and that the resulting entanglement is robust to decoherence. Such a system is of great interest for its possible application as a quantum channel and as a tool to investigate the boundary between the

classical and quantum world.

3.2 The Lieb-Robinson bound

In its simplest form, the Lieb-Robinson bound can be derived in the following way. We suppose that the total Hilbert space is the tensor product of local Hilbert spaces:

$$\mathcal{H} = \bigotimes_x \mathcal{H}_x. \tag{3.1}$$

Each local Hilbert space $\mathcal{H}_x$ is associated to an edge or to a vertex of a graph G with vertices having a maximum valency ν. The total graph is thus associated to the total Hilbert space. On this Hilbert space we have a local Hamiltonian which defines the evolution:

$$H_{local} = \sum_{X \subset G} \Phi_X, \tag{3.2}$$

where the operators Φ_X are R-local. We define an operator to be R-local if it has support on a Hilbert space with an associated subgraph X of G such that the diameter of X (the maximal distance between any two point of X) in graph distance is less than R and such that $X \cap Y = \emptyset \Rightarrow [\Phi_X, \Phi_Y] = 0$. The norm of these local operators is also assumed to be less than some positive number K. The Lieb-Robinson bound is a bound on the commutator of two local observables separated by a distance d at a time t such as

$$f(t) := [O_P(t), O_Q(0)], \tag{3.3}$$

where the operators O_P and O_Q have support on the Hilbert spaces associated with the subgraphs P and Q which are separated by a graph distance d. Taking the derivative with respect to t and rearranging using the Jacobi identity, we have that

$$f'(t) = -i \sum_{X \in Z_P} ([f(t), \Phi_X(t)] + [O_P(t), [\Phi_X(t), O_Q(0)]]) \tag{3.4}$$

where Z_P contains subgraphs of diameter at most R which have a non-empty intersection with P. Taking the norm and integrating we obtain

$$\|[O_P(t), O_Q(0)]\| \leq \|[O_P(0), O_Q](0)\| + 2\|O_P\| \sum_{X \in Z_P} \int_0^{|t|} ds \|[\Phi_X(s), O_Q(0)]\|. \tag{3.5}$$

This last equation can then be iterated to give

$$\|[O_P(t), O_Q(0)]\| \leq \|O_P\|\|O_Q\| \sum_{n=0}^{\infty} \frac{(2|t|)^n}{n!} a_n \tag{3.6}$$

where

$$a_n := \sum_{X_2 \in Z_{X_1}} \cdots \sum_{X_{n+1} \in Z_{X_n}} \prod_{j=1}^{n} \|\Phi_{X_j}\| \delta_Q^{X_n} \leq K^n l^n e^{\lambda(nR-d)} \tag{3.7}$$

for some positive number λ and where we've set $X_1 := P$. We define $\delta_Y^X = 1$ if $X \cap Y \neq \emptyset$ and $\delta_Y^X = 0$ otherwise. We also define $l := \max_X |Z(X)| < \infty$ for diameter$(X) \leq R$. A bound on a_n is obtained by bounding $\|\Phi_{X_j}\|$ by K and by noticing that there are at most l terms in each sum such that $\delta_Q^{X_n} = 0$ and $nR < d$. Using this bound for a_n we obtain a

form of the Lieb-Robinson bound

$$\|[O_P(t), O_Q(0)]\| \leq \|O_P\|\|O_Q\| \exp\left(-\lambda(d - v|t|)\right), \tag{3.8}$$

where $v \leq (2Ke^{\lambda R})/\lambda$. This last inequality implies that the "speed of signals" in the system is effectively less than v. Anything travelling faster than this speed will be exponentially suppressed.

From the above derivation of the Lieb-Robinson bound, two limitations immediately surface. First, passing from Eq.(3.4) to Eq.(3.5), the norm of the local operators is used; hence it is necessary that the local operators composing the Hamiltonian be bounded. Second, it is evident from using $\|\Phi_{X_j}\| \leq K$ in Eq.(3.7) that in obtaining the Lieb-Robinson bound, one has ignored the interplay between different types of operators (different types of interactions) weakening the bound in the case where not all of the local operators have norm K. The purpose of chapter 4 will be to resolve this second limitation. In chapter 5, we will partially resolve the first limitation by allowing unbounded operators as long as their commutators remain bounded. Finally in 6 we will put these two results together and give the final result.

Before we proceed however, we would like to point out a stunning implication of the existence of the Lieb-Robinson bound: a relativistic light-cone structure emerges in the continuum limit of certain local (non-relativistic) quantum systems. More precisely, the continuum limit of any quantum system, for which the Lieb-Robinson bound is applicable, will exhibit a sharp emergent light-cone structure with a *finite* signaling speed. A heuristic argument can be given by replacing graph distances with metric distances in some units.

For instance, let Δ be the unit graph distance in some standard unit such as metres or centimetres. If we now re-write the Lieb-Robinson bound using this standard unit instead of the graph distance we get

$$\|[O_P(t), O_Q(0)]\| \leq \tilde{M} \exp\Big(\frac{\lambda}{\Delta}\big(v_{LR} \mid t \mid -d(P,Q)\big)\Big), \tag{3.9}$$

where the Lieb-Robinson speed, v_{LR}, is measured in the standard units of length per unit time, the distance $d(P,Q)$ is measured in the same units of distance. It is now clear that if we take the continuum limit of the theory, $\Delta \to 0$, Eq.(3.9) will be exactly zero if $d(P,Q) > v_{LR} \mid t \mid$. A complete analysis of the emergence of a strict light cone in the continuum limit has been shown in [28] for general harmonic quantum systems.

The Lieb-Robinson bound will allow us to conclude that any discrete R-local quantum theory with a Hamiltonian consisting of uniformly bounded or commutator-bounded operators will have an exact emerging light-cone structure in the continuum limit, a finite speed of sound. If in the low energy limit the underlying limit cannot be detected and thus one cannot observe a preferred reference frame of the medium then operationally defined measurements will yield an emergent Lorentz symmetry. As mentioned in section 3.1, since many theories of quantum gravity are built from discrete structures such as graphs, the Lieb-Robinson bound could provide a natural mechanism for the emergence of relativity in those theories without requiring local Lorentz invariance a priori.

3.3 Maximal Speed of Signals from the Lieb-Robinson Bound

To show how the Lieb-Robinson bound implies a limiting speed to the propagation of information, we will follow, in this section, the treatment of [24] where this implication was shown, to our knowledge, for the first time. Let us consider two observers: Alice and Bob. Alice, who wants to send a message to Bob, acts on a bounded subgraph Q with a set of unitary operators: $\{O_Q^k\}$, where k labels the particular message she wishes to send with the particular choice $O_Q^0 = \mathbb{1}$. Bob, at distance d (in graph distance) away makes a measurement with observable O_P on a bounded subgraph P. If we define the global evolution of the system for a time t to be given by $U(t) = \exp(tH)$ so that $O_P(t) := U(t)O_PU(t)^\dagger$, then, from the Lieb-Robinson bound we have that

$$\|[O_P(t), O_Q^k(0)]\| \leq M\|O_P\|\|O_Q^k\| \exp\Big(\frac{1}{\xi}\big(v_{LR} \mid t \mid -d\big)\Big), \tag{3.10}$$

where M is a constant. If we now suppose that the global initial state is given by ρ_0, we have that the input state of the quantum channel over which Alice communicates with Bob is

$$\rho^k(0) = O_Q^k \rho_0 (O_Q^k)^\dagger. \tag{3.11}$$

Designating Γ to be the global system and Γ/P to be the whole system except for the local system where Bob makes his measurement, we have that the output state available to Bob

at time t is

$$\sigma_P^k(t) = \mathrm{Tr}_{\Gamma/P}\Big[U(t)O_Q^k\rho_0(O_Q^k)^\dagger U(t)^\dagger\Big]. \tag{3.12}$$

We can now look at what effect Alice's signaling has on Bob's observation by looking at the difference in what Bob observes if Alice signals a message or does nothing:

$$\begin{aligned}|\mathrm{Tr}_P\Big\{O_P(\sigma_Q^0(t)-\sigma_Q^k(t))\Big\}| &= |\mathrm{Tr}_P\Big\{\rho_0(O_Q^k)^\dagger[O_Q^k,O_P(t)]\Big\}| \\ &\leq \|[O_P(t),O_Q^k]\| \leq \|O_P\|\epsilon,\end{aligned} \tag{3.13}$$

where $\epsilon = M\exp\Big(\frac{-1}{\xi}(d-v_{LR}\mid t\mid)\Big)$ is given by Eq.(3.10). This implies that for any k, $\sigma_P^k(t)$ and $\sigma_P^0(t)$ are ϵ-close in the trace norm:

$$\forall k, \quad \|\sigma_P^k(t)-\sigma_P^0(t)\|_1 \leq \epsilon. \tag{3.14}$$

Supposing then that in the particular language used by Alice to communicate, the probability for her to implement the unitary operator O_Q^k is p_k, then we have that the amount of information she can transmit to Bob with each message is given by the Holevo capacity:

$$C_\chi = S\big(\sum_k p_k\sigma_P^k(t)\big) - \sum_k p_k S\big(\sigma_P^k(t)\big), \tag{3.15}$$

where $S(\rho) = -\mathrm{Tr}\big(\rho\log_2(\rho)\big)$ is the von Neumann entropy. If n_P is the dimension of the Hilbert space associated with the subgraph P, then Fannes' inequality asserts that given

two density operators ρ_P^1 and ρ_P^2 on the Hilbert space we have that

$$|S(\rho_P^1) - S(\rho_P^2)| \leq \|\rho_P^1 - \rho_P^2\|_1 \log_2 \left(\frac{n_P}{\|\rho_P^1 - \rho_P^2\|_1} \right). \tag{3.16}$$

Thus, combining Eq.(**??**) we obtain:

$$\begin{aligned}
C_\chi &= \sum_k p_k \left(S\big(\sum_j p_j \sigma_P^j(t)\big) - S\big(\sigma_P^k(t)\big) \right) \\
&\leq \sum_k p_k \left(|S\big(\sum_j p_j \sigma_P^j(t)\big) - S\big(\sigma_P^0(t)\big)| + |S\big(\sigma_P^0(t)\big) - S\big(\sigma_P^k(t)\big)| \right) \\
&\leq \sum_k p_k \left(\|\sum_j p_j (\sigma_P^j(t) - \sigma_P^0(t))\|_1 \log_2(n_P / \|\sum_j p_j (\sigma_P^j(t) - \sigma_P^0(t))\|_1) + \epsilon \log_2(n_p/\epsilon) \right) \\
&\leq \sum_k p_k \left((\sum_j p_j \|\sigma_P^j(t) - \sigma_P^0(t)\|_1 \log_2 \left[n_P / \{\sum_j p_j \|\sigma_P^j(t) - \sigma_P^0(t)\|_1\} \right]) + \epsilon \log_2(n_p/\epsilon) \right) \\
&\leq 2\epsilon \log_2(n_P/\epsilon)
\end{aligned} \tag{3.17}$$

which shows that the capacity of the quantum channel is exponentially suppressed as $\exp[-(d - v_{LR}|t|)/\xi]$.

Chapter 4

Interaction-Strength-Dependent Bound

In previous derivations of the Lieb-Robinson bound, the focus was on proving its existence not on providing a tight bound. One of the most significant places where tightness was sacrificed in favour of generality is the strength of the interactions: the complex interplay between non-commuting local operators of the Hamiltonian was ignored by approximating the norm of all operators by the largest norm. In this chapter, modified from [94], we show how some of the interaction type and strength dependence can be accounted for.

4.1 Theories of Two Interactions

Before taking into account the subtle interplay between a finite number of interaction types in the Hamiltonian, we will derive the Lieb-Robinson bound for a Hamiltonian with two interactions. This will give us the intuition needed to derive the bound for a system with more than two interactions. We will consider R-Local quantum systems with Hamiltonians composed of bounded operators containing only two interactions. We will begin by defining precisely what an R-Local quantum system is.

4.1.1 R-Local Quantum Systems

We consider quantum systems of the following kind. Let G be a graph (finite or infinite) having a maximum valence ζ[1] such that to every edge e we associate a Hilbert space $\mathcal{H}_e$ and to every vertex v we associate a Hilbert space $\mathcal{H}_v$. The total Hilbert space of the system is then defined to be

$$\mathcal{H}_{tot} \equiv \bigotimes_{\text{e an edge of G}} \mathcal{H}_e \otimes \bigotimes_{\text{v a vertex of G}} \mathcal{H}_v. \tag{4.1}$$

We then take the evolution of the system to be R-local for R a natural number. By this we mean that the evolution is governed by a Hamiltonian composed of a sum of operators each having support on a Hilbert space which is associated with a subgraph of G having a diameter less than R (i.e. the graph distance between any two points of the subgraph on which the operator acts is at most R). By association, we will also refer to the diameter of an operator as the diameter of its associated subgraph. Also, we use the notation that if Φ is an operator and it does not have an explicit time dependence then it is considered to be an operator evaluated at time $t = 0$, i.e. $\Phi = \Phi(0)$; furthermore, we have $\Phi(t) \equiv e^{itH}\Phi e^{-itH}$.

4.1.2 General Hamiltonians With Two Bounded Interactions

A common type of Hamiltonian is one with two coupling constants and two different types of operators. We say a Hamiltonian is a general Hamiltonian with two coupling constants

[1] This ensures that the continuum limit of G be locally compact. The requirement will be needed so that the sum $\sum_{n=0}^{\infty} c_n \frac{w^n}{n!}$, which we will encounter later, converges for all real w.

if it is of the following type

$$H \equiv \sum_{i \in S_0} h_0 \Phi_0^i + \sum_{j \in S_1} h_1 \Phi_1^j, \tag{4.2}$$

with the properties that for $a \in \mathbb{Z}_2 = \{0, 1\}$ and $(i, j) \in S_a \times S_a$ we have $[\Phi_a^i, \Phi_a^j] = 0$ and $\|\Phi_a^i\| = \|\Phi_a^j\| = 1$. In other words the operators are normalised and operators of the same type at different locations on the graph commute. Here, the set S_a is the set of labels of the subgraphs of G for which the operators of type a have support.

Let $\Gamma(q, m)$ be the subgraph associated with the operator Φ_q^m and let $(a, b) \in \mathbb{Z}_2^2$. We define the function

$$K_{a\ b}^{i\ j}(t) \equiv [\Phi_a^i(t), \Phi_b^j], \tag{4.3}$$

in analogy with Eq. (3.3). We will generalise the Lieb-Robinson bound as calculated in [42] to R-local Hamiltonians of bounded operators having two interactions by deriving a bound for $K_{a\ b}^{i\ j}(t)$. Note that since we are dealing with bounded operators, it is possible to absorb the norm of the operators into the coupling constants and we may thus assume $\|\Phi_c^k\| = 1$. In the following, we will show that if P and Q are two separate regions of the graph which are small, as compared to the typical size of the total graph and O_P and O_Q are bounded local operators acting on the subgraphs P and Q respectively, then

$$\|[O_P(t), O_Q(0)]\| \leq \tilde{C} \exp\left(\xi\big(2\frac{\gamma}{\xi} e\sqrt{h_0 h_1}t - d(P, Q)\big)\right), \tag{4.4}$$

where $\tilde{C}$ is a positive constant depending on P,Q,$\|O_P\|$, $\|O_Q\|$ and H. Here γ and ξ are

positive constants depending on the graph structure, and $d(P,Q)$ is the graph distance between P and Q. As shown in section 3.3 this implies that information cannot propagate at speeds greater than $v_{LR} = 2\frac{\gamma}{\xi}e\sqrt{h_0 h_1}$ without suffering exponential suppression of the bandwidth as a function of distance. We will call this limit on the speed of information propagation the Lieb-Robinson speed. Note that if one of h_1 or h_0 equals zero the speed is zero and no information can propagate. This is indeed true for any system having a Hamiltonian composed of local operators which all commute with each other: imagine for example for example an Ising Model on a spin chain with no transverse field having for Hamiltonian $H = \sum_i S_i^z S_{i+1}^z$, no matter how one decides to flip or change the spin at site i, no discernable effect will ever observed at site $j \neq i$ no matter how long one waits. This is reminiscent of electromagnetism, information cannot propagate using only the electrostatic interaction or only the magnetostatic interaction, both are needed to send a signal and indeed, the quantised electric field and magnetic field do not commute. We obtain Eq.(4.4) through recursion as described below.

Taking the derivative of Eq.(4.3) with respect to t we get

$$
\begin{aligned}
(K_{a\ b}^{i_1\ j}(t))' &= -i[[\Phi_a^{i_1}(t), H(t)], \Phi_b^j], \\
&= -ih_{a+1} \sum_{i_2 \in Z_{i_1}} [[\Phi_a^{i_1}(t), \Phi_{a+1}^{i_2}(t)], \Phi_b^j], \qquad (4.5) \\
&= -ih_{a+1} \sum_{i_2 \in Z_{i_1}} [[\Phi_a^{i_1}(t), \Phi_b^j], \Phi_{a+1}^{i_2}(t)] + [\Phi_a^{i_1}(t), [\Phi_{a+1}^{i_2}(t), \Phi_b^j]], \\
&= [K_{a\ b}^{i_1\ j}(t), \Big(-ih_{a+1} \sum_{i_2 \in Z_{i_1}} \Phi_{a+1}^{i_2}(t) \Big)] + (-ih_{a+1}) \sum_{i_2 \in Z_{i_1}} [\Phi_a^{i_1}(t), [\Phi_{a+1}^{i_2}(t), \Phi_b^j]], \qquad (4.6)
\end{aligned}
$$

where the Jacobi identity was used to obtain the third equality and for $i \in S_q$ with $q \in \mathbb{Z}_2$, we define Z_i to be the set of $k \in S_{q+1}$ such that $\Gamma(q,i) \cap \Gamma(q+1,k) \neq \emptyset$. Note that if $a \in \mathbb{Z}_2$ and $a = 1$ then $a + 1 = 0$. Thus integrating Eq.(4.6) we get

$$K_{a\ b}^{i_1\ j}(t) = T_2(t) K_{a\ b}^{i_1\ j}(0) - i h_{a+1} \int_0^t ds \sum_{i_2 \in Z_{i_1}} [\Phi_a^{i_1}(s), [\Phi_{a+1}^{i_2}(s), \Phi_b^j]], \tag{4.7}$$

where $T_2(t)$ is a unitary evolution given by the unitary matrix $U_2(t) = \exp\left(-i h_{a+1} \sum_{i_2 \in Z_{i_1}} \Phi_{a+1}^{i_2}(t)\right)$ with $T_2(t)O \equiv U_2(t)^\dagger O U_2(t)$ for any operator O. Taking the norm of Eq.(4.7) we obtain

$$\begin{aligned}
\|K_{a\ b}^{i_1\ j}(t)\| &\leq \|K_{a\ b}^{i_1\ j}(0)\| + 2h_{a+1} \int_0^t ds \sum_{i_2 \in Z_{i_1}} \|\Phi_a^{i_1}(s)\| \|[\Phi_{a+1}^{i_2}(s), \Phi_b^j]\|, \qquad (4.8) \\
&= \|[\Phi_a^{i_1}(0), \Phi_b^j(0)]\| + 2h_{a+1} \|\Phi_a^{i_1}(0)\| \int_0^t ds \sum_{i_2 \in Z_{i_1}} \|[\Phi_{a+1}^{i_2}(s), \Phi_b^j]\|, \\
&\leq 2\delta_j^{i_1} + 2h_{a+1} \int_0^t ds \sum_{i_2 \in Z_{i_1}} \|[\Phi_{a+1}^{i_2}(s), \Phi_b^j]\|, \\
&= 2\delta_j^{i_1} + 2h_{a+1} \int_0^t ds \sum_{i_2 \in Z_{i_1}} \|K_{a+1\ b}^{i_2\ j}(s)\|, \qquad (4.9)
\end{aligned}$$

where we define

$$\delta_i^k = \begin{cases} 1 & \text{if } \Gamma(a_i, i) \cap \Gamma(a_k, k) \neq \emptyset, \\ 0 & \text{otherwise}, \end{cases} \tag{4.10}$$

and where the last inequality is obtained by realizing that $\|[\Phi_c^k, \Phi_d^l]\| \leq 2$ and is necessarily zero if $\Gamma(c,k)$ and $\Gamma(d,l)$ have an empty intersection. Applying Eq.(4.9) to itself, we get by

induction that

$$\|K_a^{i_1}{}_b^{\,j}(t)\| \leq M \sum_{n=0}^{\infty} \frac{(2 \mid t \mid \sqrt{h_a h_{a+1}})^n}{n!} \underbrace{\Big(\sum_{i_2 \in Z_{i_1}} \cdots \sum_{i_{n+1} \in Z_{i_n}} \delta_j^{i_n} \Big)}_{c_n}, \tag{4.11}$$

where $M = \max\Big\{\sqrt{\frac{h_1}{h_0}}, \sqrt{\frac{h_0}{h_1}}\Big\}$. Note that c_n counts the number of chains associated to n local operators (and thus n subgraphs $\Gamma(c,k)$) starting with $\Gamma(a,i_1)$ and ending with $\Gamma(b,j)$. In all such chains a $\Gamma(0,k)$ is followed by a $\Gamma(1,l)$ where $\Gamma(0,k) \cap \Gamma(1,l) \neq \emptyset$ and vice versa. If we repeat exactly the same procedure, but this time with $O_P(t)$ instead of $\Phi_a^{i_1}(t)$ and $O_Q(0)$ instead of Φ_b^j where O_P, O_Q are operators defined on some regions P, Q we get

$$\|[O_P(t), O_Q(0)]\| \leq N\|O_P\|\|O_Q\| M \times \sum_{n=0}^{\infty} \frac{(2 \mid t \mid \sqrt{h_a h_{a+1}})^n}{n!} \underbrace{\Big(\sum_{i_2 \in Z_{i_1}} \cdots \sum_{i_{n+1} \in Z_{i_n}} \delta_Q^{i_n} \Big)}_{c_n}, \tag{4.12}$$

where M is defined as above and N is the (finite) number of local operators of the Hamiltonian intersecting P. Here, c_n counts the number of chains associated to n local operators (and thus n subgraphs $\Gamma(c,k)$) starting with $\Gamma(a,i_1)$ which must intersect P and ending with $\Gamma(b,i_n)$ which must intersect Q. Furthermore, we can always find a bound of the following type for c_n

$$c_n \leq \tilde{M} \gamma^n e^{\lambda(\frac{n}{\xi} - d)}, \tag{4.13}$$

where λ is an arbitrary positive real number. This is because the $\Gamma(a,i)$'s have a diameter of R or less. Hence, if the distance, d, between P and Q is greater than nR then there are no possible chains of n local operators linking P and Q. Since there is always less than ν other local operators intersecting $\Gamma(a,i)$ (ν must be finite because all vertices have a valence of not more than ζ), there is a maximum of ν^n possible chains of n local operators starting from any given position. Thus, like before, we certainly have that

$$c_n \leq \nu^n e^{\lambda(Rn-d)}. \tag{4.14}$$

Using Eq.(4.13) in Eq.(4.12) we obtain

$$\|[O_P(t), O_Q(0)]\| \leq \tilde{\tilde{M}} \exp\lambda \left(2\sqrt{h_0 h_1}\frac{\gamma}{\lambda}e^{\frac{\lambda}{\xi}}t - d\right), \tag{4.15}$$

where $\tilde{\tilde{M}} = M\tilde{M}N\|O_P\|\|O_Q\|$. This gives us an upper bound on the speed information can travel

$$v_{LR} = 2\sqrt{h_0 h_1}\frac{\gamma}{\lambda}e^{\frac{\lambda}{\xi}}, \tag{4.16}$$

which can be minimised by choosing $\lambda = \xi$. We thus get the following upper bound on the speed information can travel

$$v_{LR} = 2\frac{\gamma}{\xi}e\sqrt{h_0 h_1}. \tag{4.17}$$

4.1.3 Lieb-Robinson Bound on a Lattice

In the case where the graph is a regular lattice, it is possible to give a bound of the form given in Eq.(4.13) as a function of the lattice and the Hamiltonian. We will show here how this can be done.

For the Hamiltonian given in Eq.(4.2) on a regular lattice we have the following properties (in addition to the properties on a general graph): by passing from a Φ_0 to a Φ_1 in an operator chain, one always moves along the lattice by a lattice distance of D_1 and by passing from a Φ_1 to a Φ_0 in an operator chain, one invariably moves along the lattice by a lattice distance of D_0. In addition, for a given i the finite number $n_{a\to b}$ of j's such that $\Gamma(a,i)$ and $\Gamma(b,j)$ have a non-empty intersection is independent of i and j and depends only on a and b, i.e. the interaction types. Since the chains must alternate between operators of type 0 and operators of type 1, the number of operator chains of length n starting at a specified point on the lattice, but with an unconstrained endpoint, is at most

$$c_n \leq \max\left\{\sqrt{\frac{n_{0\to1}}{n_{1\to0}}}, \sqrt{\frac{n_{1\to0}}{n_{0\to1}}}\right\}\sqrt{n_{0\to1}n_{1\to0}}^{n}. \tag{4.18}$$

where the max prefactor takes care of both even and odd chains. In this case, for $d(P,Q) > \frac{n+1}{2}(D_0+D_1)$, there cannot be any chains of n operators linking the initial and final point. This means that for $\lambda > 0$, $e^{\lambda\left(\frac{n+1}{2}(D_0+D_1)-d(P,Q)\right)}$ is necessarily greater than 1 if there exists at least one operator chain of length n linking P and Q. Thus, instead of Eq.(4.18) we can write

$$c_n \leq \tilde{M}\sqrt{n_{0\to1}n_{1\to0}}^{n} e^{\lambda\left(\frac{n}{2}(D_0+D_1)-d(P,Q)\right)}, \tag{4.19}$$

where $\tilde{M} = \max\left\{\sqrt{\frac{n_{0\to1}}{n_{1\to0}}}, \sqrt{\frac{n_{1\to0}}{n_{0\to1}}}\right\} e^{\frac{\lambda}{2}(D_0+D_1)}$. Referring back to Eq.(4.13) we obtain:

$$\gamma = \sqrt{n_{0\to1}n_{1\to0}}, \tag{4.20}$$

$$\xi = \frac{2}{D_0 + D_1}. \tag{4.21}$$

Combining these results with Eq.(4.17) gives

$$v_{LR} = e\sqrt{n_{0\to1}n_{1\to0}h_0h_1}(D_0 + D_1). \tag{4.22}$$

Of course, the restriction to lattices is a significant one; however, as we shall see next, it is possible to obtain an equivalent bound on c_n for more general graphs.

4.1.4 Lieb-Robinson Bound on a Homogeneous and Isotropic Graph

Let us now suppose that we have a general graph, and not necessarily a lattice. In this case, the D's of Section 4.1.3 gain a dependence on the specific local operators Φ^i and Φ^j, i.e. instead of simply D_0 and D_1 we have $D_0^{i\to j}$ and $D_1^{j\to k}$. Similarly, the n's gain a dependence on i: instead of simply $n_{0\to1}$ and $n_{1\to0}$ we have $n^i_{0\to1}$ and $n^j_{1\to0}$. For a given operator chain of n operators $\{\phi_a^{i_1}, \phi_{a+1}^{i_2}, \ldots, \phi_b^{i_{n-1}}, \phi_{b+1}^{i_n}\}$ the end points of the chain can be separated by at most a graph distance of $\sum_{k=1}^{n-1} D_{a_k}^{i_k\to i_{k+1}}$. Hence if $d(P,Q) > \sum_{k=1}^{n-1} D_{a_k}^{i_k\to i_{k+1}}$ the chain cannot link P to Q.

Let us consider chains of n operators starting at i_1. Let i_k and j_k be different chains

such that $i_1 = j_1$. Then if we have

$$\frac{1}{n} \sum_{\text{chain i}} \sum_{k=1}^{n-1} D_{a_k}^{i_k \to i_{k+1}} \approx \frac{1}{n} \sum_{\text{chain j}} \sum_{k=1}^{n-1} D_{a_k}^{j_k \to j_{k+1}} \text{ and,} \tag{4.23}$$

$$\sqrt[n]{\prod_{\text{chain i}} \prod_{k=1}^{n-1} n_{a_k \to a_k+1}^{i_k}} \approx \sqrt[n]{\prod_{\text{chain j}} \prod_{k=1}^{n-1} n_{a_k \to a_k+1}^{j_k}}, \tag{4.24}$$

then the Lieb-Robinson speed will be the same in all directions. By $\approx$ we mean that the quantities converge for large n and are thus independent of the path the chain makes on the lattice. Moreover, if the quantities in Eqs. (4.23) and (4.24) depend on i_n then the Lieb-Robinson speed will vary in different regions of the graph. Finally, if the quantities in Eqs. (4.23) and (4.24) depend on n, then the speed will depend on the distance d.

We say a graph is homogeneous if the quantities in Eqs. (4.23) and (4.24) do not depend on n. Furthermore, we say a graph is isotropic at i_1 if Eqs. (4.23) and (4.24) do not depend on i_n, in which case the Lieb-Robinson speed will be the same in all directions. If these conditions are satisfied, the Lieb-Robinson speed will be constant in all directions and areas of the graph (or subgraph) considered.

It follows that in the case of a homogeneous and isotropic graph, we can define

$$\overline{n} = \sqrt[n]{\prod_{\text{chain i}} \prod_{k=1}^{n-1} n_{a_k \to a_k+1}^{i_k}}, \tag{4.25}$$

$$\overline{D} = \frac{1}{n} \sum_{\text{chain i}} \sum_{k=1}^{n-1} D_{a_k}^{i_k \to i_{k+1}}, \tag{4.26}$$

for some chain of length n where n is large. By definition these quantities will not depend on the particular chain chosen. We then have that $\overline{n}^n$ is equal to the number of chains of n

operators starting at a given point and ending anywhere. Note that for $d(P,Q) > n\overline{D}$ there cannot be any chains of n operators linking the initial and final point. This means that for $\lambda > 0$, $e^{\lambda\left(n\overline{D}-d(P,Q)\right)}$ is necessarily greater than 1 if there exists at least one operator chain of length n linking P and Q. Thus, we can write the analogue of Eq.(4.19) by

$$c_n \leq \overline{n}^n e^{\left(\lambda\left(n\overline{D}-d(P,Q)\right)\right)}, \tag{4.27}$$

which gives

$$\gamma = \overline{n}, \tag{4.28}$$

$$\xi = \frac{1}{\overline{D}}. \tag{4.29}$$

Combining these results with Eq.(4.17) gives us

$$v_{LR} = 2e\overline{D}\overline{n}\sqrt{h_0 h_1}. \tag{4.30}$$

As in Sections 4.1.3, we require a bound for the coefficient c_n in order to provide a Lieb-Robinson speed in terms of the parameters of the system. Let

$$\begin{aligned}
\overline{n} &= \begin{cases} \sqrt{n_{0\to1} n_{1\to0}}, & \text{lattice}, \\ \sqrt[n]{\prod_{\text{chain i}}^{n-1}{}_{k=1}\, n_{a_k\to a_k+1}^{i_k}}, & \text{h\&i graph}, \end{cases} \\
\overline{D} &= \begin{cases} \frac{1}{2}(D_0 + D_1), & \text{lattice}, \\ \frac{1}{n}\sum_{\text{chain i}}^{n}{}_{k=1}\, D_{a_k}^{i_k\to i_{k+1}}, & \text{h\&i graph}, \end{cases}
\end{aligned} \tag{4.31}$$

where "h&i" stands for homogeneous and isotropic. Using the definitions of Eq.(4.31) we have that Eq.(4.30) is the general equation for the Lieb-Robinson speed for both lattice systems and homogeneous and isotropic systems.

4.1.5 Example: The Ising Model

The quantum Ising model describes a spin network with a preferred alignment that is subjected to a magnetic field transverse to this preferred direction. In 1-dimension, the model is exactly solvable and is known to exhibit a second order phase transition at zero temperature [98]. The quantum Ising chain has a wide range of applications from condensed matter physics [104] to quantum gravity [17].

The quantum Ising chain is an example of a bounded system on a lattice having a Hamiltonian with two coupling constants. Accordingly, we can use the framework developed above to calculate the Lieb-Robinson bound.

The Hamiltonian for the quantum Ising chain is given by

$$H = -J \sum_i \left(g\sigma_i^x + \sigma_i^z \sigma_{i+1}^z \right), \tag{4.32}$$

where σ^x and σ^z are Pauli matrices. At zero temperature the Ising chain exhibits two phases: paramagnetic ($g > 1$) and ferromagnetic ($g < 1$) with a quantum critical point at $g = 1$. By varying g, i.e. the transverse magnetic field, the system can undergo a quantum phase transition from the paramagnetic phase (disordered) to the ferromagnetic phase (ordered) or vice versa.

In order to calculate the Lieb-Robinson speed we need an upper bound on the coef-

ficients c_n defined in Eq.(4.13). The c_n coefficients represent the number operator chains of length n consisting of alternating σ_i^x and $\sigma_i^z\sigma_{i+1}^z$ operators such that the subgraphs corresponding to the operators intersect (in this case only nearest neighbours). Since we are dealing with a lattice we can use Eq.(4.20) and Eq.(4.21). There are 2 possible steps from a vertex to an edge and 2 possible steps from an edge to a vertex. Thus by Eq.(4.20), in this case, $\gamma = \sqrt{2 \times 2} = 2$. Furthermore, by passing from a vertex to an edge, and vice versa, we move by half of a lattice spacing, thus by virtue of Eq.(4.21), $\xi = 2$.

It follows, from Eq. (4.17) that the Lieb-Robinson bound for the speed of propagation in the quantum Ising model is found to be

$$v_{LR} = 2e\sqrt{g}J. \tag{4.33}$$

Close to the quantum phase transition (which happens at $g = 1$), at small deviations from criticality, $|g - 1| \ll 1$, it is possible to take the continuum limit which gives a relativistic Majorana fermion field theory in one dimension with a speed of light of $c = J$ and a mass of $m = (g-1)J$ [37]. This means at up to a constant of order 1, $2e$, which we expect due to the approximations made, the Lieb-Robinson gives the right value for the speed of information propagation, at least near the phase transition where it can be checked.

4.1.6 Example: String Net Condensate Model of Emerging Light

The *principle of locality* is one of the most fundamental ideas of modern physics. It states that every physical system can be influenced only by those in its neighbourhood. The

concept of *field* is the outcome of taking this principle seriously: if object A causes a change on object B, there must be changes involving the points in between. The field is exactly what changes. In addition, if something is "happening" at all the intermediate points, then the interaction between the objects must propagate with a finite speed. Relativistic quantum mechanics is built by taking the locality principle as a central feature.

In this section, we will give a concrete example of a Galilean quantum system on a lattice which becomes Special Relativistic in the continuum limit because of a finite speed of information propagation that can be predicted by the Lieb-Robinson bound. This is an example of the general situation described in section 3.1. In the model under study, we can take the continuum limit exactly to find what the true maximum speed of interactions is and compare it with the Lieb-Robinson speed we derived in the previous section. This will give us an idea on how tight an upper bound on the maximum speed of information propagation we can expect the Lieb Robinson speed to be. Also, we will see explicitly how the theory in the continuum limit is Special Relativistic as we concluded should be the case in section 3.1. In fact the theory we are considering is a theory of emergent light, and so in this particular case, the Lorentz transformation parameter c will indeed correspond to a speed of light.

The concept of topological order, on which the emergent light model is based is one of the most productive recent ideas in condensed matter theory [106]. It provides explanations for phases of matter (for example, fractional quantum Hall liquids) that cannot be described by the paradigm of local order parameters and symmetry breaking. If local order parameters cannot describe such phenomena, then their order could be topological in nature [106]. Topological order gives rise to a ground state degeneracy that depends on the

topology of the system and is robust against any local perturbations [107]. Because of this property, topologically ordered systems appear to be good candidates for robust quantum memory and fault-tolerant quantum computation [60].

Not only can topological order explain exotic phases of matter, but it offers a whole new perspective to the problem of elementary particles. Currently, there are particles that we regard as fundamental, like photons and fermions, and other particles that can be interpreted as collective modes of a crystal. For example, we can describe phonons in this way because of the symmetry of the crystal. The understanding of the phases of matter provides an explanation for the phonon and other gapless excitations. However, one can also ask whether photons, electrons, or gravitons are emergent phenomena too, not elementary particles. Let us consider the case of light. Photons are $U(1)$ gauge bosons and they cannot correspond to the breaking of any local symmetry [108]. Nevertheless, they can be collective modes of a different kind of order, and this is the case of topological order. Indeed models with topological order can feature photons, fermions and even gravitons as emerging collective phenomena [106, 39].

Light emerges from topological order as the effective low-energy theory of a quantum spin system. The quantum spin system is built as a *local bosonic model*, namely a system in which the principle of locality is enforced by the fact that the Hilbert space decomposes in a direct product of local Hilbert spaces and all the observables have to commute when far apart. Moreover, the Hamiltonian must be a sum of local operators. In the low-energy sector, and in the continuum limit, the effective theory can be described by the Lagrangian of electromagnetism. Therefore low-energy excitations behave like photons. Maybe this is what photons really are, collective excitations of a spin system on a lattice with Planck-

scale distance. But then, why do we not see signals that are faster than light? There could be all sorts of interactions that can propagate as fast as permitted by the coupling constants of the underlying spin model. A theory of light as an emergent phenomenon needs to explain why we do not see signals faster than light.

Topological Order and Artificial Light.— If we want to impose the principle of locality in a strong sense, we must consider *local bosonic models* [108]. Fermionic models are not really local because fermionic operators do not generally commute even at distance. A local bosonic model is a theory where the total Hilbert space is the tensor product of local Hilbert spaces, local physical operators are finite products acting on nearby local Hilbert spaces, and the Hamiltonian is a sum of local physical operators. Thus local physical operators must commute when they are far apart. If we restrict ourselves to the case of a discrete number of degrees of freedom and finite-dimensional local Hilbert spaces, we have a *quantum spin model*. A quantum spin model can be therefore defined as follows. To every vertex x in a graph G we associate a finite dimensional Hilbert space $\mathcal{H}_x$. The total Hilbert space of the theory is $\mathcal{H} = \otimes_{x\in G}\mathcal{H}_x$. To every finite subset of vertices $X \subset G$, we associate the local physical operators with support in X as the algebra $\mathcal{B}(\mathcal{H}_X)$ of the bounded linear operators over the Hilbert space $\mathcal{H}_X = \otimes_{x\in X}\mathcal{H}_x$. The Hamiltonian will have the form $H_{local} = \sum_{X\subset G}\Phi_X$, where to every finite subset $X \subset G$ we associate an hermitian operator Φ_X with support in X. An example of local bosonic model is given by a spin $1/2$ system on a lattice. To every vertex x in the lattice we associate a local Hilbert space $\mathcal{H}_x \cong \mathbb{C}^2$. Local physical operators are finite tensor products of the Pauli matrices at every vertex.

The bosonic model we consider is a lattice of quantum rotors. Its low-energy effective

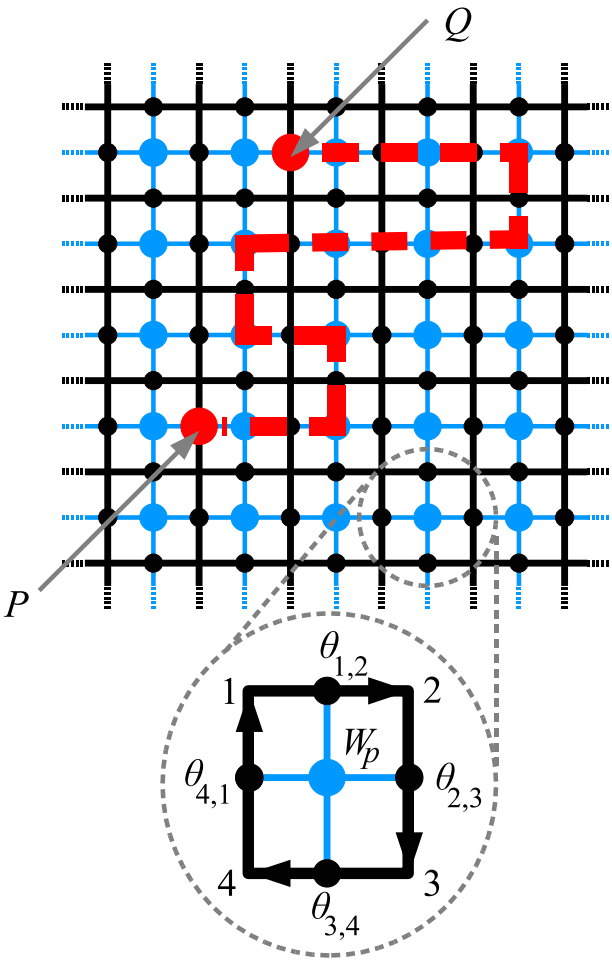

Figure 4.1: (Colour online) A $2D-$dimensional rotor lattice. To every plaquette p is associated a rotor operator W_p as a function of the variables θ_{ij}. The graph G is the one drawn in thin black lines. The graph G' is the graph with black and blue (lighter, bigger) dots as vertices and blue thin lines as edges. The red dashed line shows a path of length $n = 22$ from the point P to the point Q which are at a distance $2d(P, Q) = 8$ on G' or $d(P, Q) = 4$ on G. These paths contain alternating link and plaquette operators.

theory is a $U(1)$ lattice gauge theory whose deconfined phase contains emergent light. Consider a square lattice whose vertices are labeled by $\mathbf{i}$, with angular variable $\hat{\theta}_{\mathbf{ij}}$ and angular momentum $S^z_{\mathbf{ij}}$ on its links. The Hamiltonian for the quantum rotor model is given by

$$\begin{aligned} H_{rotor} &= U\sum_{\mathbf{i}}\left(\sum_{\alpha} S^z_{\mathbf{i},\alpha}\right)^2 + J\sum_{\mathbf{i},\alpha}(S^z_{\mathbf{i},\alpha})^2 \\ &+ \sum_{\substack{\mathbf{i},\{\alpha_1,\alpha_2\} \\ s.t.\ \alpha_1\cdot\alpha_2=0}} \left(t_{<\alpha_1\alpha_2>} e^{i\left(\theta_{\mathbf{i}+\alpha_1}-\theta_{\mathbf{i}+\alpha_2}\right)} + h.c.\right), \end{aligned} \tag{4.34}$$

where $\alpha = \pm 1/2(1,0), \pm 1/2(0,1)$ are the vectors of length $1/2$ pointing towards the lattice axes [108] and the t's are coupling constants. In the limit $t, J \ll U$, the first term of the Hamiltonian H_{rotor} behaves like a local constraint and makes the model a local gauge theory. Defining $g := 2/U(t_{12}t_{-1-2} + t_{2-1}t_{-21})$, the effective low-energy theory becomes the spin Hamiltonian

$$H_{eff} = J\sum_{<\mathbf{ij}>}(S^z_{\mathbf{ij}})^2 - g\sum_{\mathbf{p}}\frac{W_{\mathbf{p}} + h.c.}{2} \tag{4.35}$$

where now $\theta_{ij} = S^z_{ij}$ and $W_{\mathbf{p}} = S^+_{12}S^-_{23}S^+_{34}S^-_{41}$ is the operator that creates a string around the plaquette $\mathbf{p}$ (see Fig. 4.1). The smaller S, the smaller is the energy at which emergent light emerges [108]. In the following we assume $S = 1$. Although a lattice gauge theory is not a local bosonic model, this does not violate locality because H_{eff} is just an effective theory. The fundamental theory is local and H_{eff} is still a sum of local terms. In the large g/J limit,

the continuum theory for the Hamiltonian H_{eff} is the Lagrangian of electromagnetism

$$L = \int d^2\mathbf{x} \left(\frac{1}{4J}\mathbf{E^2} - \frac{g}{2}\mathbf{B}^2 \right),$$

with speed of light given by $c = \sqrt{2gJ}$.

Lieb-Robinson Bound for the emergent $U(1)$ model.— What do the Lieb-Robinson bounds tell us about the model H_{eff} with emergent light? Is the maximum speed of the interactions something like the speed of the emergent light or something completely different? As we have seen, this is of great importance if we want to take seriously the theory of light as an emergent phenomenon.

Using Eq.(4.22), and noticing that plaquettes are adjacent to four edges ($n_{\text{plaq}\to\text{edg}} = 4$), edges are adjacent to two plaquettes ($n_{\text{edg}\to\text{plaq}} = 2$) and that moving from the centre of the plaquette to an adjacent edge and *vice versa* one travels a graph distance of one half ($D = \frac{1}{2}$) we get that the Lieb-Robinson speed for the effective Hamiltonian is $v_{LR} = 2e\sqrt{2gJ} = 2e \times c$, where $c = \sqrt{2gJ}$ is the exact speed of the emerging light in the model. Again, as for the Ising model, we obtain the correct speed up to a constant of order 1 which, as mentioned previously, we would expect due to the approximations made. What is important though is that the functional dependence on the interaction strength is exact as this is very important information. Interestingly, in this case, the Lieb-Robinson speed is larger than the actual speed of information propagation by a factor of $2e$, the same factor that was obtained in the case of the Ising model. We do not know the reason for this, if any.

This calculation was done using the effective infrared Hamiltonian and so gives the

speed and a bound on the speed in that limit only. Probing energies of order U we could still find faster signals.

4.2 Theories of Finitely Many Interactions

Now that we have established in detail how to calculate the Lieb-Robinson bound for two interactions, we will apply the intuition we gained to derive a bound for any finite number of interactions. The essential intuition which we gained for two interactions was that, in an operator chain, because one type of interaction commutes with interactions of the same type, each operator in a chain must be of a different type than the preceding one. In the case of only two types of interaction, this requirement uniquely defines the interaction type of each operator in the chain, i.e. they must alternate. However, in the case of m-interactions, the situation is more complicated because we have a choice of as many as $m-1$ interaction types for each operator along the chain. The way we will deal with this added complication is by considering periodic chains of operators. Since the bound for an arbitrary chain will be the geometric mean of the bounds for such periodic chains, a bound on any chain can be derived from the bounds on the periodic chains.

Let us now consider general Hamiltonians possessing m types of interactions. We define a type of interaction to be a subset of the the local operators making up the Hamiltonian such that all the operators commute with each other and such that they appear with the same coupling constant in the Hamiltonian. Intuitively we think of all the operators of a single type as performing the same action at different locations on the graph. For example, in the quantum Ising model, the set of local operators $\{\sigma_i^x\}_{i\in\mathbb{Z}}$ implementing

the transverse magnetic field is considered to be one type of interaction. We will derive the Lieb-Robinson bound for such a Hamiltonian and provide the specific dependence of the Lieb-Robinson speed on the strength of the interactions. For simplicity, we will restrict ourselves to the case of bounded operators on a lattice. Generalisations to the commutator-bounded case and to homogeneous and isotropic graphs are straightforward applications of the methods shown in the previous sections, the results for which we will state at the end of this section.

We consider a Hamiltonian of the following type:

$$H \equiv \sum_{l=1}^{m} \sum_{i_l \in S_l} h_l \Phi_l^{i_l}, \tag{4.36}$$

where l labels the interaction type. We assume that all the terms in the sum are non-zero and that for all $l \in \{1, \ldots, m\}$ and $\forall (i,j) \in S_l^2$ we have $[\Phi_l^i, \Phi_l^j] = 0$ and $\|\Phi_l^i\| = \|\Phi_l^j\| = 1$. Note that the normalisation of the operators can be imposed without any loss of generality in the case of bounded interactions. Further, we assume that for all $(l_1, l_2) \in \{1, \ldots, m\}^2$ and $i \in S_{l_1}$, there are exactly $n_{l_1 \to l_2}$ j's such that $j \in S_{l_2}$ and $\Gamma(l_1, i) \cap \Gamma(l_2, j) \neq \emptyset$ where $n_{l_1 \to l_2}$ depends only on l_1 and l_2. In addition, the graph distance traveled along the graph by passing from $\Gamma(l_1, i)$ to one such $\Gamma(l_2, j)$ is $D_{l_1}^{l_1 \to l_2}$ which also depends only on l_1 and l_2. The last two properties arise from the fact that we are supposing the graph to be a lattice.

4.2.1 Lieb-Robinson Bound

For Hamiltonians with two interaction types it was easy to calculate the Lieb-Robinson bound. This is because in order for a signal to propagate the two types of interactions

had to alternate in the operator chains which showed up in the bound. Therefore, we knew that half the operators were of one type of interaction while the other half were of the other type. For m types of interactions, different chains could have many different combinations of each type of operator, the only requirement being that each operator in the chain implements a different interaction than the previous operator. The intuition is then to consider all possible chains which are periodic in the interaction type and then bound all chains by the periodic sequence of operators which has the maximal norm. This will work because even if a chain is not periodic, it can be subdivided into components which are subchains of periodic chains.

Everything up to Eq.(4.11) does not depend on the number of interaction types. In the case of m interactions, Eq.(4.11) becomes

$$\|K_{a\ b}^{i_1\ j}(t)\| \leq M \sum_{n=0}^{\infty} \frac{|\ t\ |^n}{n!} \Big(\sum_{i_2 \in Z_{i_1}} 2h(i_2) \ldots \sum_{i_{n+1} \in Z_{i_n}} 2h(i_{n+1}) \delta_j^{i_n} \Big), \tag{4.37}$$

where $h(i_k) \in \{h_1, h_2, \ldots, h_m\}$ and of course $h(i_k) \neq h(i_{k+1})$. This situation is now more complicated than for two interactions because there is not necessarily the same number of each coupling constant in each term. The power of a particular coupling constant in a particular term depends on the operator chain and can range from anywhere from 0 to $\lceil n/2 \rceil$.

In Eq.(4.37) the end points of the chain are separated by at most a graph distance of $\sum_{k=1}^{n-1} D_{a(i_k)}^{a(i_k) \to a(i_{k+1})}$, where $a(i_k) \in \{1, 2, \ldots, m\}$ labels the operator type of i_k. Hence if $d(P, Q) > \sum_{k=1}^{n-1} D_{a(i_k)}^{a(i_k) \to a(i_{k+1})}$ the chain cannot link P to Q. As we did previously, we can bound $\|K_{a\ b}^{i_1\ j}(t)\|$ by multiplying every term in Eq.(4.37) by $\exp\Big(\lambda\big(\sum_{k=1}^{n-1} D_{a(i_k)}^{a(i_k) \to a(i_{k+1})} -$

$d(P,Q))\Big)$ which takes care of the endpoint condition (i.e. the $\delta_j^{i_n}$ factor in Eq.(4.37)). By doing this, it can be shown (see Appendix A for details) that the Lieb-Robinson bound takes the form

$$\|[O_P(t), O_Q(0)]\| \leq \tilde{M}(\lambda) \exp\Big(\lambda\big(\frac{2(m-1)L(\lambda)}{\lambda} \mid t \mid -d(P,Q)\big)\Big), \tag{4.38}$$

where λ is again an arbitrary positive number, $\tilde{M} < \infty$ for finite λ and

$$L(\lambda) \equiv \max_{2\leq r\leq m(m-1)} \max_{(a_1,a_2,\ldots,a_r)\in\{1,\ldots,m\}^r} \Big\{ k_{a_1\ldots a_r} e^{\lambda \xi_{a_1\ldots a_r}} | 1 \leq p < q \leq r, (a_p, a_{p+1}) \neq (a_q, a_{q+1}) \Big\}, \tag{4.39}$$

where

$$\begin{aligned} k_{a_1 a_2 \ldots a_q} &\equiv \sqrt[q]{\prod_{l=1}^{q} h_{a_l} n_{a_l \to a_{l+1}}}, \\ \xi_{a_1 a_2 \ldots a_q} &\equiv \frac{\sum_{l=1}^{q} D_{a_l}^{a_l \to a_{l+1}}}{q}, \end{aligned} \tag{4.40}$$

and where we assume $a_{r+1} \equiv a_1$. This implies a Lieb-Robinson speed of

$$v_{LR} = \inf_{\lambda>0} \frac{2(m-1)L(\lambda)}{\lambda}. \tag{4.41}$$

We can generalise this result to homogeneous and isotropic graphs using the same methods used in the previous sections. All that is needed is to redefine the k's and ξ's in Eq.(4.40). By the definition of a homogeneous and isotropic graph, the result of taking the arithmetic mean of the D's and the geometric mean of the n's over a chain will not

depend on the chain taken. In other words, if we let $Ch(P, x, l_1, l_2, \ldots, l_r)$ be the set of operator chains of x operators whose first operator's support intersects P and is of type l_1 and whose q^{th} operator is of type l_g where $g = [(q-1) \mod r] + 1$; we may define:

$$\begin{aligned}
\overline{n}_{l_1 l_2 \ldots l_r} &= \sqrt[|Ch(P,x,l_1,l_2,\ldots,l_r)|]{\prod_{i \in Ch(P,x,l_1,l_2,\ldots,l_r)} \prod_{k=1}^{r} n_{l_k \to l_{k+1}}^{i_{fr+k}}} \\
\overline{D}_{l_1 l_2 \ldots l_r} &= \frac{1}{|Ch(P, x, l_1, l_2, \ldots, l_r)|} \sum_{i \in Ch(P,x,l_1,l_2,\ldots,l_r)} \sum_{k=1}^{r} D_{l_k \to l_{k+1}}^{i_{fr+k} \to i_{fr+k+1}}.
\end{aligned} \tag{4.42}$$

We will now summarise our results for the Lieb-Robinson bound for a system of m interactions on a lattice or a homogeneous and isotropic (h&i) graph. The derivation was for bounded operators but we also state the result for commutator bounded systems which are discussed in [93]. To state all results concisely we define a constant C and state the forms of $k_{l_1 \ldots l_r}$ and $\xi_{l_1 \ldots l_r}$ for the different possible systems:

$$C = \begin{cases} 2(m-1) \end{cases} \tag{4.43}$$

$$k_{l_1 \ldots l_r} = \begin{cases} \sqrt[r]{\prod_{i=1}^{r} h_{l_i} n_{l_i \to l_{i+1}}} & \text{lattice,} \\ \sqrt[r]{\prod_{i=1}^{r} h_{l_i}} \overline{n}_{l_1 l_2 \ldots l_r} & \text{h\&i graph,} \end{cases} \tag{4.44}$$

$$\xi_{l_1 \ldots l_r} = \begin{cases} \frac{\sum_{i=1}^{r} D^{l_i \to l_{i+1}}}{r} & \text{lattice,} \\ \overline{D}_{l_1 \ldots l_r} & \text{h\&i graph.} \end{cases} \tag{4.45}$$

With these redefinitions, the general version of the Lieb-Robinson bound and speed are

$$\| [O_P(t), O_Q(0)] \| \leq \tilde{M}(\lambda) \exp\Big(\lambda\big(\frac{CL(\lambda)}{\lambda} \mid t \mid - d(P,Q)\big)\Big), \tag{4.46}$$

giving that

$$v_{LR} = \inf_{\lambda>0} \frac{CL(\lambda)}{\lambda}. \tag{4.47}$$

4.2.2 Calculating the Lieb-Robinson Speed

Using Eqs. (4.44), (4.45), and (4.47) we will calculate the Lieb-Robinson speed for a system of m interactions. If there are only two interactions labeled by 0 and 1 then the max is over a set containing only one element so we have

$$v_{LR} = C \inf_{\lambda>0} \left\{ \frac{k_{01}}{\lambda} e^{\xi_{01}\lambda} \right\} = Cek_{01}\xi_{01}, \tag{4.48}$$

which agrees with our previous result for systems with two interactions. For more than two interactions the max is taken over a set containing more than one element which brings about a qualitative difference: One obtains a different functional dependence on the strengths of the interactions (the h's) as well as the structure of the graph (the n's and D's) as compared to the algebraic dependence in the case of two interactions.

To calculate v_{LR} for more than two interactions we must take the maximum of a set of functions of the form $k_{i_1\ldots i_r} e^{\xi_{i_1\cdots i_r}\lambda}$. Since the maximal element of this set can change for different values of λ some care must be taken. In view of Eq.(4.47) we will divide these elements by λ since it won't change which element is maximal and we will call this set A. That is

$$A = \left\{ \frac{k_{i_1 \ldots i_r} e^{\xi_{i_1 \ldots i_r} \lambda}}{\lambda} \right\}, \tag{4.49}$$

for the different possible subchain labellings $i_1 \ldots i_r$ as given in Eq.(4.39). Further, we will define a function $A_{\max}(\lambda) = \max A$. Therefore

$$v_{LR} = C \inf_{\lambda > 0} A_{\max}(\lambda). \tag{4.50}$$

The element of A which has the largest value of k will be maximal for $\lambda \to 0$. The value of λ at which two elements of A intersect is given by $\frac{k_{l_1 \ldots l_r} e^{\xi_{l_1 \ldots l_r} \lambda}}{\lambda} = \frac{k_{j_1 \ldots j_s} e^{\xi_{j_1 \ldots j_s} \lambda}}{\lambda}$ and corresponds to the value

$$\lambda^{(l_1 \ldots l_t)}_{(j_1 \ldots j_s)} = \frac{\ln(k_{l_1 \ldots l_t}) - \ln(k_{j_1 \ldots j_s})}{\xi_{j_1 \ldots j_s} - \xi_{l_1 \ldots l_t}}. \tag{4.51}$$

Notice that for $\lambda^{(l_1 \ldots l_t)}_{(j_1 \ldots j_s)}$ to be positive we must have $\xi_{j_1 \ldots j_s} > \xi_{l_1 \ldots l_t}$ which is also the condition for the two curves to intersect. Now suppose that $k_{i_1 \ldots i_r}$ is the largest value of k of the elements in A and that $\lambda^{(j_1 \ldots j_s)}_{(i_1 \ldots i_r)}$ is the smallest intersection point involving this element. Next suppose that $\lambda^{(l_1 \ldots l_t)}_{(j_1 \ldots j_s)}$ is the smallest intersection point greater than $\lambda^{(j_1 \ldots j_s)}_{(i_1 \ldots i_r)}$ involving the element labeled by $j_1 \ldots j_s$. Continuing in this way the function $A_{\max}(\lambda)$ will be given by

$$A_{\max}(\lambda) = \begin{cases} \frac{k_{i_1\ldots i_r} e^{\xi_{i_1\ldots i_r}\lambda}}{\lambda}, & 0 < \lambda \leq \lambda^{(j_1\ldots j_s)}_{(i_1\ldots i_r)}, \\ \frac{k_{j_1\ldots j_s} e^{\xi_{j_1\ldots j_s}\lambda}}{\lambda}, & \lambda^{(j_1\ldots j_s)}_{(i_1\ldots i_r)} \leq \lambda \leq \lambda^{(l_1\ldots l_t)}_{(j_1\ldots j_s)}, \\ \vdots & \end{cases} \tag{4.52}$$

Since the function $\frac{k_{j_1\ldots j_s} e^{\xi_{j_1\ldots j_s}\lambda}}{\lambda}$ has only one minimum at $\lambda = 1/\xi_{j_1\ldots j_s}$ it follows that if $\lambda^{(j_1\ldots j_s)}_{(i_1\ldots i_r)} \leq 1/\xi_{j_1\ldots j_s} \leq \lambda^{(l_1\ldots l_t)}_{(j_1\ldots j_s)}$ for any one of the intervals then the infimum of $A_{\max}(\lambda)$ is given by $A(1/\xi_{j_1\ldots j_s})$. Otherwise, the infimum of $A_{\max}(\lambda)$ will be at one of the points $\lambda^{(l_1\ldots l_t)}_{(j_1\ldots j_s)}$. This completes the algorithm for finding the Lieb-Robinson speed v_{LR} for any finite number of interactions.

For concreteness we will work out some general scenarios for the case of three interactions. We will label the interactions by 1,2, and 3 in which case

$$A = \left\{ \frac{k_{12}e^{\xi_{12}\lambda}}{\lambda}, \frac{k_{23}e^{\xi_{23}\lambda}}{\lambda}, \frac{k_{31}e^{\xi_{31}\lambda}}{\lambda}, \frac{k_{123}e^{\xi_{123}\lambda}}{\lambda}, \frac{k_{132}e^{\xi_{132}\lambda}}{\lambda}, \right. \\ \left. \frac{k_{2131}e^{\xi_{2131}\lambda}}{\lambda}, \frac{k_{1232}e^{\xi_{1232}\lambda}}{\lambda}, \frac{k_{1323}e^{\xi_{1323}\lambda}}{\lambda}, \frac{k_{123132}e^{\xi_{123132}\lambda}}{\lambda} \right\}. \tag{4.53}$$

Note that we have only considered distinct elements of the set. For example, we did not consider $\frac{k_{231}e^{\xi_{231}\lambda}}{\lambda}$ because $\frac{k_{231}e^{\xi_{231}\lambda}}{\lambda} = \frac{k_{123}e^{\xi_{123}\lambda}}{\lambda}$.

There are two possible scenarios. The first is that one of the k's and its associated ξ are greater than all the other k's and ξ's. In that case, one element of A will be greater than all the others regardless of the value of λ and the Lieb-Robinson speed will be given by

minimising that particular element of A. If, for example k_{132} is greater or equal to all the other k's while simultaneously ξ_{132} is greater or equal to all the other ξ's, then $\frac{k_{132}e^{\xi_{132}\lambda}}{\lambda}$ will be the maximum element irrespective of λ and so we will have

$$\begin{aligned} v_{LR} &= C \inf_{\lambda>0} \frac{k_{132}e^{\xi_{132}\lambda}}{\lambda}, \\ &= Cek_{132}\xi_{132}. \end{aligned} \tag{4.54}$$

For a bounded system on a lattice $C = 2(m-1)$ and

$$k_{123} = \sqrt[3]{h_1h_2h_3}\sqrt[3]{n_{1\to3}n_{3\to2}n_{2\to1}}, \tag{4.55}$$

$$\xi_{123} = \frac{D^{1\to3} + D^{3\to2} + D^{2\to1}}{3}, \tag{4.56}$$

which allows us to solve for the Lieb-Robinson speed explicitly in terms of the coupling constants and lattice distances as

$$v_{LR} = \frac{4e}{3}\sqrt[3]{h_1h_2h_3}\sqrt[3]{n_{1\to3}n_{3\to2}n_{2\to1}}(D^{1\to3} + D^{3\to2} + D^{2\to1}). \tag{4.57}$$

In the second scenario, no single element of A is greater than all the others for all values of λ. Let us suppose, in that case, that we have $k_{12} > k_{23} > k_{123} > k_{31} > k_{132} > k_{1232} > k_{123132} > k_{2131} > k_{1323}$ and $\xi_{123} > \xi_{23} > \xi_{12} > \xi_{1323} > \xi_{2131} > \xi_{123132} > \xi_{1232} > \xi_{31} > \xi_{132}$.

inc. or dec.:		$\searrow$	$\searrow$	$\searrow$	$\searrow$	$\nearrow$	$\nearrow$	$\nearrow$
max term:		$\frac{k_{12}e^{\xi_{12}\lambda}}{\lambda}$	$\frac{k_{23}e^{\xi_{23}\lambda}}{\lambda}$			$\frac{k_{123}e^{\xi_{123}\lambda}}{\lambda}$		
λ :	0	$\lambda_{(12)}^{(23)}$	ξ_{123}^{-1}	$\lambda_{(12)}^{(123)}$	$\lambda_{(23)}^{(123)}$	ξ_{23}^{-1}	ξ_{12}^{-1}	

Table 4.1: This table shows that the minimal point of the function $A_{\max}(\lambda)$ is located at $\lambda = \lambda_{(23)}^{(123)}$. The top row indicates whether the function $A_{\max}(\lambda)$ is increasing or decreasing in the intervals of λ determined by the various critical points. The middle row indicates the maximal element of the set A while the bottom row is a scale for λ beginning at $\lambda = 0$. Also shown are ξ_{12}^{-1}, ξ_{23}^{-1}, and ξ_{123}^{-1} which are the minima of their respective elements in A. In this case they are not minima of $A_{\max}(\lambda)$ because they do not lie in the intervals for which their corresponding element of A is maximal.

With these assumptions one finds that

$$A_{\max}(\lambda) = \begin{cases} \frac{k_{12}e^{\xi_{12}\lambda}}{\lambda}, & 0 < \lambda \leq \lambda_{(12)}^{(23)}, \\ \frac{k_{23}e^{\xi_{23}\lambda}}{\lambda}, & \lambda_{(12)}^{(23)} \leq \lambda \leq \lambda_{(23)}^{(123)}, \\ \frac{k_{123}e^{\xi_{123}\lambda}}{\lambda}, & \lambda_{(23)}^{(123)} \leq \lambda \leq \ldots, \\ \vdots & \end{cases} \tag{4.58}$$

and also that ξ_{12}^{-1}, ξ_{23}^{-1}, and ξ_{123}^{-1} do not lie in the intervals of λ for which their corresponding element in A is maximal, i.e. none of these are the minimal point of $A_{\max}(\lambda)$.

In Table 4.1 we state the maximal element of A in the different relevant intervals of λ. We also indicate whether the function $A_{\max}(\lambda)$ is increasing or decreasing in each interval. From the table we see that the function $A_{\max}(\lambda)$ is minimised for $\lambda = \lambda_{(23)}^{(123)}$.

Thus we have

$$v_{LR} = C\frac{k_{23}e^{\xi_{23}\lambda_{(23)}^{(123)}}}{\lambda_{(23)}^{(123)}}. \tag{4.59}$$

For a bounded system on a lattice we have $C = 2(m-1)$ and

$$k_{23} = \sqrt{h_2 h_3}\sqrt{n_{2\to3}n_{3\to2}}, \tag{4.60}$$

$$\xi_{23} = \frac{D^{2\to3} + D^{3\to2}}{2}, \tag{4.61}$$

which allows us to solve for the Lieb-Robinson speed explicitly in terms of the coupling constants and lattice distances as

$$\begin{aligned} v_{LR} &= 2(m-1)\frac{(\xi_{123}-\xi_{23})}{\ln(k_{23})-\ln(k_{123})}k_{23}^{\frac{\xi_{123}}{\xi_{123}-\xi_{23}}}k_{123}^{\frac{\xi_{23}}{\xi_{23}-\xi_{123}}} \qquad (4.62)\\ &= 4^{\frac{[\frac{h_2+h_3}{2} - \frac{h_1+h_2+h_3}{3}] + [\frac{n_{2\to3}+n_{3\to2}}{2} - \frac{n_{1\to2}+n_{2\to3}+n_{3\to1}}{3}]}{\frac{D^{1\to2}+D^{2\to3}+D^{3\to1}}{3} - \frac{D^{2\to3}+D^{3\to2}}{2}}} \\ &\times \sqrt{h_2h_3n_{2\to3}n_{3\to2}}^{\frac{\frac{D^{1\to2}+D^{2\to3}+D^{3\to1}}{3}}{\frac{D^{1\to2}+D^{2\to3}+D^{3\to1}}{3} - \frac{D^{2\to3}+D^{3\to2}}{2}}} \\ &\times \sqrt[3]{h_1h_2h_3n_{1\to2}n_{2\to3}n_{3\to1}}^{\frac{\frac{D^{2\to3}+D^{3\to2}}{2}}{\frac{D^{2\to3}+D^{3\to2}}{2} - \frac{D^{1\to2}+D^{2\to3}+D^{3\to1}}{3}}}. \qquad (4.63) \end{aligned}$$

In general, when the minimum of $A_{\max}$ is attained at a minimum of one of the elements in A the Lieb-Robinson speed will be of the form of Eq.(4.54). When the minimum of $A_{\max}$ occurs at the point where two elements of A are equal, the Lieb-Robinson speed will be of

the form of Eq.(4.62). Thus the Lieb-Robinson speed will always be of one of the two forms

$$v_{LR}^{s}(k,\xi) = 2ce(m-1)k\xi \tag{4.64}$$

or

$$v_{LR}^{d}(k_1,k_2,\xi_1,\xi_2) = 2c(m-1)\frac{(\xi_1-\xi_2)k_1^{\frac{\xi_2}{\xi_2-\xi_1}}k_2^{\frac{\xi_1}{\xi_1-\xi_2}}}{\ln(k_2)-\ln(k_1)}, \tag{4.65}$$

where $c = 1$ for bounded systems and $c = \sqrt{2}$ for commutator-bounded systems. This is true also for any $m \geq 3$ since adding more interactions merely increases the number of elements of A. Now that we have seen how to calculate the Lieb-Robinson speed for any number of interactions, let us consider a physical example.

4.2.3 Example: XY-Model

We investigate the anisotropic quantum XY-model on a 2-dimensional square lattice. This model is well understood and is studied mainly in connection with quantum phase transitions. This model is also of practical interest for example in understanding the isolator-superconductor phase transition in cuprate type II superconductors [100]. At zero temperature the system exhibits two phases, one with an energy gap and another which is gapless.

The Hamiltonian for the quantum XY-model is given by

$$H = J\sum_{\langle n,m\rangle}(S_n^xS_m^x + S_n^yS_m^y) + D\sum_n (S_n^z)^2, \tag{4.66}$$

where $\langle n, m \rangle$ represents the sum over nearest neighbours on the sites, n, of a square lattice. Note that the gapless and gapped phases are determined by $\delta < \delta_c$ and $\delta > \delta_c$ respectively where $\delta = \frac{D}{2J}$ and where δ_c has been estimated to be approximately 3.6 [91]. For $\delta > \delta_c$ the correlation length of the system approaches a finite value leading to a quantum paramagnetic ground state with no long range order. We label the $S^x S^x$, $S^y S^y$ and S^z operator types by X, Y, and Z respectively[2].

Since the k's and ξ's are symmetric under cyclic permutations as well as the interchange of X and Y the set A will have only four distinct elements

$$A = \left\{ \frac{k_{XY} e^{\lambda \xi_{XY}}}{\lambda}, \frac{k_{XZ} e^{\lambda \xi_{XZ}}}{\lambda}, \frac{k_{XYZ} e^{\lambda \xi_{XYZ}}}{\lambda}, \frac{k_{XYZY} e^{\lambda \xi_{XYZY}}}{\lambda} \right\}. \tag{4.67}$$

Note that $XZYZ = XZ$ and $XYZXZY = XYZ$ by breaking the larger chains in two and using the symmetries.

The operators X and Y are located on edges of the graph whereas the operators of type Z are located on the plaquettes. Moving from a plaquette to an edge corresponds to moving a lattice distance of $1/2$ while moving from a plaquette to another plaquette corresponds to moving a lattice distance of 1. Therefore

[2]Note that even though $S_n^x S_m^x$ and $S_n^y S_m^y$ have the same coupling constant, we must nevertheless consider them as two separate interactions because otherwise the conditions laid out in between Eq.(4.2) and Eq.(4.3) would not be satisfied.

$$D_{X\to Z} = D_{Y\to Z} = 1/2, \tag{4.68}$$

$$D_{X\to Y} = 1. \tag{4.69}$$

Note that these distances are symmetric. Furthermore, from an edge one can move to one of two plaquettes or one of 7 other edges (including the one currently on). From a plaquette one can move to one of four edges. Therefore,

$$n_{X\to Z} = n_{Y\to Z} = 2, \tag{4.70}$$

$$n_{Z\to X} = n_{Z\to Y} = 4, \tag{4.71}$$

$$n_{X\to Y} = n_{Y\to X} = 7. \tag{4.72}$$

Using this information and the coupling constants $h_X = J$, $h_Y = J$, and $h_Z = D$ in Eqs. (4.44) and (4.45) we get

$$\begin{aligned} k_{XY} &= 7JS, & \xi_{XY} &= 1, \\ k_{XZ} &= \sqrt{8JD}S, & \xi_{XZ} &= \frac{1}{2}, \\ k_{XYZ} &= \sqrt[3]{7\cdot 8J^2D}S, & \xi_{XYZ} &= \frac{2}{3}, \\ k_{XYZY} &= \sqrt[4]{7^2\cdot 8J^3D}S, & \xi_{XYZY} &= \frac{3}{4}, \end{aligned} \tag{4.73}$$

where S is a half integer giving us the type of spins on the lattice. From Eq.(4.51), we obtain

$$\lambda_{(XZ)}^{(XY)} = \lambda_{(XYZ)}^{(XY)} = \lambda_{(XYZY)}^{(XY)} = \lambda_{(XZ)}^{(XYZ)} = \lambda_{(XZ)}^{(XYZY)} = \lambda_{(XYZ)}^{(XYZY)} = 2\ln(4/7) + \ln\left(\frac{D}{2J}\right). \tag{4.74}$$

This implies that all of the elements of A intersect at the same value of λ. First note that this value is negative for $D/2J < (7/4)^2$ and thus the curves do not intersect. In this case, $\frac{k_{XY}e^{\lambda\xi_{XY}}}{\lambda}$ is maximal for all λ and so the Lieb-Robinson speed is

$$\begin{aligned} v_{LR} &= 2e(m-1)k_{XY}\xi_{XY}, \\ &= 28eJS. \end{aligned} \tag{4.75}$$

For $D/2J > (7/4)^2$ we have

$$A_{\max}(\lambda) = \begin{cases} \frac{k_{XY}e^{\xi_{XY}\lambda}}{\lambda}, & 0 < \lambda \leq \lambda_{(XY)}^{(XZ)}, \\ \frac{k_{XZ}e^{\xi_{XZ}\lambda}}{\lambda}, & \lambda_{(XY)}^{(XZ)} \leq \lambda \leq \infty. \end{cases} \tag{4.76}$$

First let us consider the cases when the minima occur within the intervals. The minimum occurs in the first interval when $0 < \xi_{XY}^{-1} \leq \lambda_{(XY)}^{(XZ)}$ which corresponds to $(7/4)^2 < D/2J < e(7/4)^2$ and gives the same speed as for $D/2J < (7/4)^2$. The second interval contains the minimum when $\lambda_{(XY)}^{(XZ)} < \xi_{XZ}^{-1} \leq \infty$ which occurs for $D/2J > e^2(7/4)^2$. In this case the

minimum value is $A_{\max}(\xi_{XZ}^{-1})$ and gives a Lieb-Robinson speed of

$$\begin{aligned} v_{LR} &= 2e(m-1)k_{XZ}\xi_{XZ}, \\ &= 4e\sqrt{2JD}S. \end{aligned} \tag{4.77}$$

Finally, in the region $e(7/4)^2 < D/2J < e^2(7/4)^2$ the minimum occurs for $\lambda = \lambda_{(XY)}^{(XZ)}$ and so

$$\begin{aligned} v_{LR} &= 2(m-1)\frac{k_{XY}e^{\xi_{XY}\lambda_{(XY)}^{(XZ)}}}{\lambda_{(XY)}^{(XZ)}}, \\ &= \frac{32}{7}\frac{DS}{2\ln(4/7)+\ln(D/2J)}. \end{aligned} \tag{4.78}$$

The results and the various conditions are summarised in Table (4.2). The first column gives the Lieb-Robinson speed in the region of phase space defined by the inequalities of the third column. By phase space we simply mean the space $\mathbb{R}_+^2$ of all possible values of the coupling constants J and D. The different values of the Lieb-Robinson speed in the different regions of the phase space are plotted in Fig. 4.2. In general, the number of functional forms for the Lieb-Robinson speed could be as many as twice the number of distinct intersection points obtained in Eq.(4.74) plus one, i.e. the minimum could occur at each intersection point or in each interval.

Also plotted in Fig. 4.2 is the critical line for the quantum phase transition (dotted line) which occurs for $\frac{D}{2J} \approx 3.6$. It is important to remember that the regions of phase space with different Lieb-Robinson speeds do not correspond to different quantum phases.

v_{LR}	Conditions	Simplified Cond.
$v^s_{LR}(k_{XZ},\xi_{XZ})$ $= 4e\sqrt{2JDS}$	$\lambda^{(XY)}_{(XZ)} \geq \xi^{-1}_{XZ}$ $\lambda^{(XYZ)}_{(XZ)} \geq \xi^{-1}_{XZ}$ $\lambda^{(XYZY)}_{(XZ)} \geq \xi^{-1}_{XZ}$	$\frac{D}{2J} \geq \left(\frac{7}{4}\right)^2 e^2$
$v^d_{LR}(k_{XZ},k_{XY},$ $\xi_{XZ},\xi_{XY})$ $= \frac{32}{7}\frac{DS}{2\ln(\frac{4}{7})+\ln\left(\frac{D}{2J}\right)}$	$\xi^{-1}_{XY} \leq \lambda^{(XY)}_{(XZ)}$ $\lambda^{(XY)}_{(XZ)} \leq \xi^{-1}_{XZ}$ $\lambda^{(XY)}_{(XYZY)} \leq \lambda^{(XY)}_{(XZ)}$ $\lambda^{(XY)}_{(XYZ)} \leq \lambda^{(XY)}_{(XZ)}$	$\left(\frac{7}{4}\right)^2 e \leq \frac{D}{2J} \leq \left(\frac{7}{4}\right)^2 e^2$
$v^s_{LR}(k_{XY},\xi_{XY})$ $= 28eJS$	$\lambda^{(XY)}_{(XYZ)} \leq \xi^{-1}_{XY}$ $\lambda^{(XY)}_{(XZ)} \leq \xi^{-1}_{XY}$ $\lambda^{(XY)}_{(XYZY)} \leq \xi^{-1}_{XY}$	$\frac{D}{2J} \leq \left(\frac{7}{4}\right)^2 e$

Table 4.2: The Lieb-Robinson speed for the XY-model. The first column gives the functional form of the Lieb-Robinson speed in terms of the interaction strengths. The second column gives the region of applicability of each of the six functional forms of the Lieb-Robinson speed in terms of the λ's and ξ's. The last column gives the regions in terms conditions of the interaction strengths. The results of this table are depicted graphically in Fig. 4.2.

Quantum phases occur in the ground state at a particular point of the phase space whereas the Lieb-Robinson speed is the maximum speed of any signals in any state and not just small excitations over the ground state.

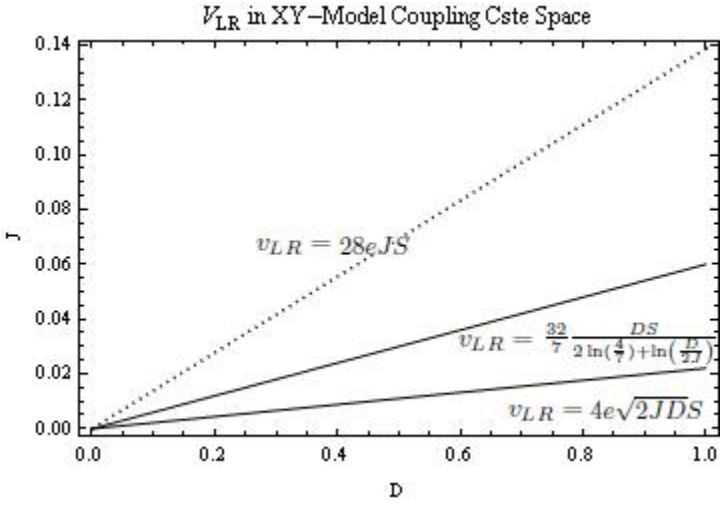

Figure 4.2: The (D,J)-plane of the XY-Model and the three different formulas for the Lieb-Robinson speed: if $\frac{D}{2J} \geq \left(\frac{7}{4}\right)^2 e^2$ then the Lieb-Robinson speed is $4e\sqrt{2JD}S$, if $\left(\frac{7}{4}\right)^2 e \leq \frac{D}{2J} \leq \left(\frac{7}{4}\right)^2 e^2$ then the Lieb-Robinson speed is $\frac{32}{7}\frac{DS}{2\ln(\frac{4}{7})+\ln\left(\frac{D}{2J}\right)}$ and finally if $\frac{D}{2J} \leq \left(\frac{7}{4}\right)^2 e$ the Lieb-Robinson speed is $28eJS$. The dotted line indicates the critical line for the phase transition which runs along the line $\frac{D}{2J} = 3.6$

Chapter 5

Lieb-Robinson Bound for Unbounded Operators

In this chapter, which is a modified version [93], we will show how one can find a bound to the maximum speed of interactions in the case of a class of unbounded spin Hamiltonians. Here we want to show that one can derive a Lieb-Robinson bound if the Hamiltonian is the sum of local operators, *whose commutators are bounded*. Therefore, there is no necessity for even the non-local terms to be bounded, as long as their commutators are.

More specifically, we suppose the following: The Hilbert space of the quantum system is the tensor product of local Hilbert spaces associated to vertices and edges of a graph. The Hamiltonian is the sum of local operators Φ_i, each with a support on a region of the graph with diameter less then a fixed number R. Each of the local operators Φ_i of the Hamiltonian is non-commuting with less than ν other local operator terms of the Hamiltonian Φ_j. For any two of these operators we have $\|[\Phi_i, \Phi_j]\| < K$ and for any three operators $\|[\Phi_i, [\Phi_j, \Phi_k]]\| < Q$ for two positive numbers K and Q.

Supposing all this we then have that for any two local operators Φ_i and Φ_j which are terms in the Hamiltonian and whose support is separated by a graph distance d, that

$$\|[\Phi_i(t), \Phi_j(0)]\| \leq \tilde{\tilde{M}} \exp\Big(\lambda\left(v_{LR}t - d\right)\Big), \tag{5.1}$$

where $\tilde{\tilde{M}}$ is a constant and v_{LR}, the limit on the speed of propagation of information, depends only on local operators of the Hamiltonian as it is they who effect the propagation. This bound can be generalised to any local observables O_P and O_Q with supports P and Q respectively, that satisfy the following local observable operator conditions: $i)$ the graph distance d separating P and Q is greater than R $ii)$ the number of terms Φ_i of the Hamiltonian whose support has non-empty intersection with P is $n_P < \infty$ $iii)$ there exists F_P and F_Q such that for all terms Φ_i and Φ_j of the Hamiltonian the inequalities $\|[O_P, \Phi_i]\| < F_P K$, $\|[O_Q, \Phi_i]\| < F_Q K$ and $\|[O_Q, [\Phi_i, \Phi_j]]\| < F_Q Q$ are satisfied. The generalised bound is then:

$$\|[O_P(t), O_Q(0)]\| \leq \tilde{\tilde{M}} F_P F_Q n_P (n_P + 1) \exp\Big(\lambda\left(v_{LR}t - d\right)\Big). \tag{5.2}$$

To motivate our discussion let us start by the most trivial example: Consider the case of a Hamiltonian $H = \sum h_i$ which is composed of a sum of local terms h_i which are commuting, such as the quantum Ising model without transverse field. In such a case there is simply no propagation of signals: indeed, for any local operator O_A we have: $O_A(t) = e^{itH} O_A e^{-iHt} = e^{itH_A} O_A e^{-iH_A t}$ where $H_A = \sum_{i:[h_i, O_A]\neq 0} h_i$, since there is a finite number of h_i in H_A, and they are of finite range, $O_A(t)$ is also strictly local for arbitrary long times t, and irrespective of the norm of the h_i operators. This suggests that it is desirable to

find Lieb-Robinson bounds in terms of the norm of the commutators rather than the norm of the local terms h_i.

Let us outline a simple example of a commutator bounded system satisfying the conditions we just outlined. Consider a system of parallel quantum wires. We place fermions on the wires. These are usually described by what are called one dimensional Luttinger liquids, and have approximately a linear dispersion relation. We place a density-density interaction between the wires. Labeling the wires by the index j, Luttinger liquids are described by the following Hamiltonian:

$$H_{wires} = \sum_j \left(-i\frac{\partial}{\partial x_j} + V(x_j - x_{j+1}) \right), \tag{5.3}$$

which is commutator bounded in the sense of this chapter as long as both $|\partial_{x_j} V|$ and $|\partial_{x_i}\partial_{x_j} V|$ are bounded. Another example involves a generalised Dicke model, describing an array of spins interacting with a boson field via

$$H = \sum h_n \quad ; \quad h_n = \sigma_n^z (b_n^\dagger + b_n + i b_{n+1}^\dagger - i b_{n+1}) \tag{5.4}$$

where b_n are boson creation operators and σ_n^z is the nth spin. It is easy to check that in this case the commutator $[h_n, h_{n+1}] = -2i\sigma_n^z \sigma_{n+1}^z$ is bounded. (In fact, this particular hamiltonian can also be written as a sum of commuting terms $\tilde{h}_n = b_n(\sigma_n^z - i\sigma_{n-1}^z) + h.c.$)

We consider Hamiltonians that are the sum of two different types of operators Φ_0 and

Φ_1 :

$$H \equiv \sum_{i \in S_0} h_0 \Phi_0^i + \sum_{j \in S_1} h_1 \Phi_1^j. \tag{5.5}$$

Here S_0, S_1 are two sets of labels and h_0 and h_1 are two coupling constants and $[\Phi_0^i, \Phi_0^j] = [\Phi_1^i, \Phi_1^j] = 0$ for every i, j. As an example, consider the Ising model. Then $\Phi_0^i = \sigma_i^x \sigma_{i+1}^x$ and $\Phi_1^i = \sigma_i^z$. We call the subgraph which is the support of the operator $\Phi_q^m,\ \Gamma(q,m)$ and for $(a,b) \in \{0,1\}^2$, we define

$$K_{a\ b}^{i\ j}(t) \equiv [\Phi_a^i(t), \Phi_b^j]. \tag{5.6}$$

We consider what we will refer to as commutator bounded R-local quantum systems. For such systems the commutators and the commutators of commutators of operators of the Hamiltonian are uniformly bounded while the operators themselves may be unbounded and the operators of the Hamiltonian have support on subgraphs of size less than R, for R an arbitrary natural number. Explicitly, the diameter of all $\Gamma(q,m)$ is less than R and for any three operators Φ_a^i, Φ_b^j and Φ_c^kappearing in the Hamiltonian with the coupling constants h_a, h_b and h_c we have that $h_a h_b \|[\Phi_a^i, \Phi_b^j]\| < K$ and $h_a h_b h_c \|[[\Phi_a^i, \Phi_b^j], \Phi_c^k]\| < Q$ where K and Q are positive real numbers. Note that a bounded system which is uniformly bounded by $\tilde{K}$ must satisfy $K \leq 2\tilde{K}^2$ as well as $Q \leq 4\tilde{K}^3$ and thus boundedness implies commutator-boundedness.

Taking the derivative of Eq.(5.6) with respect to t we obtain $(K_{a\ b}^{i_1\ j}(t))' = [[-iH(t), \Phi_a^i(t)], \Phi_b^j]$, after keep only the terms in $H(t)$ which do not commute with $\Phi_a^i(t)$ and after some algebra,

we get (here and in the following by $a+1$ we mean $a+1\ mod(2)$)

$$(K_{a\ b}^{i_1\ j}(t))' = [K_{a\ b}^{i_1\ j}(t), \Big(-ih_{a+1} \sum_{i_2 \in Z_{i_1}} \Phi_{a+1}^{i_2}(t) \Big)] + (-ih_{a+1}) \sum_{i_2 \in Z_{i_1}} [\Phi_a^{i_1}(t), [\Phi_{a+1}^{i_2}(t), \Phi_b^j]], \quad (5.7)$$

where if $i \in S_0$, then Z_i is the finite subset of S_1 such that $j \in Z_i \Leftrightarrow \Gamma(0,i) \bigcap \Gamma(1,j) \neq \emptyset$ and vise-versa for $i \in S_1$.

Taking the second derivative, and using the fact that $[\Phi_a^i(t), \Phi_a^j(t)] = 0$ we obtain, after some algebraic manipulation,

$$\begin{aligned} K_{a\ b}^{i_1\ j}{}''(t) = \quad & -i[K_{a\ b}^{i_1\ j}{}'(t), \sum_{j_2 \in Z_{i_1}} h_{a+1} \Phi_{a+1}^{j_2}(t) + \sum_{i_3 \in Z_{i_2}} h_a \Phi_a^{i_3}(t)] \\ & -h_{a+1}^2 \sum_{j_2 \in Z_{i_1}} \sum_{i_2 \in Z_{i_1}} [[\Phi_a^{i_1}(t), \Phi_{a+1}^{i_2}(t)], [\Phi_{a+1}^{j_2}(t), \Phi_b^j]] \\ & -h_a h_{a+1} \sum_{i_2 \in Z_{i_1}} \sum_{i_3 \in Z_{i_2}} [[\Phi_a^{i_1}(t), \Phi_{a+1}^{i_2}(t)], [\Phi_a^{i_3}(t), \Phi_b^j]]. \end{aligned} \quad (5.8)$$

Defining the following unitary operator $U_{2+3}(t) \equiv e^{-it\Big(\sum_{j_2 \in Z_{i_1}} h_{a+1} \Phi_{a+1}^{j_2}(t) + \sum_{i_3 \in Z_{i_2}} h_a \Phi_a^{i_3}(t)\Big)}$ and its associated unitary evolution $T_{2+3}(t)O \equiv U_{2+3}(t)^\dagger O U_{2+3}(t)$, integrating Eq.(5.8) and taking the norm we obtain, after some manipulations:

$$\begin{aligned} \|K_{a\ b}^{i_1\ j}{}'(t)\| \leq \quad & h_{a+1} \sum_{i_2 \in Z_{i_1}} \|[[\Phi_a^{i_1}, \Phi_{a+1}^{i_2}], \Phi_b^j]\| \\ + \int_0^t ds \Bigg(& 2h_{a+1}^2 K \sum_{j_2 \in Z_{i_1}} \sum_{i_2 \in Z_{i_1}} \|[\Phi_{a+1}^{j_2}(s), \Phi_b^j]\| + 2h_a h_{a+1} K \sum_{i_2 \in Z_{i_1}} \sum_{i_3 \in Z_{i_2}} \|[\Phi_a^{i_3}(s), \Phi_b^j]\| \Bigg) \end{aligned} \quad (5.9)$$

where we used the fact that $\|[\Phi_a^i(t), \Phi_{a+1}^j(t)]\| \leq K$. By integrating Eq.(5.9) we get

$$\|K_{ab}^{i_1 j}(t)\| \leq \|[\Phi_a^{i_1}, \Phi_b^j]\| + h_{a+1} \sum_{i_2 \in Z_{i_1}} \|[[\Phi_a^{i_1}, \Phi_{a+1}^{i_2}], \Phi_b^j]\| t$$
$$+ \int_0^t ds \int_0^s dl \left(2h_{a+1}^2 K \sum_{i_2 \in Z_{i_1}} \sum_{j_2 \in Z_{i_1}} \|K_{a+1b}^{j_2 j}(l)\| + 2h_a h_{a+1} K \sum_{i_2 \in Z_{i_1}} \sum_{i_3 \in Z_{i_2}} \|K_{ab}^{i_3 j}(l)\| \right). \tag{5.10}$$

Since the commutators are bounded we have $\|[\Phi_a^{i_1}, \Phi_b^j]\| \leq K$ and $\|[[\Phi_a^{i_1}, \Phi_{a+1}^{i_2}], \Phi_b^j]\| \leq Q$ for some $K, Q > 0$. Noting that $\|[\Phi_a^{i_1}, \Phi_b^j]\| = 0$ if $\Gamma(a, i_1)$ and $\Gamma(b, j)$ do not overlap and $\|[[\Phi_a^{i_1}, \Phi_{a+1}^{i_2}], \Phi_b^j]\| = 0$ if $\Gamma(b, j)$ does not overlap with either $\Gamma(a, i_1)$ or $\Gamma(a+1, i_2)$ we see that Eq.(5.10) implies

$$\|K_{ab}^{i_1 j}(t)\| \leq K\delta_{i_1}^j + \sum_{i_2 \in Z_{i_1}} h_{a+1} Q \delta_{i_1 \cup i_2}^j t +$$
$$\int_0^t ds \int_0^s dl \left(2h_{a+1}^2 \sum_{j_2 \in Z_{i_1}} \sum_{i_2 \in Z_{i_1}} \|K_{a+1b}^{j_2 j}(l)\| + 2h_a h_{a+1} \sum_{i_2 \in Z_{i_1}} \sum_{i_3 \in Z_{i_2}} \|K_{ab}^{i_3 j}(l)\| \right), \tag{5.11}$$

where we have used the following symbol

$$\delta_i^k := \begin{cases} 1 & \text{if } \Gamma(a_i, i) \cap \Gamma(a_k, k) \neq \emptyset, \\ 0 & \text{otherwise}, \end{cases} \tag{5.12}$$

Solving for $\|K_{ab}^{i_1 j}(t)\|$, we find

$$\begin{aligned}
\|K_{ab}^{i_1 j}(t)\| \leq\ & K\delta_{i_1}^{j} + \sum_{i_2 \in Z_{i_1}} Q h_{a+1} \delta_{i_1 \cup i_2}^{j} t + \sum_{j_2 \in Z_{i_1}} \sum_{i_2 \in Z_{i_1}} 2h_{a+1}^2 K \delta_{j_2}^{j} \frac{t^2}{2!} \\
& + \sum_{i_2 \in Z_{i_1}} \sum_{i_3 \in Z_{i_2}} 2h_a h_{a+1} K \delta_{i_3}^{j} \frac{t^2}{2!} \\
& + \sum_{j_2 \in Z_{i_1}} \sum_{i_2 \in Z_{i_1}} \sum_{i_3 \in Z_{j_2}} 2h_{a+1}^2 h_a K Q \delta_{j_2 \cup i_3}^{j} \frac{t^3}{3!} \\
& + \sum_{i_2 \in Z_{i_1}} \sum_{i_3 \in Z_{i_2}} \sum_{i_4 \in Z_{i_3}} 2h_{a+1} h_a^2 K Q \delta_{i_3 \cup i_4}^{j} \frac{t^3}{3!} \\
& + \int_0^t dv \int_0^v du \int_0^u ds \int_0^s dl \Bigg((2h_{a+1}h_a)^2 K^2 \sum_{i_2 \in Z_{i_1}} \sum_{j_2 \in Z_{i_1}} \sum_{i_3 \in Z_{j_2}} \sum_{j_3 \in Z_{j_2}} \|K_{ab}^{j_3 j}(l)\| \\
& + (2h_{a+1}^2)(2h_{a+1}h_a) K^2 \sum_{i_2 \in Z_{i_1}} \sum_{j_2 \in Z_{i_1}} \sum_{i_3 \in Z_{j_2}} \sum_{i_4 \in Z_{i_4}} \|K_{a+1b}^{j_4 j}(l)\| \\
& + (2h_{a+1}h_a)^2 K^2 \sum_{i_2 \in Z_{i_1}} \sum_{i_2 \in Z_{i_1}} \sum_{i_3 \in Z_{i_2}} \sum_{i_4 \in Z_{i_3}} \|K_{a+1b}^{i_4 j}(l)\| \\
& + (2h_a^2)(2h_{a+1}h_a) K^2 \sum_{i_2 \in Z_{i_1}} \sum_{i_3 \in Z_{i_2}} \sum_{i_3 \in Z_{1_2}} \sum_{j_3 \in Z_{i_2}} \|K_{ab}^{j_3 j}(l)\| \Bigg).
\end{aligned} \tag{5.13}$$

Iterating this procedure we obtain by induction

$$\|K_{ab}^{i_1 j}(t)\| \leq M \sum_{n=0}^{\infty} \sqrt{2h_0 h_1 K}^{n} \frac{|\ t\ |^n}{n!} c_n, \tag{5.14}$$

where $M = \sqrt{2} \max\{\frac{h_0}{h_1}, \frac{h_1}{h_0}\} \times \max\{\frac{1}{K}, 1\} \times \max\{\frac{\sqrt{K}}{Q}, 1\}$ and where c_n is a combinatorial factor counting the number of linking operator chains of n operators between $\Gamma(a, i_1)$ and $\Gamma(b, j)$. What we call an operator chain is heuristically a sequence of intersecting operators linking the initial and final operators. The process of constructing the sequence of operators forming the chain is as follows: the $2j^{th}$ operator in the chain has to be non-

commuting with the $(2j-1)^{th}$ one. This imposes that the two consecutive operators of a chain have to: 1) be of a different interaction type and 2) have overlapping support. For the odd-numbered operators there is an extra choice: the $(2k+1)^{th}$ operator can be an operator that does not commute with the $2k^{th}$ operator (as for the even case) *or* an operator that does not commute with the $(2k-1)^{th}$ operator. That is, even operators in the sequence must be non-commuting with the previous operator in the sequence and odd operators in the sequence must be non-commuting with either of the two previous operators in the sequence. From the recursive Eq.(5.11) we see that if we start with an operator i_1 of type a, the next operator in the chain must be an operator $i_2 \in Z_{i_1}$ of the other type $(a+1)$. The fact that it is in Z_{i_1} means that its support overlaps with i_1's, which is similar to what was found in the bounded case. However if we look at the operator that comes after i_2, we see that we have two distinct possibilities. The first (second double sum under the integrals of Eq.(5.11)) is that it can be $i_3 \in Z_{i_2}$ an operator of type a (different than $a+1$) whose support overlaps with i_2's. If this were the only possibility, we would have exactly the same situation as we had for bounded systems. However, the first double sum under the integrals of Eq.(5.11) adds another possibility. That second possibility (first double sum) is choosing an operator $j_2 \in Z_{i_1}$ after the operator i_2. j_2 is, like i_2, an operator of type $a+1$ which (by virtue of being in Z_{i_1}) has a support that overlaps i_1's support. To find the next operator after that, we reiterate Eq.(5.11). Hence, like the first operator after i_1 we need to choose an operator which is of a different type than the last one (be it j_2 or i_3), and has overlapping support with the last one; thus, at this point, we can not "change our mind". We can thus see the process of building the chain as every two choices we must choose an operator that links with the previous one, but for every other choice we can also choose an

operator that links to the penultimate one instead.

Because for every two choices in building up the chain we must choose an operator of a different type than the previous one, in the end, the chain contains the same number of operators of type 0 as of type 1 (plus or minus one). This means that there will be the same number of factors of h_1 as of h_0 in every term. Hence we can pull them out of the sums over chains and simply write an overall factor of $\sqrt{h_0 h_1}$ in front while passing from Eq.(5.13) to Eq.(5.14).

Furthermore, as mentioned previously, we can always find a bound of the following type for c_n

$$c_n \leq \tilde{M}\gamma^n e^{\lambda(\frac{n}{\xi}-d)}, \tag{5.15}$$

where λ is an arbitrary positive real number. This is because the $\Gamma(a,i)$'s have a diameter of R or less. Hence, if the distance d, between the initial and final points, is greater than R^n, then there are no possible linking operator chains of n local operators between the initial and final point. Furthermore, since at every odd step along the chain there is a choice of at most ν local operators to choose from for the next operator in the chain and at every even step there is at maximum 2ν operators to choose from, there is a maximum of $(\sqrt{2}\nu)^n$ possible local operator chains of n operators starting from any given position. Thus, we certainly have that

$$c_n \leq \sqrt{2}^n \nu^n e^{\lambda(Rn-d)}, \tag{5.16}$$

where λ is arbitrary. Using Eq.(5.15) with Eq.(5.14), we obtain the Lieb-Robinson bound Eq.(5.1):

$$\|[\Phi_a^i(t), \Phi_b^j(0)]\| \leq \tilde{\tilde{M}} \exp \lambda \left(2\sqrt{h_0 h_1 K}\frac{\gamma}{\lambda} e^{\frac{\lambda}{\xi}} t - d\right) \tag{5.17}$$

where $\tilde{\tilde{M}} = \tilde{M}M$. To obtain the generalisation to local operators O_P and O_Q satisfying the local observable operator conditions enounced in the introduction, we introduce $\tilde{K}_a^{i_1}(t) \equiv [\Phi_a^i(t), O_Q(0)]$. Using exactly the same procedure used to obtain Eq.(5.9), we get

$$\begin{aligned}
&\|[O_P(t), O_Q(0)]'(t)\| \leq \\
&\int_0^t ds \left(2h_b h_a K F_P \sum_{j_2 \in Z_P} \sum_{i_2 \in Z_P} \|\tilde{K}_b^{j_2}(s)\| \right. \\
&\left. + 2h_a h_{a+1} K F_P \sum_{i_2 \in Z_P} \sum_{i_3 \in Z_{i_2}} \|\tilde{K}_a^{i_3}(s)\| \right) \\
&\leq 2\max\{h_0^2, h_1^2\} n_P (n_P + 1) \int_0^t ds \|\tilde{K}_a^k(s)\|,
\end{aligned} \tag{5.18}$$

where Z_P is the set of of labels of the terms of the Hamiltonian which do not commute with O_P ($\|Z_P\| = n_P$), where k is such that $\int_0^t ds \|\tilde{K}_a^k(s)\| = \max_{i \in Z_P} \int_0^t ds \|\tilde{K}_a^i(s)\|$ and where unlike in Eq.(5.9), the terms containing no integrals do not appear here because of the condition that $d > R$. $\|\tilde{K}_a^k(s)\|$ can then be treated in exactly the same way as $\|K_{ab}^{i_1 j}(s)\|$ was, with the only exception that while bounding the final commutators (i.e. when we place the δ of Eq.(5.12)), we will need an extra factor of F_Q. Thus we obtain Eq.(5.2):

$$\|[O_P(t), O_Q(0)]\| \leq F_P F_Q n_P (n_P + 1) \tilde{\tilde{M}} \exp \lambda \left(2\sqrt{h_0 h_1 K}\frac{\gamma}{\lambda} e^{\frac{\lambda}{\xi}} t - d\right). \tag{5.19}$$

Optimising for λ, the Lieb-Robinson speed is thus:

$$v_{LR} = 2\frac{\gamma}{\xi} e \sqrt{h_0 h_1 K}. \tag{5.20}$$

We can compare Eq.(5.19) this with the bound obtained for Hamiltonians composed of bounded local operators and for bounded local observable O_P and O_Q which is [42]:

$$\|[O_P(t), O_Q(0)]\| \leq \|O_P\| \|O_Q\| n_P \tilde{\tilde{M}} \exp \lambda \left(2\sqrt{h_0 h_1} \frac{\gamma}{\lambda} e^{\frac{\lambda}{\xi}} t - d \right). \tag{5.21}$$

Thus, we have shown that a Lieb-Robinson bound exists for those Hamiltonians that are the sum of local operators whose commutator is bounded. This allows to treat a class of systems with unbounded operators.

Chapter 6

General Results

Now that we have generalised the Lieb-Robinson bound to a class of commutator-bounded systems with two interactions, we see that we can easily generalise the bound to the case of multiple interactions by a slight modification of Eq.(4.43,4.44,4.45). Thus, our final results are the following:

Take an R-Local quantum system with m interaction types such that each local operator Φ_i^l of the Hamiltonian is non-commuting with less than a finite integer ν other local operators of the Hamiltonian. We suppose that the local operators of the Hamiltonian satisfy one of the following criteria:

- Uniform boundedness: $\exists K > 0$ such that for all local operators of the Hamiltonian we have $\|\Phi_i^l\| < K$

  or

- Commutator boundedness: $\exists K > 0$ and $Q > 0$ such that for all triples of local operators $\Phi_i^a, \Phi_j^b, \Phi_k^c$ we have $\|[\Phi_i^a, \Phi_j^b]\| < K$ and $\|[\Phi_i^a, [\Phi_j^b, \Phi_k^c]]\| < Q$.

Take any two observable operators O_P and O_Q such that O_P has support on a finite

subgraph P intersecting at most $n_P < \infty$ local operators of the Hamiltonian and O_Q has support on subgraph Q such that the graph distance between P and Q is $d > R$. Suppose further that one of the following is satisfied:

- $\|O_P\| < \infty$ and $\|O_Q\| < \infty$ in the uniform boundedness case,

  or

- there exists F_P and F_Q such that for all terms Φ_i^a and Φ_j^b of the Hamiltonian the inequalities $\|[O_P, \Phi_i^a]\| < F_P K$, $\|[O_Q, \Phi_i^a]\| < F_Q K$ and $\|[O_Q, [\Phi_i^a, \Phi_j^b]]\| < F_Q Q$ are satisfied in the commutator boundedness case.

Consider

$$L(\lambda) \equiv \max_{2 \leq r \leq m(m-1)} \max_{(a_1, a_2, \ldots, a_r) \in \{1, \ldots, m\}^r} \left\{ k_{a_1 \ldots a_r} e^{\lambda \xi_{a_1 \ldots a_r}} | 1 \leq p < q \leq r, (a_p, a_{p+1}) \neq (a_q, a_{q+1}) \right\}, \tag{6.1}$$

where

$$C = \begin{cases} 2(m-1) & \text{bounded,} \\ \sqrt{8}(m-1) & \text{commutator-bounded,} \end{cases} \tag{6.2}$$

$$k_{l_1 \ldots l_r} = \begin{cases} \sqrt[r]{\prod_{i=1}^{r} h_{l_i} n_{l_i \to l_{i+1}}} & \text{bounded, lattice,} \\ \sqrt[r]{\prod_{i=1}^{r} h_{l_i}}\, \overline{n}_{l_1 l_2 \ldots l_r} & \text{bounded, h\&i graph,} \\ \sqrt[r]{\prod_{i=1}^{r} h_{l_i} K_{l_i l_{i+1}} n_{l_i \to l_{i+1}}} & \text{commutator-bounded, lattice,} \\ \sqrt[r]{\prod_{i=1}^{r} h_{l_i}}\, \overline{n}_{l_1 l_2 \ldots l_r} & \text{commutator-bounded, h\&i graph,} \end{cases} \tag{6.3}$$

$$\xi_{l_1 \ldots l_r} = \begin{cases} \frac{\sum_{i=1}^{r} D^{l_i \to l_{i+1}}}{r} & \text{lattice,} \\ \overline{D}_{l_1 \ldots l_r} & \text{h\&i graph,} \end{cases} \tag{6.4}$$

$$M(\lambda) = \begin{cases} \|O_P\| \|O_Q\| n_P e^{\lambda \xi(\lambda)} & \text{bounded,} \\ F_P F_Q n_P (n_P + 1) e^{\lambda \xi(\lambda)} & \text{commutator-bounded,} \end{cases} \tag{6.5}$$

$$\tag{6.6}$$

where for commutator bounded systems we define $K_{l_i l_{i+1}} = \|[\Phi_{l_i}, \Phi_{l_{i+1}}]\|$ for $(l_i, l_{i+1}) \in \{1, \ldots, m\}^2$ and where $\xi(\lambda) = \xi_{a_1 \ldots a_r}$ where $a_1 \ldots a_r$ maximises Eq.(6.1). Then, with these redefinitions, the general version of the Lieb-Robinson bound for both bounded and commutator bounded cases cases is:

$$\|[O_P(t), O_Q(0)]\| \leq M(\lambda) \exp\Big(\lambda\big(\frac{CL(\lambda)}{\lambda} \mid t \mid -d(P,Q)\big)\Big). \tag{6.7}$$

Hence we deduce a Lieb-Robinson speed in the general case to be

$$v_{LR} = \inf_{\lambda>0}\{\frac{CL(\lambda)}{\lambda}\}, \tag{6.8}$$

where $L(\lambda)$ is defined by Eq. (6.1,6.2,6.3,6.4). Explicit calculations of Eq.(6.8) then proceed exactly as shown in sections 4.2.2 and 4.2.3.

In summary, in this part, we derived a bound which was sensitive to the relative interaction strengths and which was applicable not only systems where local operators are bounded but also to those where they are commutator bounded. We observed that for $m \geq 3$ interactions, the space of coupling constants was subdivided into a finite number of regions, each of which produced a different functional form for the Lieb-Robinson speed. Interestingly, the dependence of the speed on the coupling is not necessarily algebraic anymore for three or more interactions as it was for two interactions; it was found that the logarithm of the coupling constants could appear in the speed.

It is also important, especially for applications in such domains as quantum gravity, that we be able to calculate the bound not only for a system on a lattice but also for general graphs. We derived explicit equations for the Lieb-Robinson bound and speed in the case of homogeneous and isotropic graphs. This is the best we can hope to have since if the graph is not homogeneous and isotropic, the speed will not be constant. It was important, particulary when thinking of applications to Quantum Graphity to derive as tight a bound as possible so that the actual maximal speed of information can be closely estimated and the relativistic metric of Quantum Graphity deduced from assuming, as mentioned in section 3.1 that the maximal speed is constant and that it is the metric which changes. Also,

if the transition from pre-geometric to geometric phase is a quantum phase transition in Quantum Graphity, we can gain more information on it from an interaction-strength dependent Lieb-Robinson speed.

PART III

PHENOMENOLOGY

Chapter 7

The Loop Quantum Black Hole

Introduction

Quantum gravity is the theory attempting to reconcile general relativity and quantum mechanics. In general relativity the space-time is dynamical and so it is not possible to study other interactions on a fixed background because the background itself is a dynamical field. "Loop quantum gravity" (LQG) [97] [26] [75] is a major contestant amongst the theories aiming at unifying gravity and quantum mechanics. It is one of the non perturbative and background independent approaches to quantum gravity. Since LQG is a quantum geometric fundamental theory that reconciles general relativity and quantum mechanics at the Planck scale, we expect that this theory could resolve the classical singularity problems of general relativity. Much progress has been made in this direction in the last years. In particular, the application of LQG technology to the early universe in the context of minisuperspace models have resolved the initial singularity problem [19], [10].

Black holes are another interesting place for testing the validity of LQG. In the past years applications of LQG ideas to the Kantowski-Sachs space-time [56] [66] lead to some

interesting results. In particular, it has been shown [72] [8] that it is possible to solve the black hole singularity problem by using tools and ideas developed in the full LQG. Other remarkable results have been obtained in the non homogeneous case [36]. We think the resolution of the black hole singularity problem is a crucial first step to solve the information loss problem [54].

There is also work of a semiclassical nature which tries to solve the black hole singularity problem [73],[18]. In these papers the authors use an effective Hamiltonian constraint obtained by replacing the Ashtekar connection A of Eq.(2.14) with the holonomy $h(A)$ and they solve the classical Hamilton equations of motion exactly or numerically.

In what follows, we review a modification to the holonomic version of the Hamiltonian constraint. The main result is that the minimum area [96] of full LQG is the fundamental ingredient to solve the black hole space-time singularity problem at $r = 0$. The S^2 sphere bounces on the minimum area $A_{min} \equiv 8\pi a_0$ of LQG and the singularity disappears. We show that the Kretschmann invariant is regular in all of space-time and the position of the maximum is independent of the mass and of the polymeric parameter introduced to define the holonomic version of the scalar constraint. The radial position of the curvature maximum depends only on G_N and $\hbar$.

Part III is organised as follows. In this chapter, modified from the first part of [76], we start by reviewing the singularity free semiclassical black hole solution obtained in [74] by Modesto. We also recall the causal space-time structure and the Carter-Penrose diagram for the maximal space-time extension. Then, in section 7.2 show the self-duality property of the metric which we derived in [76]. In chapter 8, we discuss the thermodynamical properties of the Loop Quantum black hole. In chapter 9, we take special notice of ultra-

light black holes which differ qualitatively from Schwarzschild black holes even outside the horizon. We show that their horizons are hidden behind a wormhole of Planck diameter. In chapter 10 we study the formation of a black hole and its subsequent evaporation. Using the static solution, we examine the more realistic dynamical case by generalising the static case with help of the Vaidya metric [105]. We track the formation and evolution of trapped surfaces during collapse and evaporation and examine the buildup of quantum gravitationally caused stress-energy preventing the formation of a singularity. In chapter 11 we study the phenomenology of LQBHs (Loop Quantum black holes), we examine the possibility that they could make up a significant portion of dark matter. We study the production rate of black holes in the early universe and using Stefan's law we calculate the black hole mass today. In chapter 12 we pursue the phenomenological line of investigation initiated in chapter 11 and we estimate the production of ultra-high-energy-cosmic-rays (UHECR) by the ULBH portion of the dark matter. We show the production of UHECR is compatible with observation. The ultra light black holes could be the missing source for the UHECRs.

7.1 A regular Black Hole from LQG

In this section we recall the classical Schwarzschild solution inside the event horizon $r \leqslant 2m$ [74], [72] [8]. Because we are inside the event horizon the radial coordinate is time-like and the temporal coordinate is space-like. For this reason the space-time for $r \leqslant 2m$ is the homogeneous Kantowski-Sachs space-time of spatial topology $\mathbb{R} \times S^2$. The Ashtekar

variables [5] of Eq. (2.14,2.13) are

$$A = \tilde{c}\tau_3 dx + \tilde{b}\tau_2 d\theta - \tilde{b}\tau_1 \sin\theta d\phi + \tau_3 \cos\theta d\phi,$$
$$E = \tilde{p}_c \tau_3 \sin\theta \frac{\partial}{\partial x} + \tilde{p}_b \tau_2 \sin\theta \frac{\partial}{\partial \theta} - \tilde{p}_b \tau_1 \frac{\partial}{\partial \phi}, \tag{7.1}$$

where A is an $\mathfrak{su}(2)$ connection of mass dimension 0 and E, its canonical conjugate is a densitised triad of mass dimension -2. The component variables in the phase space have length dimension: $[\tilde{c}] = L^{-1}$, $[\tilde{p}_c] = L^2$, $[\tilde{b}] = L^0$, $[\tilde{p}_b] = L$. Using the general relation $E^a_i E^b_j \delta^{ij} = \det(q) q^{ab}$ (q_{ab} is the metric on the spatial section) we obtain $q_{ab} = (\tilde{p}_b^2/|\tilde{p}_c|, |\tilde{p}_c|, |\tilde{p}_c| \sin^2\theta)$. In the Hamiltonian constraint and in the symplectic structure we restrict integration over x to a finite interval L_0 and we rescale the variables as follows: $b = \tilde{b}$, $c = L_0 \tilde{c}$, $p_b = L_0 \tilde{p}_b$, $p_c = \tilde{p}_c$. The length dimensions of the new phase space variables are: $[c] = L^0$, $[p_c] = L^2$, $[b] = L^0$, $[p_b] = L^2$. From the symmetry reduced connection and density triad we can read the component variables in the phase space: (b, p_b), (c, p_c), with Poisson algebra $\{c, p_c\} = 2\gamma G_N$, $\{b, p_b\} = \gamma G_N$. The Hamiltonian constraint in terms of the rescaled phase space variables and the holonomies is

$$\mathcal{C}_H = -\frac{N}{\kappa}\left\{ 2\frac{\sin\delta_c c}{\delta_c}\frac{\sin\Delta_b b}{\delta_b}\sqrt{|p_c|} + \frac{\sin^2\Delta_b b + \gamma^2\delta_b^2}{\sqrt{|p_c|}\delta_b^2} p_b \right\},$$

where $\kappa = 2G_N\gamma^2$; δ_b, δ_c are the polymeric parameters introduced to define the lengths of the paths along which we integrate the connection to define the holonomies and by definition $\Delta_b = \delta_b/\sqrt{1+\gamma^2\delta_b^2}$ [74]. The reason $\sin$'s appear in the above expression for the Hamiltonian constraint is that holonomies appear in the curvature and the $\sin$'s and $\cos$'s

appear in the parallel transport group elements. For example, let $U(x)$ be the $SU(2)$ group element performing the parallel transport along a path of length x in the direction $\partial/\partial x$. Then U satisfies the equation for parallel transport:

$$\frac{\partial U(x)}{\partial x} + A(x)[\partial/\partial x]U(x) = 0. \tag{7.2}$$

Using Eq.(7.1)this becomes

$$\begin{aligned} &\frac{\partial U(x)}{\partial x} = -\tilde{c}\tau_3 U(x) \\ &\Rightarrow U(\delta_c) = \exp(-\delta_{\tilde{c}}\tilde{c}\tau_3) = -\big[\cos(\delta_{\tilde{c}}\tilde{c})\mathbb{1} + \sin(\delta_{\tilde{c}}\tilde{c})\tau_3\big]. \end{aligned} \tag{7.3}$$

So, multiplying such parallel transports together to form a holonomy, dividing by the area of the loop ($\propto \delta^2$) we get the curvature. Then taking the appropriate traces we obtain Eq.(7.2).

The Gauss-constraint and the Diff-constraints are identically zero because of the homogeneity. Using the gauge $N = (\gamma\sqrt{|p_c|}\text{sgn}(p_c)\delta_b)/(\sin\Delta_b b)$, we can solve the Hamilton equation of motion and the Hamiltonian constraint (see [74] for details): $\mathcal{C}_H(q_i) = 0$, $\dot{q}_i = \{q_i, C_H\}$; where $q_i = (c, p_c, b, p_b)$ obtaining a solution on the four dimensional phase space: $(c(t), p_c(t), b(t), p_b(t))$. The relations between the Ashtekar and metric variables is explicit in the following line element:

$$ds^2 = -N^2\frac{dt^2}{t^2} + \frac{p_b^2}{|p_c|\,L_0^2}dx^2 + |p_c|(\sin^2\theta d\phi^2 + d\theta^2). \tag{7.4}$$

In [74], the solution inside the event horizon ($r < 2m$) was calculated and because of the

regularity of the solution $\forall\, r$, the solution was have analytically extended to $0 < r < +\infty$. In particular the Kretschmann invariant ($K = \mathrm{R}_{\mu\nu\rho\sigma}\mathrm{R}^{\mu\nu\rho\sigma}$) is regular $\forall r$ and it is possible to extend analytically the solution beyond the horizons (because as will be recounted below, the new metric has an inner event horizon). In [74] regular coordinates were found in any patch where the metric has a coordinate singularity showing explicitly that the metric is regular everywhere and can be extended to all of space-time.

Because of the regularity of the metric, we can use the usual Schwarzschild coordinates where r is space-like and t is time-like outside the event horizon. The semiclassical metric is

$$\begin{aligned} ds^2 = &-\frac{(r-r_+)(r-r_-)(r+r_\star)^2}{r^4+a_0^2}dt^2 \\ &+\frac{dr^2}{\frac{(r-r_+)(r-r_-)r^4}{(r+r_\star)^2(r^4+a_0^2)}} + \Big(\frac{a_0^2}{r^2}+r^2\Big)d\Omega^{(2)}, \end{aligned} \tag{7.5}$$

where $r_+ = 2m$, $r_- = 2m\mathcal{P}(\delta_b)^2$, $r_\star = 2m\mathcal{P}(\delta_b)$, $a_0 = A_{\mathrm{Min}}/8\pi$ and A_{Min} is the minimum area of LQG. r_+ is the location of the outer horizon while r_- is the location of the inner horizon. r_*, geometric mean of the coordinates of the two horizons is in between the two horizons. $\mathcal{P}(\delta_b)$ is a function of the polymeric parameter δ_b,

$$\mathcal{P}(\delta_b) = \frac{\sqrt{1+\gamma^2\delta_b^2}-1}{\sqrt{1+\gamma^2\delta_b^2}+1}. \tag{7.6}$$

The area operator in LQG has a discrete spectrum. Irreducible units of area in LQG — associated to an edge on a spin-network — have area $A(j) = 8\pi\gamma\sqrt{j(j+1)}l_P^2$ where γ is the Immirzi parameter believed to be $\gamma = 0.2375$ [71]. j is a half-integer labelling an

irreducible representation of $SU(2)$ and l_P is the Planck length. Looking at this, it is natural to assume that the minimum area in LQG is $A_{\text{Min}} = A(1/2) = 4\pi\gamma\sqrt{3}l_P^2 \approx 5l_P^2$. One should however not take this exact value too seriously for various reasons. First, the value of γ is not necessarily definite and the consensus on its value has changed a few times already. Second there are other Casimirs possible besides $\sqrt{j(j+1)}$. Third, we are looking for a minimum area for a closed surface so, the spin-network being most likely a closed graph, it is probable that least two edges cross the surface, in which case the minimum area is at least twice the previously given value. In addition, if we consider a surface enclosing a non-zero volume, LQG stipulates that at least one 4-valent vertex must be present, in which case we might have four edges intersecting the surface making A_{Min} be four times the aforementioned value. We will parameterise our ignorance with a parameter β and define $A_{\text{Min}} = \beta A(1/2) = 4\pi\gamma\beta\sqrt{3}\, l_P^2 \approx 5\beta l_P^2$, and so $a_0 = A_{\text{Min}}/(8\pi) = \gamma\beta\sqrt{3}\, l_P^2/2 \approx 0.2\beta l_P^2$ where the expectation is that β is not many orders of magnitude bigger or smaller than 1. In what follows we mostly consider $\beta \approx 1$ or $\beta = 4$ when more precision is needed, but in the end the precise choice of β does not change much.

There is also *another argument* we can make to justify the analytic extension of the metric to all of space-time. We can interpret the black hole solution (7.5) as having been generated by an effective matter fluid that simulates the loop quantum gravity corrections (in analogy with [21]). The effective gravity-matter system satisfies by definition the Einstein equations $G = 8\pi\, T$, where T is the effective energy tensor. In this case $T \neq 0$ in contrast to the classical Schwarzschild solution. The stress energy tensor for a perfect fluid compatible with the space-time symmetries is $T^\mu_\nu = (-\rho, P_r, P_\theta, P_\theta)$ and in terms of the Einstein tensor the components are $\rho = -G^t_t/8\pi G_N$, $P_r = G^r_r/8\pi G_N$ and $P_\theta = G^\theta_\theta/8\pi G_N$.

The semiclassical metric to zeroth order in δ_b and a_0 is the classical Schwarzschild solution ($g^C_{\mu\nu}$) that satisfies $G^\mu_\nu(g^C) \equiv 0$. When we calculate explicitly the energy density and pressure we obtain that those quantities are *spatially homogeneous* inside the event horizon and *static* outside. Using this property of the energy tensor we can repeat the argument used to extend the classical Schwarzschild solution to all of space-time. The crucial difference is that in our case $T^\mu_\nu \neq 0$ but the logic is identical. In particular T^μ_ν is *static* or *spatially homogeneous* depending on the nature of the surfaces $\sqrt{|p_c|} = const.$ and we can repeat the analysis given at the end of [46]. The analytic form of the energy density is,

$$\begin{aligned}\rho = 4r^4[&a_0^4 m(1+\mathcal{P})^2 + 2m^2\mathcal{P}(1+\mathcal{P})^2 r^7 + \\ &-a_0^2 r^2(2m\mathcal{P}+r)(12m^2\mathcal{P}^2 - m(7+\mathcal{P}(2+7\mathcal{P}))r \\ &+3r^2)]/[8\pi G_N(2m\mathcal{P}+r)^3(a_0^2+r^4)^3]. \end{aligned} \tag{7.7}$$

The regular properties of the metric are summarised in the following table,

Properties of $g_{\mu\nu}$
$\lim_{r\to+\infty} g_{\mu\nu}(r) = \eta_{\mu\nu}$
$\lim_{r\to 0} g_{\mu\nu}(r) = \eta_{\mu\nu}$
$\lim_{m,a_0\to 0} g_{\mu\nu}(r) = \eta_{\mu\nu}$
$K(g) < \infty \ \forall r$
$r_{\rm Max}(K(g)) \propto l_P$

where $r_{\rm Max}(K(g))$ is the radial position where the Kretschmann invariant achieves its maximum value. Fig.7.3 is a graph of K. It is regular in all of space-time and its large r behaviour is asymptotically identical to the classical scalar $\mathrm{R}_{\mu\nu\rho\sigma}\mathrm{R}^{\mu\nu\rho\sigma} \cong 48m^2/r^6$. The

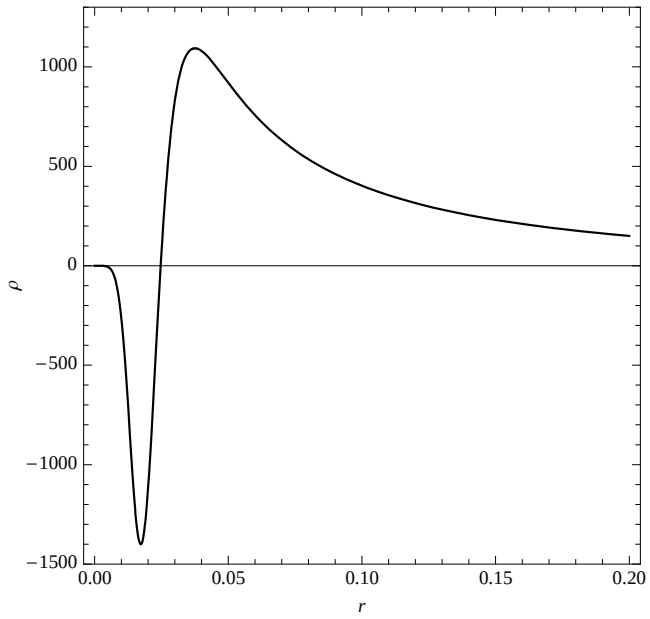

Figure 7.1: Effective energy density for $m = 10$ and $a_0 = 0.01$.

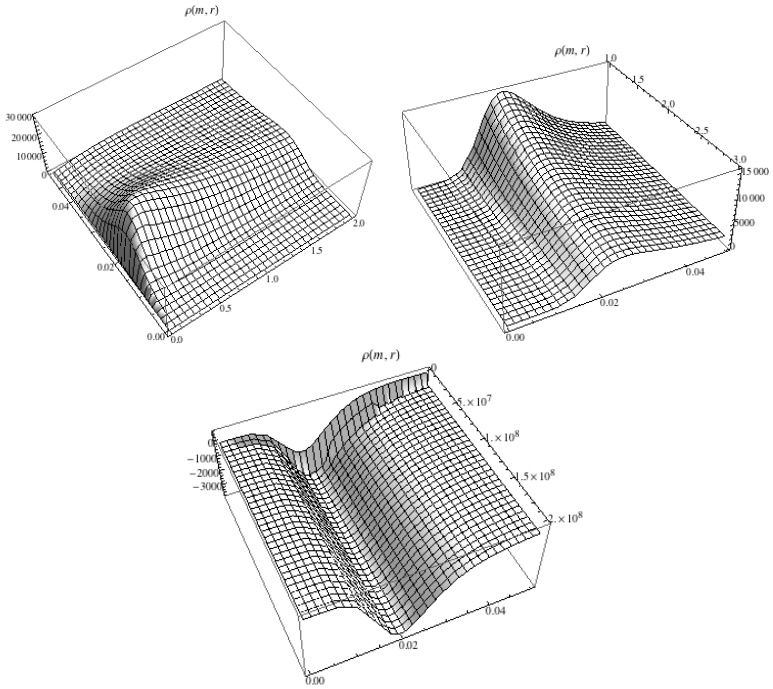

Figure 7.2: Effective energy density as function of r and m. In the upper plot on the left $m \in [0, 2]$ and $r \in [0, 0.045]$, in the upper plot on the right $m \in [1, 3]$ and $r \in [0, 0.045]$ and in the lower plot $m \in [0, 2\,10^8]$ and $r \in [0, 0.045]$. The plots show that the energy density is localised around the Planck scale for any value of the mass and decrees rapidly for $r \gtrsim l_P$.

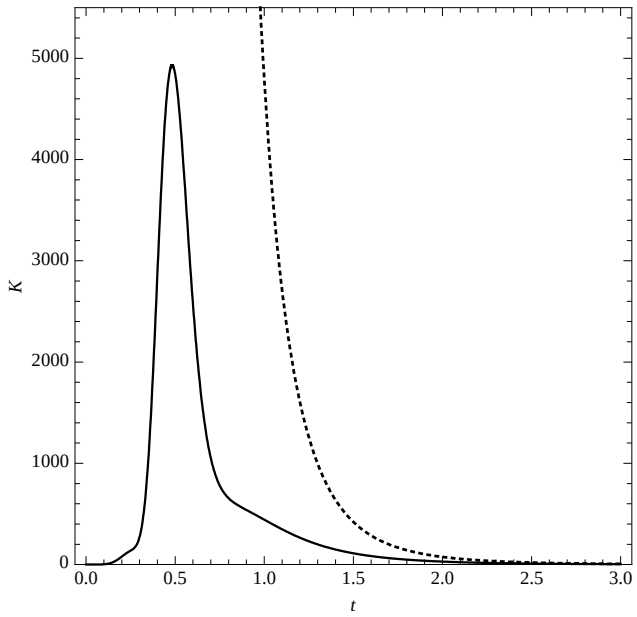

Figure 7.3: Plot of the Kretschmann scalar invariant $\mathrm{R}_{\mu\nu\rho\sigma}\mathrm{R}^{\mu\nu\rho\sigma}$ for $m = 10$, $p_b^0 = 1/10$ and $\gamma\delta_b = \log(4)/\pi$, $\forall t \geqslant 0$; the large t behaviour is $1/t^6$. The dotted line is the value the Kretschmann scalar would take in the Schwarzschild case.

resolution of the singularity of K is a non perturbative result, in fact for small values of the radial coordinate r, $K \approx 3145728\pi^4 r^6/A_{\mathrm{Min}}^4\gamma^8\delta_b^8 m^2$ diverges for $A_{\mathrm{Min}} \to 0$ or $\delta_b \to 0$. A crucial difference with the classical Schwarzschild solution is that the 2-sphere S^2 has a minimum for $r_{min} = \sqrt{a_0}$ and the minimum square radius is $p_c(r_{min}) = 2a_0$. The solution has a spacetime structure very similar to the Reissner-Nordström metric because of the inner horizon in $r_- = 2m\mathcal{P}(\delta_b)^2$. For $\delta_b \to 0$, $r_- \approx m\gamma^4\delta_b^4/8$. We observe that the position of the inside horizon is $r_- \neq 2m\ \forall\gamma \in \mathbb{R}$ (we recall that γ is the Barbero-Immirzi parameter). The metric (7.5) for $\delta_b, a_0 = 0$ is exactly the Schwarzschild metric.

The metric (7.5) has an asymptotic Schwarzschild core near $r \approx 0$. To show this property we develop the metric very close to the point $r \approx 0$ and we consider the coordinate changing $R = a_0/r$. In the new coordinate the point $r = 0$ is mapped in the point $R = +\infty$.

The metric in the new coordinates is

$$ds^2 = -\left(1 - \frac{2m_1}{R}\right)dt^2 + \frac{dR^2}{1 - \frac{2m_2}{R}} + R^2 d\Omega^{(2)}, \tag{7.8}$$

where m_1 and m_2 are functions of $m, A_{\text{Min}}, \delta_b, \gamma$,

$$m_1 = \frac{A_{\text{Min}}}{8\pi m\gamma^2\delta_b^2\mathcal{P}(\delta_b)} \ , \quad m_2 = \frac{A_{\text{Min}}(1+\gamma^2\delta_b^2)}{8\pi m\gamma^2\delta_b^2\mathcal{P}(\delta_b)}. \tag{7.9}$$

For small δ_b we obtain $m_1 \approx m_2$ and (7.8) converges to a Schwarzschild metric of mass $M \approx A_{\text{Min}}/2m\pi\gamma^4\delta_b^4$. We can conclude the space-time near the point $r \approx 0$ is described by an effective Schwarzschild metric of mass $M \propto A_{\text{Min}}/m$ in the large distance limit $R \gg M$. An observer in the asymptotic region $r = 0$ experiences a Schwarzschild metric of mass $M \propto a_0/m$ because such an observer sees the same metric that an observer at assymptotic infinity of a Schwarzschild metric with mass M sees.

Now we are going to show that a massive particle cannot reach $r = 0$ in a finite proper time. We consider the radial geodesic equation for a massive point particle

$$(-g_{tt}\, g_{rr})\dot{r}^2 = E_n^2 + g_{tt}, \tag{7.10}$$

where " $\dot{}$ " is the proper time derivative and E_n is the point particle energy. If the particle falls from infinity with zero initial radial velocity the energy is $E_n = 1$. We can write (7.10)

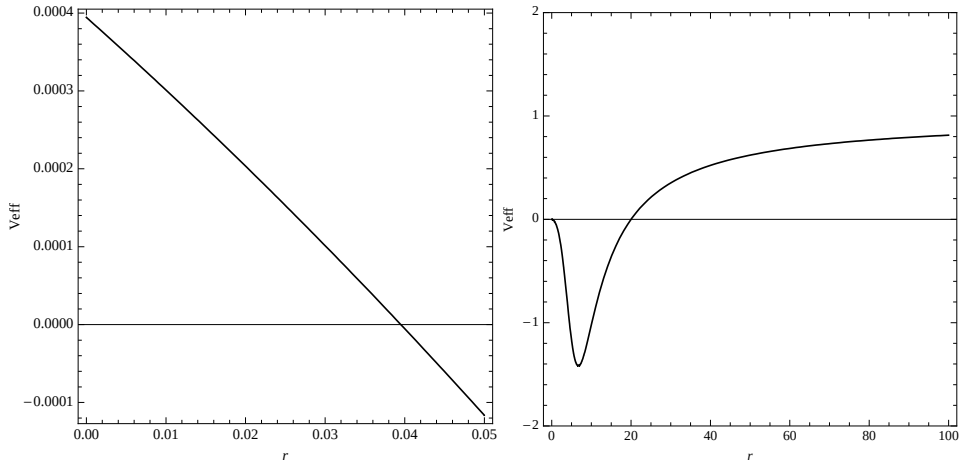

Figure 7.4: Plot of $V_{eff}(r)$. On the left there is a zoom of V_{eff} for $r \approx 0$.

in a more familiar form

$$\underbrace{(-g_{tt}\, g_{rr})}_{\geqslant 0\ \forall r}\dot{r}^2 + \underbrace{V_{eff}}_{-g_{tt}\geq 0}(r) = \underbrace{E}_{E_n^2}, \tag{7.11}$$

V_{eff} is plotted in Fig.7.4. For $r = 0$, $V_{eff}(r = 0) = 1024m^4\pi^2\mathcal{P}(\delta_b)^4/A^2_{\rm Min}$ then a particle with $E < V_{eff}(0)$ can never reach $r = 0$. If the particle energy is $E > V_{eff}(0)$, the geodesic equation for $r \approx 0$ is $\dot{r}^2 \propto r^4$ which gives $\tau \propto 1/r - 1/r_0$ or $\Delta\tau \equiv \tau(0) - \tau(r_0) \to +\infty$ for the proper time to reach $r = 0$. The space-time structure of the semiclassical solution is given in Fig.7.5.

7.2 Selfduality

In this section, taken from [76] where it was first shown, we explicitly show that the black hole solution obtained in LQG is *selfdual* in the sense the metric is invariant under the transformation $r \to a_0/r$. The self-dual transformation will transform the relevant quantities as

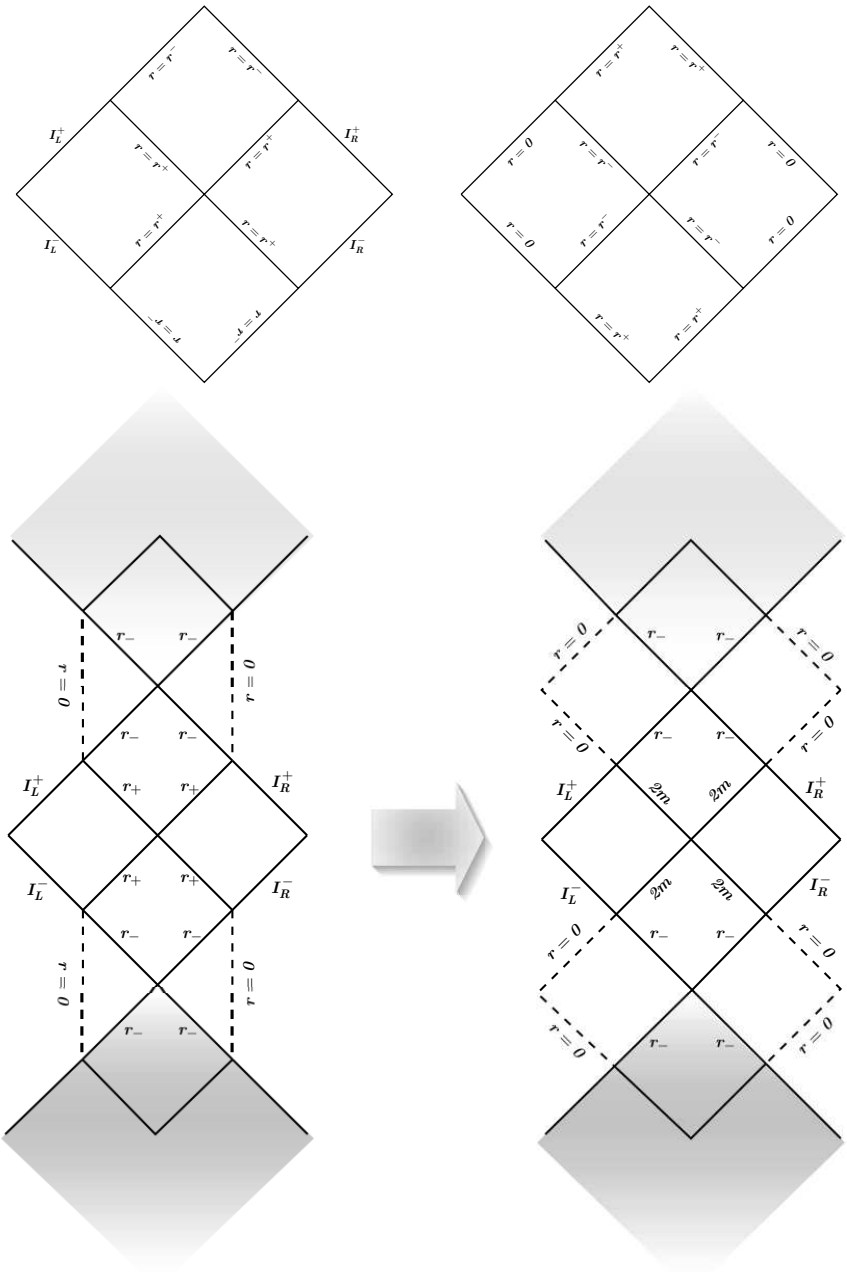

Figure 7.5: The upper picture on the left represents the Carter-Penrose diagram in the region outside r_- and the upper picture on the right represents the diagram for $r_- \leqslant r \leqslant 0$. The lower pictures represent the maximal space-time extension Reissner-Nordström black hole on the left and maximal space-time extension of the LQBH on the right.

shown in the following table:

$\text{Self} - \text{duality}$
$r \to R = \frac{a_0}{r}$
$r_+ \to R_- = \frac{a_0}{r_+} = \frac{a_0}{2m}$
$r_- \to R_+ = \frac{a_0}{r_-} = \frac{a_0}{2m\mathcal{P}(\delta_b)^2}$
$r_\star \to R_\star = \frac{a_0}{r_\star} = \frac{a_0}{2m\mathcal{P}(\delta_b)}$

(note that $R_+ > R_- \; \forall \delta_b$ because $\mathcal{P}(\delta_b) < 1$). If we apply to this transformation to the metric (7.5), we obtain

$$ds^2 = -\frac{(R-R_+)(R-R_-)(R+R_\star)^2}{R^4+a_0^2}dt^2 + \frac{dR^2}{\frac{(R-R_+)(R-R_-)R^4}{(R+R_\star)^2(R^4+a_0^2)}} + \Big(\frac{a_0^2}{R^2}+R^2\Big)d\Omega^{(2)}, \tag{7.12}$$

where we have complemented the transformation $r \to a_0/r$ with a rescaling of the time coordinate $t \to \mathcal{P}(\delta_b)(r_+^{3/2}r_-^{1/2}/a_0)\,t$. It is evident from the explicit form (7.12) that the metric is *selfdual*. We can define the selfdual radius identifying $R = a_0/r$, $r^{sd} = \sqrt{a_0}$. The existence of a selfdual radius implies a selfdual mass because we have

$$R_- = r_- \;,\; R_+ = r_+ \;,\; R_\star = r_\star \to m_{sd} = \frac{\sqrt{a_0}}{2\mathcal{P}(\delta_b)}. \tag{7.13}$$

In the global extension of the space-time any black hole with mass $m < m_{sd}$ is equivalent to a black hole of mass $m > m_{sd}$ by the selfdual symmetry.

Chapter 8

Thermodynamics

In this chapter, modified from an analogous section in [76], we review the thermodynamics found in [21] [3]: temperature, entropy and evaporation.

The form of the metric calculated in the previous section has the general form, $ds^2 = -g(r)dt^2 + dr^2/f(r) + h^2(r)(d\theta^2 + \sin^2\theta d\phi^2)$, where the functions $f(r)$, $g(r)$ and $h(r)$ depend on the mass parameter m and are the components of the metric (7.5). We can introduce the null coordinate v to express the metric above in the Bardeen form. The null coordinate v is defined by the relation $v = t + r^*$, where $r^* = \int^r dr/\sqrt{f(r)g(r)}$ and the differential is $dv = dt + dr/\sqrt{f(r)g(r)}$. In the new coordinate the metric is, $ds^2 = -g(r)dv^2 + 2\sqrt{g(r)/f(r)}\, drdv + h^2(r)d\Omega^{(2)}$.

8.1 Temperature

In this paragraph we calculate the temperature for the quantum black hole solution and analyze the evaporation process. The Bekenstein-Hawking temperature is given in terms of the surface gravity κ by $T = \kappa/2\pi$, the surface gravity is defined by $\kappa^2 = -g^{\mu\nu}g_{\rho\sigma}\nabla_\mu\chi^\rho\nabla_\nu\chi^\sigma/2 =$

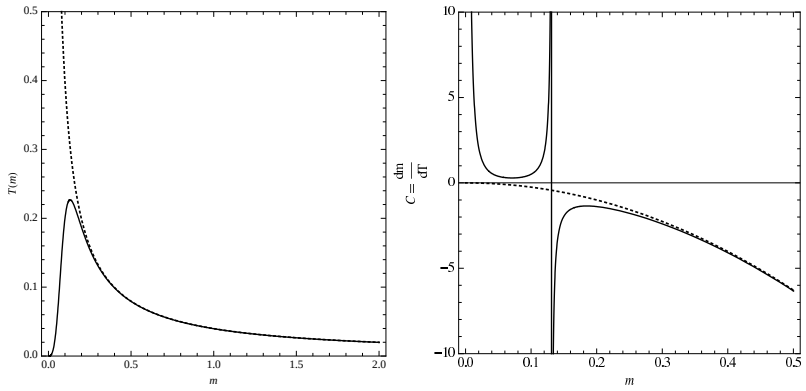

Figure 8.1: Plot of the temperature $T(m)$ on the left and of the heat capacity $C_s = \frac{dm}{dT}$ on the right. The continuous plots represent the LQBH quantities, the dashed lines represent the classical quantities.

$-g^{\mu\nu}g_{\rho\sigma}\Gamma^{\rho}_{\mu 0}\Gamma^{\sigma}_{\nu 0}/2$, where $\chi^{\mu} = (1, 0, 0, 0)$ is a timelike Killing vector and $\Gamma^{\mu}_{\nu\rho}$ is the connection compatible with the metric $g_{\mu\nu}$. Using the semiclassical metric (7.5)we can calculate the surface gravity in $r = 2m$

$$\kappa^2 = -g^{00}g^{11}\left(\partial g_{00}/\partial r\right)^2/4 = \left(16m/64m^2 + \gamma^2\delta^2\right)^2. \tag{8.1}$$

From this we obtain the temperature,

$$T(m) = \frac{128\pi\sigma(\delta_b)\sqrt{\Omega(\delta_b)}\,m^3}{1024\pi^2 m^4 + A^2_{\rm Min}}, \tag{8.2}$$

where $\Omega(\delta_b) = 16(1+\gamma^2\delta_b^2)^2/(1+\sqrt{1+\gamma^2\delta_b^2})^4$. The temperature (8.2) coincides with the Hawking temperature in the large mass limit. In Fig.8.1 we have a plot of the temperature as a function of the black hole mass m. The dashed trajectory corresponds to the Hawking temperature and the continuum trajectory corresponds to the semiclassical one. There is a substantial difference for small values of the mass, in fact the semiclassical temper-

ature tends to zero and does not diverge for $m \to 0$. The temperature is maximum for $m^* = 3^{1/4}\sqrt{A_{\rm Min}}/\sqrt{32\pi}$ and $T^* = 3^{3/4}\sigma(\delta_b)\sqrt{\Omega(\delta_b)}/\sqrt{32\pi A_{\rm Min}}$. Also this result, as for the curvature invariant, is a quantum gravity effect, in fact m^* depends only on the Planck area $A_{\rm Min}$. The transition from negative heat capacity for large classical black holes to positive heat capacity at or close to the Planck mass (here m^*) had already been anticipated on general grounds in [55]. In fact, when one compares the graph for the heat capacity in [55] to Fig. 8.1 one sees that although the two graphs differ in zero, they are strikingly similar everywhere else, and most importantly around the transition point which as predicted in [55] is of second order.

8.2 Entropy

In this section we calculate the entropy for the LQBH metric. By definition the entropy as a function of the ADM energy is $S_{BH} = \int dm/T(m)$. Calculating this integral for the LQBH we find

$$S = \frac{1024\pi^2 m^4 - A_{\rm Min}^2}{256\pi m^2 \sigma(\delta_b)\sqrt{\Omega(\delta_b)}} + \text{const.}. \tag{8.3}$$

We can express the entropy in terms of the event horizon area. The event horizon area (at $r = 2m$) is

$$A = \int d\phi d\theta \sin\theta \, p_c(r)\Big|_{r=2m} = 16\pi m^2 + \frac{A_{\rm Min}^2}{64\pi m^2}. \tag{8.4}$$

Inverting (8.4) for $m = m(A)$ and introducing the roots in (8.3) we obtain

$$S = \pm \frac{\sqrt{A^2 - A_{\text{Min}}^2}}{4\sigma(\delta_b)\sqrt{\Omega(\delta_b)}}, \tag{8.5}$$

where S is positive for $m > \sqrt{a_0}/2$, and negative otherwise. We are not sure how to interpret the negative entropy for black holes lighter than the Planck mass, however we hypothesise that it might relate to the conditional quantum entropy of the black hole being negative due to entanglement [52]. In a simple example to show how quantum entropy might be negative let us consider a system made up of two spin-$\frac{1}{2}$s constrained to be in the total spin-0 state. The total state has a total entropy of 0, but if we have access to only one of those spins, we have access to one q-bit of information, thus the other q-bit we cannot access must have -1 q-bit of information. A plot of the entropy is given in Fig.8.2. The first plot represents entropy as a function of the event horizon area A. The second plot in Fig.8.2 represents the event horizon area as function of m. The semiclassical area has a minimum value in $A = A_{\text{Min}}$ for $m = \sqrt{A_{\text{Min}}/32\pi}$.

We want to underline that the parameter δ_b does not appear in the quantities $T(m)$, T^*, m^* and so it does not play any regularisation role for those observable quantities. Because of this, in the evaporation process that we will study in the following section, δ_b does not play a significant role and we can take to 0. We obtain finite quantities taking the limit $\delta_b \to 0$, because $\lim_{\delta_b \to 0} \sigma(\delta_b)\sqrt{\Omega(\delta_b)} = 1$.

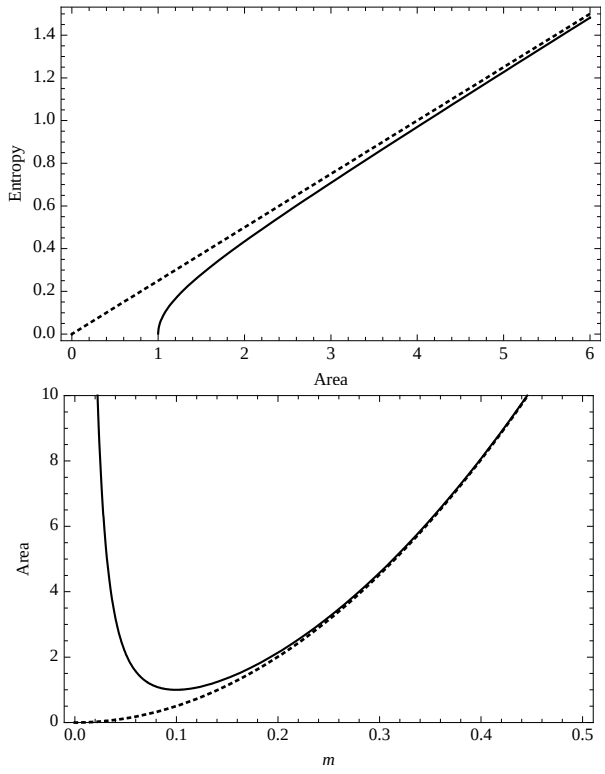

Figure 8.2: In the first plot we have the entropy for the LQBH as function of the event horizon area (dashed line represents the classical area low $S_{cl} = A/4$). In the second plot we represent the event horizon area as a function of the mass (dashed line represents the classical area $A_{cl} = 16\pi m^2$).

8.3 Evaporation

In this section we focus our attention on the evaporation process of the black hole mass and in particular in the energy flux from the hole.

The form of the metric of the LQBH has the general form, $ds^2 = -g(r)dt^2 + dr^2/f(r) + h^2(r)(d\theta^2 + \sin^2\theta d\phi^2)$, where the functions $f(r)$, $g(r)$ and $h(r)$ depend on the mass parameter m and are the components of the metric (7.5). We can introduce the null coordinate v to express the metric above in the Bardeen form. The null coordinate v is defined by the relation $v = t + r^*$, where $r^* = \int^r dr/\sqrt{f(r)g(r)}$ and the differential is $dv = dt + dr/\sqrt{f(r)g(r)}$. In the new coordinate the metric is, $ds^2 = -g(r)dv^2 + 2\sqrt{g(r)/f(r)}\, drdv + h^2(r)d\Omega^{(2)}$.

The luminosity can be estimated using the Stefan-Boltzmann law and it is given by $\mathcal{L}(m) = \alpha A(m) T_{BH}^4(m)$, where (for a single massless field with two degree of freedom) $\alpha = \pi^2/60$, $A(m)$ is the event horizon area and $T(m)$ is the temperature calculated in the previous section. At the first order in the luminosity the metric above that incorporates the decreasing mass is obtained by replacing the mass m with $m(v)$. Introducing the results (8.2) and (8.4) of the previous paragraphs in the luminosity $\mathcal{L}(m)$ we obtain

$$\mathcal{L}(m) = \frac{4194304\, m^{10}\pi^3\alpha\,\sigma^4\Omega^2}{(A_{\rm Min}^2 + 1024\, m^4\pi^2)^3}. \tag{8.6}$$

Using (8.6) we can solve the first order differential equation

$$-\frac{dm(v)}{dv} = \mathcal{L}[m(v)] \tag{8.7}$$

to obtain the mass function $m(v)$. The result of integration with initial condition $m(v =$

$0) = m_0$ is

$$
\begin{aligned}
&-\frac{n_1 A_{\rm Min}^6 + n_2 A_{\rm Min}^4 m^4\pi^2 + n_3 A_{\rm Min}^2 m^8\pi^4 - n_4 m^{12}\pi^6}{n_5 m^9\pi^3\alpha\,\sigma(\delta_b)^4\Omega(\delta_b)^2} \\
&+\frac{n_1 A_{\rm Min}^6 + n_2 A_{\rm Min}^4 m_0^4\pi^2 + n_3 A_{\rm Min}^2 m_0^8\pi^4 - n_4 m_0^{12}\pi^6}{n_5 m_0^9\pi^3\alpha\,\sigma(\delta_b)^4\Omega(\delta_b)^2} \\
&= -v, \qquad (8.8)
\end{aligned}
$$

where $n_1 = 5$, $n_2 = 27648$, $n_3 = 141557760$, $n_4 = 16106127360$, $n_5 = 188743680$. From the solution (8.8) we see that the mass evaporates in an infinite time because in the limit $m \approx 0$ Eq.(8.8) becomes $v = k_1(1/m^9 - 1) + k_2)$ with $k_1 > 0$ and k_2 two constants so $m = 0$ corresponds to $v = \infty$. Also in (8.8) we can take the limit $\delta_b \to 0$ obtaining a regular quantity independent from δ_b. In the limit $m \to 0$ equation (8.8) becomes

$$
\frac{n_1 A_{\rm Min}^6}{n_5\pi^3\alpha\,\sigma(\delta_b)^4\Omega(\delta_b)^2\,m^9} = v. \qquad (8.9)
$$

In the limit $\delta_b \to 0$, we obtain $n_1 A_{\rm Min}^6/n_5\pi^3\alpha\,m^9 \approx v$. Inverting this equation for small m we obtain: $m \approx (A_{\rm Min}^6/\alpha\,v)^{1/9}$.

Chapter 9

Ultra Light Black Hole

Outside the exterior horizon, the LQBH metric (7.5) differs from the Schwarzschild metric only by Planck size corrections. As such, the exterior of heavy LQBHs (where by "heavy" we mean significantly heavier than the Plank mass which is of the order of $20\,\mu\mathrm{g}$) is not qualitatively different than that of a Schwarzschild black hole of the same mass. This is shown in Fig.9.1 where the embedding diagrams of the LQG and Schwarzschild black holes of 50 Planck masses are compared just outside the horizon.

In order to see a qualitative departure from the Schwarzschild black hole outside the horizon we must consider the "sub-Planckian" regime, when the mass of the black hole is less than the Planck mass, as that is when quantum effects will become significant. In this chapter, modified from part of [76], we investigate ultra light quantum black hole, where by ultra light we mean that $m < \sqrt{a_0}/ \approx m_P$.

Due to Planck scale corrections the radius of the 2-sphere is not r, as is the case for the

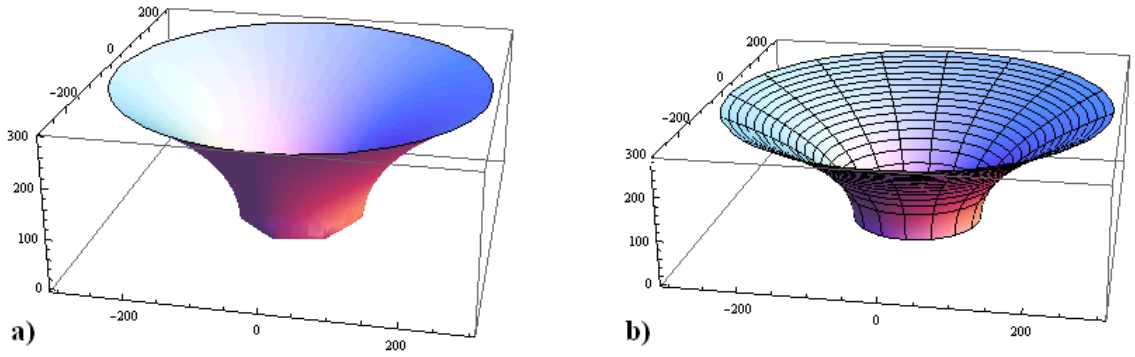

Figure 9.1: Embedding diagram of a spatial slice just outside the horizon of a 50 Planck mass ($\approx 1\text{mg}$) black hole. In (a) we have the LQBH with metric (7.5); in (b) is the Schwarzschild black hole. In both cases the foliation is done with respect to the time-like Killing vector and the scales are in Planck units. The lowermost points in each diagram correspond to the horizon (the outer horizon in the LQG case).

Schwarzschild metric, but looking at (7.5) we see that the radius of the 2-sphere is

$$\rho = \sqrt{r^2 + \frac{a_0^2}{r^2}}. \tag{9.1}$$

We see that ρ has a "bounce" at $r = \sqrt{a_0}$ which comes from LQG having a discrete area spectrum and thus a minimal area (here $8\pi a_0$). If the bounce happens before the outer horizon is reached, the outer horizon will be hidden behind the Planck-sized (space-like) "wormhole" created where the bounce takes place (see Fig. 9.2 and 9.3). As a consequence of this, even if the horizon is quite large (which it will be if $m << m_P$) it will be invisible to observers who are at $r > \sqrt{a_0}$ and who cannot probe the Planck scale because these observers would need to see the other side of the wormhole which has a diameter of the order of the Planck length. From this we conclude that to have this new phenomenon of a hidden horizon we must have $2m = r_+ < \sqrt{a_0}$, or $m < \sqrt{a_0}/2$. We illustrate this phenomenon with the embedding diagrams of a LQBH of mass $m = 4\pi\sqrt{a_0}/100$ in Fig.9.2a

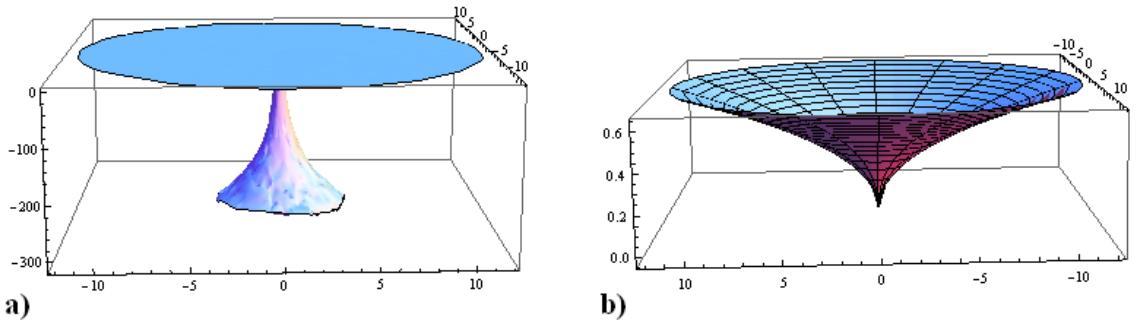

Figure 9.2: Embedding diagram of a spatial slice just outside the horizon of a 0.005 Planck mass ($\approx 100ng$) black hole. In (a) we have the LQBH with metric (7.5); in (b) is the Schwarzschild black hole. In both cases the foliation is done with respect to the time-like Killing vector and the scales are in Planck units. The lowermost points in each diagram correspond to the horizon (the outer horizon in the LQG case).

and Fig.9.3 which can be contrasted with the embedding diagram of the Schwarzschild black hole of the same mass in Fig.9.2b.

The formation of such ultra-light LQBHs is also of interest. For the Schwarzschild black hole, black hole formation occurs once a critical density is reached, i.e. a mass m is localised inside a sphere of area $4\pi(2m)^2$. The "heavy" LQBH is analogous: to create it we must achieve a critical density, putting a mass $m \geq \sqrt{a_0}/2$ inside a sphere of area $4\pi[(2m)^2 + a_0^2/(2m)^2]$. The requirement for the formation of an ultra-light LQBH is something else altogether because of the worm-hole behind which it hides: we must localise mass/energy (a particle or a few particles), irrespective of mass as long as the total mass satisfies $m < \sqrt{a_0}/2$) inside a sphere of area $8\pi a_0$ as this ensures that the mass will be inside the mouth of the wormhole. Because $A_{\rm Min} \geq 5l_P^2$ for any natural β at the currently accepted value of the Immirzi parameter, there is no theoretical semi-classical impediment to localizing matter in such a radius and thereby creating ultra-light black holes.

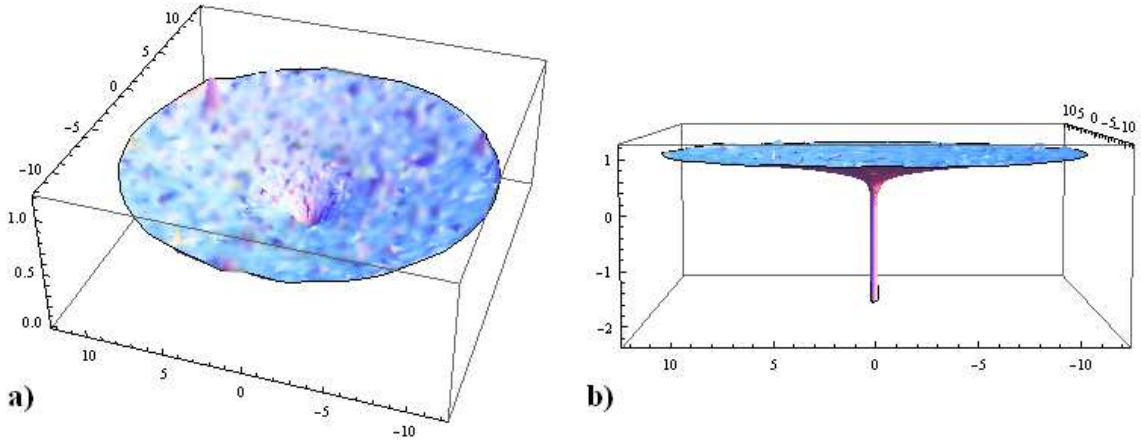

Figure 9.3: (a) Embedding diagram of a spatial slice just outside the throat of a 0.005 Planck mass LQBH. (b) zoom on the upper part of the throat of the same black hole. In both cases the foliation is done with respect to the time-like Killing vector and the scales are in Planck units.

Chapter 10

Collapse and Evaporation

Non-singular black holes were considered already by Bardeen in the late 60s and have a long history [15, 40, 41, 13, 11, 30, 69, 22, 12, 70, 48, 79, 2, 103, 81, 80]. We will here use a procedure similar to that in [48]. This chapter, modified from [53], is organised as follows. We start in the next section by recalling the regular static metric we will be using. In section 10.2 we generalise it to a collapse scenario and discuss its properties. In section 10.3 we summarise the thermodynamic properties and, in section 10.4, add the evaporation process and construct the complete causal diagram. The signature of the metric is $(-,+,+,+)$ and we use the unit convention $\hbar = c = G_N = 1$.

We will use a 4-dimensional model based on the static solution derived in [74] and generalise it to a dynamical case which then allows us to examine the causal structure. This generalisation holds to good accuracy in all realistic scenarios. This approach should be understood not as an exact solution to a problem that requires knowledge of a full theory of quantum gravity, but as a plausible model based on preliminary studies that allows us to investigate the general features of such regular black hole solutions.

10.1 The Static Black Hole metric

This quantum gravitationally corrected Schwarzschild metric Eq.(7.5) can be expressed in the form

$$ds^2 = -G(r)dt^2 + \frac{dr^2}{F(r)} + H(r)d\Omega\,, \tag{10.1}$$

with $d\Omega = d\theta^2 + \sin^2\theta d\phi^2$ and

$$\begin{aligned} G(r) &= \frac{(r-r_+)(r-r_-)(r+r_*)^2}{r^4+a_0^2}\,, \\ F(r) &= \frac{(r-r_+)(r-r_-)r^4}{(r+r_*)^2(r^4+a_0^2)}\,, \\ H(r) &= r^2 + \frac{a_0^2}{r^2}\,. \end{aligned} \tag{10.2}$$

Here, $r_+ = 2m$ and $r_- = 2mP^2$ are the two horizons, and $r_* = \sqrt{r_+ r_-} = 2mP$. P is the polymeric function

$$P = (\sqrt{1+\epsilon^2} - 1)/(\sqrt{1+\epsilon^2} + 1), \tag{10.3}$$

with $\epsilon := \gamma\delta \ll 1$ the product of the Immirzi parameter (γ) and the polymeric parameter (δ). With this, it is also $P \ll 1$, such that $r_-/(2m)$ and $r_*/(2m)$ are very close to 0. The area a_0 is equal to $A_{\min}/8\pi$, $A_{\min}$ being the minimum area gap of LQG.

Note that in the above metric, r is only asymptotically the usual radial coordinate since $g_{\theta\theta}$ is not just r^2. This choice of coordinates however has the advantage of easily revealing the properties of this metric as we will see. Most importantly, in the limit $r \to \infty$ the

deviations from the Schwarzschild-solution are of order ϵ^4 and so can be neglected and m may be identified as the usual ADM-mass:

$$\begin{aligned} G(r) &\rightarrow 1 - \frac{2m}{r}(1 + O(\epsilon^4)) \,, \\ F(r) &\rightarrow 1 - \frac{2m}{r}(1 + O(\epsilon^4)) \,, \\ H(r) &\rightarrow r^2. \end{aligned} \tag{10.4}$$

The ADM mass is the mass inferred by an observer at flat asymptotic infinity; it is determined solely by the metric at asymptotic infinity.

If one now makes the coordinate transformation $R = a_0/r$ with the rescaling $\tilde{t} = t\, r_*^2/a_0$, and simultaneously substitutes $R_\pm = a_0/r_\mp$, $R_* = a_0/r_*$ one finds that the metric in the new coordinates has the same form as in the old coordinates and thus exhibits a very compelling type of self-duality with dual radius $r = \sqrt{a_0}$. Looking at the angular part of the metric, one sees that this dual radius corresponds to a minimal possible surface element. It is then also clear that in the limit $r \rightarrow 0$, corresponding to $R \rightarrow \infty$, the solution does not have a singularity, but instead has another asymptotically flat Schwarzschild region.

The causal diagram for this metric, shown in Fig 10.1, then has two horizons and two pairs of asymptotically flat regions, A, A' and B, B', as opposed to one such pair in the standard case. In the region enclosed by the horizons, space- and timelikeness is interchanged. The horizon at r_+ is a future horizon for observers in the asymptotically flat B, B' region and a past horizon for observers inside the two horizons. Similarly, the r_- horizon is a future horizon for observers inside the two horizons but a past horizon for

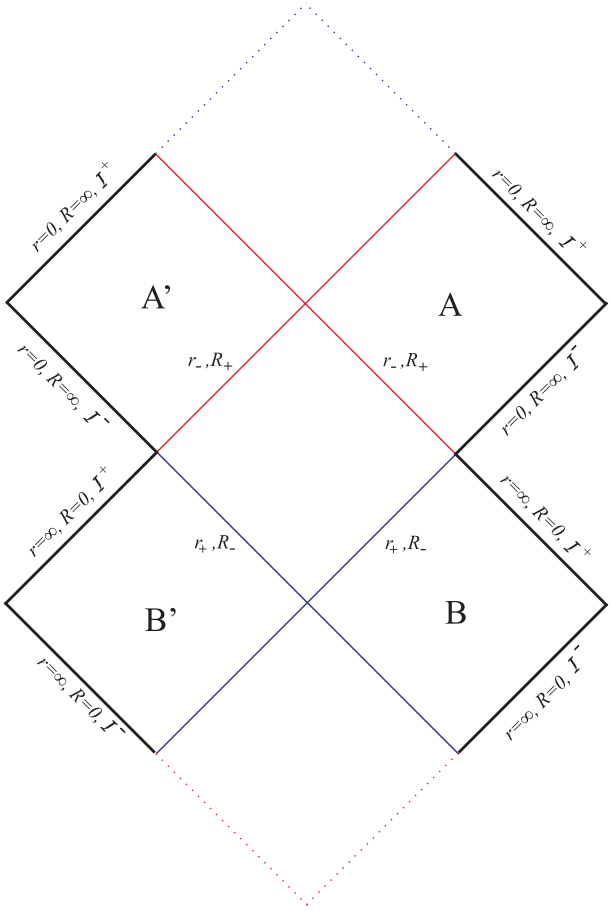

Figure 10.1: Penrose diagram of the regular static black hole solution with two asymptotically flat regions. The horizons, located at r_+ and r_-, are marked in blue and red respectively.

observes in A, A'. As we saw previously, if one computes the time it takes for a particle to reach $r = 0$, one finds that it takes infinitely long. The diagram shown in Fig. 10.1 is not analytically complete, but should be read as being continued on the dotted horizons at the bottom and top.

The metric in Eq.(10.2) is a solution of a quantum gravitationally corrected set of equations which, in the absence of quantum corrections $\epsilon, a_0 \to 0$, reproduce Einstein's field equations. However, due to these quantum corrections, the above metric is no longer a vacuum-solution to Einstein's field equations. Instead, if one computes the Einstein-

tensor and sets it equal to a source term $G_{\mu\nu} = 8\pi\widetilde{T}_{\mu\nu}$, one obtains an effective quantum gravitational stress-energy-tensor $\widetilde{T}_{\mu\nu}$. The exact expressions for the components of $\widetilde{T}$ are somewhat unsightly and can be found in appendix B. For our purposes, it is here sufficient to note that for the static metric of LQBH Eq.(7.5), the entries are not positive definite and violate the positive energy condition which is one of the assumptions for the singularity theorems.

10.2 Collapse

We will proceed by combining the static metric with a radially ingoing null-dust, such that we obtain a dynamical space-time for a black hole formed from such dust. Usually described by the Vaidya metric [105], we will in this scenario have corrections to the Vaidya metric that are negligible in the asymptotic region, but avoid the formation of a singularity in the strong-curvature region.

Explicitly, we will do the following. We take the static LQBH metric Eq.(7.5) but now we allow for m to be dependent on the ingoing null coordinate v: $m \to m(v)$. Calculating the effective energy momentum tensor we see that we gain a component G^r_v which we identify with the energy momentum T^r_v of the incoming null dust. The choosing a quantity of incoming dust by choosing the value of T^r_v will fix the value of $\partial m/\partial v$ on which G^r_v depends.

The metric constructed this way in the following is not a strict solution of the minusuperspace LQC equations. However, as long as the null-dust does not already display strong quantum gravitational effects by its mass profile, this solution should hold to good

accuracy[1].

We start by making a coordinate transformation and rewrite the static space-time in terms of the ingoing null-coordinate v. It is defined by the relation $dv = dt + dr/\sqrt{F(r)G(r)}$, which can be solved to obtain an explicit expression for v. The metric then takes the form

$$ds^2 = -G(r)dv^2 + 2\sqrt{\frac{G(r)}{F(r)}}\,drdv + H(r)d\Omega\,. \tag{10.5}$$

Now we allow the mass m in the static solution to depend on the advanced time, $m \to m(v)$. Thereby, we will assume the mass is zero before an initial value v_a and that the mass stops increasing at v_b. We can then, as before, use the Einstein equations $G = 8\pi\widetilde{T}$ to obtain the effective quantum gravitational stress-energy tensor $\widetilde{T}$. $\widetilde{T}^v_{\ v}$ and $\widetilde{T}^r_{\ r}$ do not gain any new terms through the dependence of m on v. The transverse pressure $\widetilde{T}^\theta_{\ \theta} = \widetilde{T}^\phi_{\ \phi}$ however has an additional term

$$\widetilde{T}^\theta_{\ \theta}(m(v)) = \widetilde{T}^\theta_{\ \theta}(m) - \frac{Pr^2m'(v)}{2\pi(r+2m(v)P)^4}\,, \tag{10.6}$$

where $m' = dm/dv$. Remember that P here is given by Eq.(10.3) and in the limit where the polymeric parameter goes to zero, so does P and so the transverse pressure goes to zero. Because of the ingoing radiation, the stress-energy-tensor now also has an additional non-zero component, $\widetilde{T}^r_{\ v}$, which describes radially ingoing energy flux

$$G^r_{\ v} = \frac{2(1+P)^2r^4(r^4-a_0^2)(r-r_*(v))m'(v)}{(a_0^2+r^4)^2(r+r_*(v))^3}\,. \tag{10.7}$$

[1]It has been claimed in [14] that, counterintuitively, quantum gravitational effects could become important already at the horizon when the collapse proceeds slowly. However, since we are considering null-dust, the collapse is as fast as can possibly be and these considerations do not apply.

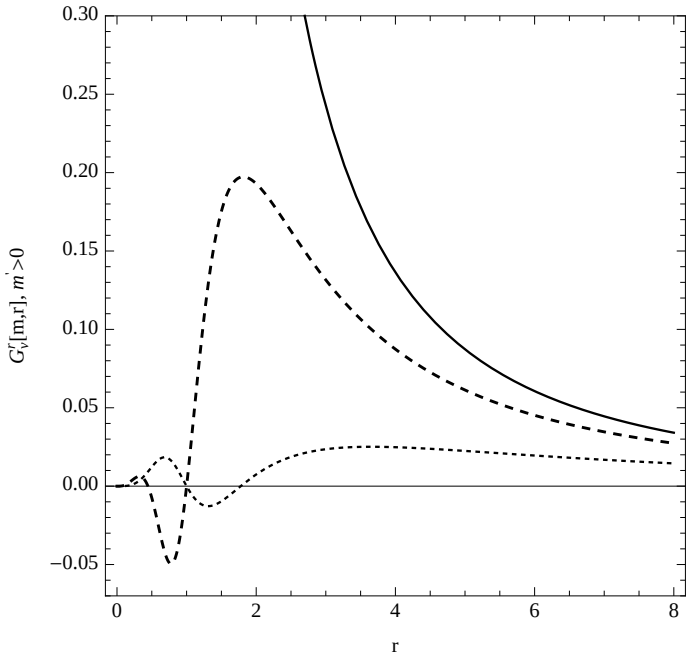

Figure 10.2: $G^r_{\ v}$ as a function of r for radially ingoing radiation and $m'(v) = 1$. The solid line depicts the classical case for $\epsilon, a_0 \to 0$. The long dashed line is for $m(v) = 20$, ($r_* > \sqrt{a_0}$) and the short dashed line is for $m(v) = 5$, ($r_* < \sqrt{a_0}$). All quantities are in Planck units.

Notice that also in the dynamical case, trapping horizons still occur where $g^{rr} = F(r, v)$ vanishes [47, 9], so we can continue to use the notation from the static case just that $r_\pm(v)$ and $r_*(v)$ are now functions of v. The r-dependence of this component is depicted in Fig 10.2.

This metric reduces to the Vaidya solutions at large radius, or for $\epsilon \to 0, a_0 \to 0$. However, in the usual Vaidya solutions, the ingoing radiation creates a central singularity. But as we see here, with the quantum gravitational correction, the center remains regular.

We note that the ingoing energy flux has two zeros, one at $r = r_*(v)$ and one at $r = \sqrt{a_0}$, and is negative between these. What happens is that the quantum gravitational correction works against the ingoing flux by making a negative contribution until the effective flux has dropped to zero at whatever is larger, the horizon's geometric mean r_* or the location

of the dual radius $r = \sqrt{a_0}$. The flux then remains dominated by the quantum gravitational effects, avoiding a collapse, until it has passed r_* and the dual radius where it quickly approaches what looks like an outgoing energy flux to the observer in the second asymptotic region.

Since in the second asymptotic region A, A' the mass assigned to the white hole is inversely proportional to the ADM mass at $r = \infty$, the white hole's mass must be decreasing, consistent with the outgoing (or rather throughfalling) energy flux. In this process, the past horizon will move towards smaller R or larger r, respectively.

10.3 Initial Conditions and Thermodynamics

Particle creation, from Hawking radiation, can take place at the horizons r_+ and r_- where there is high blueshift when tracing back lightrays. However, referring to Fig. 10.1, if the vacuum at $\mathcal{I}^-$ in the black hole's asymptotic region B, B' is empty of particles as usual, then there will be no flux from particle creation at r_- to $\mathcal{I}^+$ in the second asymptotic region A, A'. This is a consequence of causality and energy conservation, which we can see as follows.

Suppose there were particle creation at r_- resulting in a flux of Hawking radiation towards $R = \infty$. This is the time-reversed situation of the usual black hole radiation, and would mean a decrease of the white hole's mass for the observer at $R = \infty$. However, since our metric is geodesically complete, the particles emitted at the white hole's horizon r_- can be traced back all the way to $\mathcal{I}^-$ in the black hole's asymptotic region B, B'. We recall that the white hole's mass for the observer in the A, A' region is inversely proportional to the

black hole's mass and see that this particle creation at r_- would contribute to an increase of the black hole's mass corresponding to the decrease of the white hole's mass. Since there is particle emission also at the other horizon r_+, we would have to add both fluxes to obtain the net mass change.

However, we do as usual have a choice for the initial vacuum state at $\mathcal{I}^-$ and we will assume as normally that the vacuum in the black hole's asymptotic past is empty. From the above explanation we see now that this can only be the case if there is no particle flux from r_- to the white hole's asymptotic region $\mathcal{I}^+$. To achieve this, we have to chose the vacuum at $\mathcal{I}^-$ in the white hole's asymptotic region A, A' such that it contains a constant flux into the white hole with the effect that there is no outgoing particle flux created at r_-. This is the time-reversed situation of an evaporating black hole with an empty ingoing vacuum. This situation is mathematically consistent because particle production in the curved background only tells us the relation between the ingoing and outgoing vacuum states, but not the vacuum states themselves. We thus chose the vacuum state at $\mathcal{I}^-$ in the white hole's asymptotic region A, A' such that at r_- there is no additional outgoing flux created [2].

Thus, the evaporation proceeds through the Hawking emission at r_+, and the black hole's Bekenstein-Hawking temperature, given in terms of the surface gravity κ by $T_{BH} = \kappa/2\pi$, yields Eq.(8.2)

$$T_{BH}(m) = \frac{(2m)^3(1-P^2)}{4\pi[(2m)^4 + a_0^2]} \, . \tag{10.8}$$

[2] Alternatively, we could demand the vacuum at past infinity in the second asymptotic region to be free of particles, but then the vacuum in the black hole region's past infinity would have to contain particles. We will not further consider this possibility here.

This temperature coincides with the Hawking temperature in the limit of large masses but goes to zero for $m \to 0$.

The luminosity can be estimated by use of the Stefan-Boltzmann law $L(m) = \alpha A_H(m) T_{BH}^4(m)$, where (for a single massless field with two degrees of freedom) $\alpha = \pi^2/60$, and $A_H(m) = 4\pi[(2m)^2 + a_0^2/(2m)^2]$ is the surface area of the horizon. Inserting the temperature, we obtain

$$L(m) = \frac{16\, m^{10} \alpha\, (1-P^2)^4}{\pi^3 (a_0^2 + 16\, m^4)^3}\ . \tag{10.9}$$

The mass loss of the black hole is given by $-L(m)$,

$$\frac{dm(v)}{dv} = -L[m(v)] \tag{10.10}$$

and we can integrate its inverse to obtain the mass function $m(v)$. The result of this integration with initial condition $m(v=0) = m_0$ is

$$\begin{aligned} v = & \frac{5a_0^6 + 432 a_0^4 m^4 + 34560 a_0^2 m^8 - 61440 m^{12})\pi^3}{720 m^9 (1-P^2)^4 \alpha} \\ & - \frac{5a_0^6 + 432 a_0^4 m_0^4 + 34560 a_0^2 m_0^8 - 61440 m_0^{12})\pi^3}{720 m_0^9 (1-P^2)^4 \alpha}\ . \end{aligned} \tag{10.11}$$

In the limit $m \to 0$ this expression becomes $v \approx a_0^6 \pi^3/(144 m^9 (1-P^2)^4 \alpha)$, and one thus concludes that the black hole needs an infinite amount of time to completely evaporate.

10.4 Collapse and Evaporation

We are now well prepared to combine formation and evaporation of the black hole. As in section 10.2, we divide space-time into regions of advanced time. We start with empty space before v_a, let the mass increase from v_a to v_b, and stop the increase thereafter. Hawking radiation will set in, but for astrophysical black holes this evaporation will proceed very slowly, such that we have a long time span during which the black hole is quasi-stable and m remains constant to good accuracy at m_0. Then, at some later time, v_c, Hawking radiation becomes relevant and m decreases until it reaches zero again. As we have seen in the previous section, it will reach zero only in the limit $v \to \infty$.

We thus have the partition $-\infty < v_a < v_b < v_c < \infty$ with

$$\forall v \in (-\infty, v_a) : m(v) = 0, \qquad \text{[Region B1 in Fig. 10.3]} \tag{10.12}$$

$$\forall v \in (v_a, v_b) : d/dv\, m(v) > 0, \qquad \text{[Regions B2,C2 and A'2 in Fig. 10.3]} \tag{10.13}$$

$$\forall v \in (v_b, v_c) : m(v) = m_0, \qquad \text{[Regions B3, C3 and A'3 in Fig. 10.3]} \tag{10.14}$$

$$\forall v \in (v_c, +\infty) : d/dv\, m(v) < 0, \qquad \text{[Regions B4, B5, C4 and A'4 in Fig. 10.3]} \tag{10.15}$$

$$\text{for } v \to +\infty : m(v) \to 0. \tag{10.16}$$

Strictly speaking the mass would immediately start dropping without incoming energy flux and thus $v_a = v_b$, but stretching this region out will be more illuminating to clearly depict the long time during which the hole is quasistable.

To describe the Hawking-radiation we will consider the creation of (massless) particles on the horizon such that locally energy is conserved. We then have an ingoing radiation

with negative energy balanced by outgoing radiation of positive energy. Both fluxes originate at the horizon and have the same mass profile which is given by the Hawking temperature. The area with ingoing negative density is again described by an ingoing Vaidya solution, while the one with outgoing positive density is described by an outgoing Vaidya solution.

The outgoing Vaidya solution has a mass-profile that depends on the retarded time u instead of v and the mass decreases instead of increases. The retarded time is defined by $du = dt - dr/\sqrt{F(r)G(r)}$. After a coordinate transformation, the metric reads

$$ds^2 = -G(r,u)du^2 - 2\sqrt{\frac{G(r,u)}{F(r,u)}}dudr + H(r)d\Omega\,, \tag{10.17}$$

where $F(r,u)$ and $G(r,u)$ have the same form as in the static case (10.2), but with where m is replaced by a function $m(u)$. We fix the zero point of the retarded time u so that $r = r_+$ corresponds to $u_c = v_c$. Then there is a static region with total mass m_0 for $v > v_c$, $u < u_c$. Note that since the spacetime described here has neither a singularity nor an event horizon, we can consider pair creation to happen directly at the trapping horizon instead of at a different timelike hypersurface outside the horizon, as done in [50]. We have in this way further partitioned spacetime in regions, broken down by retarded time:

$$\forall u < u_c \quad : \quad m(u) = m_0\,, \tag{10.18}$$

$$\forall u > u_c \quad : \quad d/du\, m(u) < 0\,. \tag{10.19}$$

Now that we have all parts together, let us explain the complete dynamics as depicted

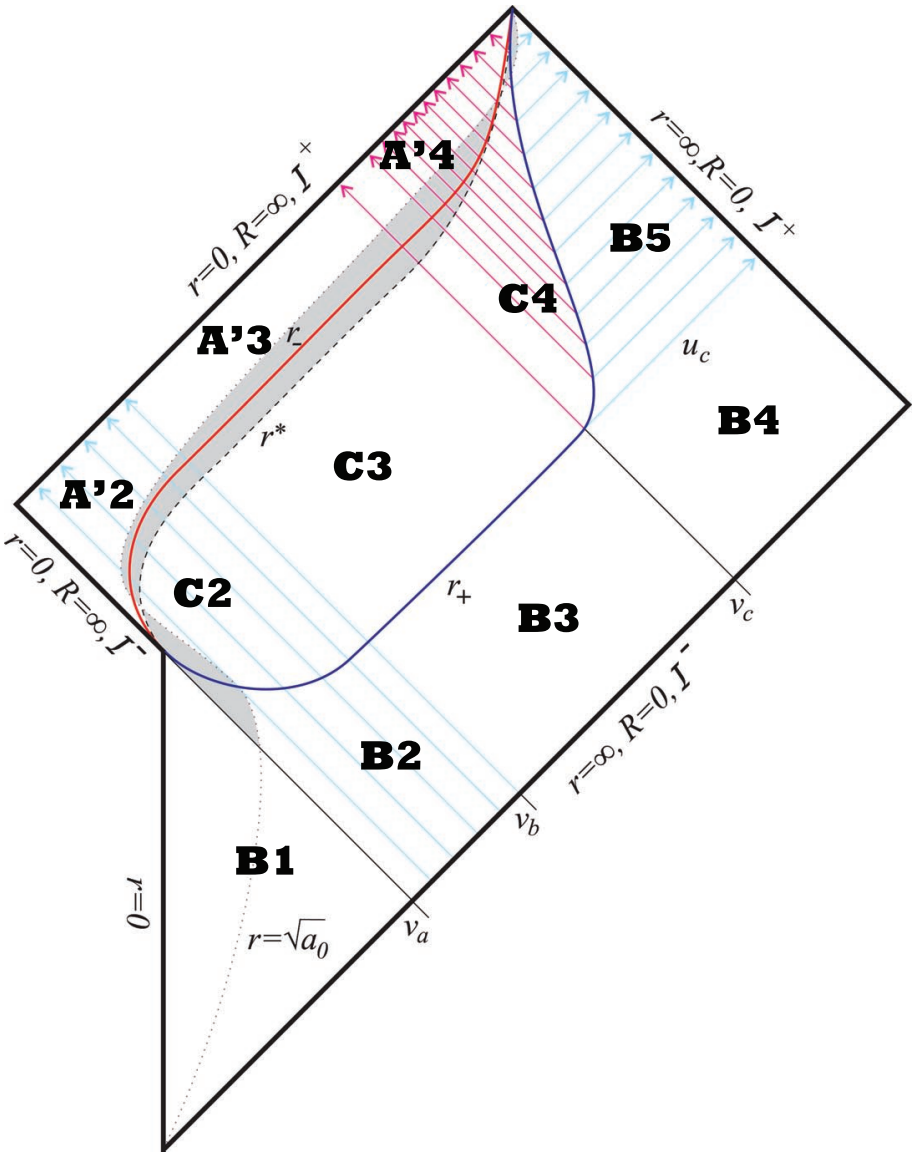

Figure 10.3: Penrose diagram for the formation and evaporation of the regular black hole metric. The red and dark blue solid lines depict the two trapping horizons r_- and r_+. The brown, dotted line is the curve of $r = \sqrt{a_0}$ and the black, short dashed one is r_*. The light blue arrows represent positive energy flux, the magenta arrows negative energy flux. The letter number combinations (B2 for example) label the different regions of the Penrose diagram. The letters are chosen to correspond with the letters in Fig. 10.1 so that all the B regions are outside the outer horizon, the C regions are all in between the two horizons and the A' regions are all on the other side of the white hole. The numbers refer to an interval of v (except for B5 which is in the same interval as 4). So for example, B2, C2 and A'2 are all inside the same interval of v. The initial conditions at $\jmath^-$ in region A'2 are given per section 10.3, different initial conditions would give a cross-flow arriving at $\jmath^+$ of B5.

in the resulting causal diagram Fig.10.3.

In the region $v < v_a$ we have a flat and empty region, described by a piece of Minkowski-space. For all times $v > v_a$, the inner and outer trapping horizons are present. These horizons join smoothly at $r = 0$ in an infinite time and enclose a non-compact region of trapped surfaces.

A black hole begins to form at $v = v_a$ from null dust which has collapsed completely at $v = v_b$ to a static state with mass m_0. It begins to evaporate at $v = v_c$, and the complete evaporation takes an infinite amount of time. The observer at $\mathcal{I}^+$ sees particle emission set in at some retarded time u_c which corresponds to the lightlike surface where the horizon has lingered for a long time. The region with $v > v_c$ is then divided into a static region for $u < u_c$, and the dynamic Vaidya region for $u > u_c$, which is further subdivided into an ingoing and an outgoing part.

As previously mentioned, the radially ingoing flux (light blue arrows) in the collapse region is not positive everywhere due to the quantum gravitational contribution. It has a flipped sign in the area between r_* (black short dashed curve) and $r = \sqrt{a_0}$ (brown dotted curve) which is grey shaded in the figure. Likewise, the ingoing negative flux during evaporation (magenta arrows) has another such region with flipped sign. It is in this region, between the two horizons' geometric mean value r_* and the dual radius corresponding to the minimal area, that the quantum gravitational corrections noticeably modify the classical and semi-classical case, first by preventing the formation of a singularity, and then by decreasing the black hole's temperature towards zero.

Chapter 11

Black Hole Dark Matter

In this chapter, modified from the corresponding section in [76], we investigate the possibility of having ultra-light quantum black holes as a major component of dark matter.

It is interesting to consider how the ultra-light LQBHs might manifest themselves if they do exist in nature. Because they are not charged, and are extremely light and have a Planck-sized cross-section (due to their Planck-sized wormhole mouth), and they interact only via their Hawking radiation and the particles they absorb, they will be very weakly interacting and hard to detect unless they are hot enough or unless we can prob the Planck scale. This is especially true as they need not be hot like a light Schwarzschild black hole, but they can be cold as can be seen in Fig.8.1. It is thus possible, if they exist, that ultra-light LQBHs are a component of the dark matter. In fact, due to (8.2), one would expect that all light enough black holes would radiate until their temperature cools to that of the CMB, at which point they would be in thermal equilibrium with the CMB and would be almost

impossible to detect. Rewriting (8.2) for small $\mathcal{P}(\delta_b)$ we get

$$T(m) = \frac{(2m)^3[1-\mathcal{P}(\delta_b)^2]}{4\pi[(2m)^4+a_0^2]} \approx \frac{(2m)^3}{4\pi[(2m)^4+a_0^2]}. \tag{11.1}$$

We thus see emerge a new phenomenon that was not present with Schwarzschild black holes: it is possible to have a black hole in a stable thermal equilibrium with the CMB radiation. In the Schwarzschild scenario, it is of course possible for a black hole to be in equilibrium with the CMB radiation, this happens for a black hole mass of 4.50×10^{22} kg (roughly 60% of the lunar mass). This equilibrium is however not a stable one because for a Schwarzschild black hole the temperature always increases as mass decreases (it has negative heat capacity) and vice versa (see the dashed line in Fig.8.1) and so if the black hole is a bit lighter than the equilibrium mass it will be a bit hotter than T_{CMB}, the temperature of the CMB radiation, and will emit more energy than it gains thus becoming lighter and lighter. Similarly, if the black hole has mass slightly larger to the equilibrium mass, it will be colder than T_{CMB} and thus absorb more energy than it emits, perpetually gaining mass. For the LQBH however, when m is smaller than the critical mass $\sqrt{a_0}/2$ of the order of the Planck mass, the black hole has positive heat capacity and the temperature increase monotonically with the mass, this allows for a stable thermal equilibrium in this region as is shown in Fig.11.1. However, for black holes even one order of magnitude heavier than m_{stable}, it would take many times the age of the universe (on average) for a black hole to reach equilibrium due to extremely weak Hawking radiation. In fact, on time scales of the age of the universe, black holes with a mass only one or two orders of magnitude smaller than the Planck mass can be treated as being stable. The values of the black hole mass in

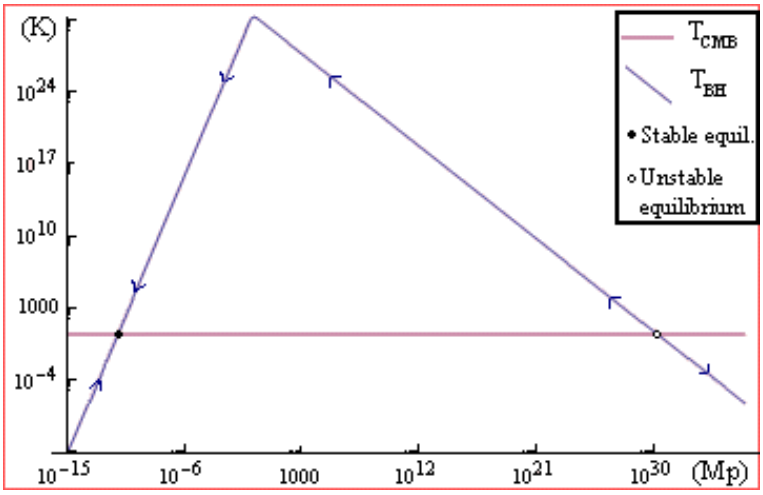

Figure 11.1: Log-log graph of (11.1) in units of Kelvin and Planck masses. The constant line denotes the temperature of the CMB radiation; above this line the black hole is hotter than the CMB and so it will lose more energy than it gains, below this line the black hole is colder than the CMB and so it will absorb more CMB radiation than it will emit radiation, thereby gaining mass. The arrows on the temperature curve denote in which direction the black hole will evolve through thermal contact with the CMB. At the two points where the temperature curve intersects the constant T_{CMB} curve, the black hole is in thermal equilibrium.

the two equilibrium positions in the LQG case are thus

$$m_{\text{unstable}} = 4.50 \times 10^{22}\,\text{kg},$$
$$m_{\text{stable}} \approx 10^{-19}\,\text{kg}, \tag{11.2}$$

where we have used $\gamma = 0.2375329...$ [71] for the Immirzi parameter and assumed $\beta \approx 1$. The unstable mass is essentially the same as in the Schwarzschild case while the stable mass, though it formally depends on the value of δ_b, it is quite insensitive to its exact value as long as δ_b is at most of the order of unity in which case m_{stable} (which is of the order of magnitude of the mass of the flu virus) is accurate to at least two decimal places.

The following picture thus emerges in LQG: black holes with a mass smaller than m_{stable}

grow by absorbing CMB radiation, black holes with a mass larger than m_{stable} but smaller than m_{unstable} evaporate towards m_{stable} and finally black holes with a mass greater than m_{unstable} grow by absorbing the CMB radiation.

11.0.1 LQBHs Production in the Early Universe

We can estimate the number of ultra-light LQBHs created as well as the extent of their subsequent evaporation. As exposed in [57], number density of black holes per Planck volume (where it assumed that there is order of unity degrees of freedom per Planck size) at local equilibrium coming from thermodynamic fluctuations is $\exp(-\Delta F/T)$, where ΔF is the change in the Helmholtz free energy and T is the temperature of the universe. From (8.3) and (11.1) the free energy of a LQBH of mass m is

$$F_{BH} = m - T_{BH}S_{BH} = m - \frac{1}{2}m\left[\frac{16m^4 - a_0^2}{16m^4 + a_0^2}\right], \tag{11.3}$$

where T_{BH} and S_{BH} are the temperature and entropy of the black hole respectively. The free energy for radiation inside the space where the black hole would form is

$$F_R = -\frac{\pi^2\kappa}{45}T^4V, \tag{11.4}$$

where V is the volume inside the 2-sphere which will undergo significant change (i.e. significant departure from the original flatness) in the event of a black hole forming. In the case of a black hole of mass $m \geq \sqrt{a_0}/2$, this is naturally the horizon. Since the horizon has an area of $4\pi[(2m)^2 + a_0^2/(2m)^2]$, we have that the volume of the flat radiation-filled space in which will undergo the transition to a black hole is $V = (4\pi/3)[(2m)^2 + a_0^2/(2m)^2]^{3/2}$.

However, as we saw earlier, for example in Fig.7.3 and 9.2, if $m \leq \sqrt{a_0}/2$, a throat of a wormhole forms at $r = \sqrt{a_0}$ and a large departure from flat space is observed. Since the mouth of the wormhole as area $A_{\text{Min}} = 8\pi a_0$ we have that the volume of flat space which will be perturbed to create the black hole is $V = (4\pi/3)(2a_0)^{3/2}$. In (11.4) κ depends on the number of particles that can be radiated where $\kappa = 1$ if only electromagnetic radiation is emitted and $\kappa = 36.5$ if all the particles of the Standard Model (including the Higgs) can be radiated. Hence, if we define

$$\Delta F = F_{BH} - F_R \tag{11.5}$$

to be the difference between the black hole free energy and the radiation free energy inside the volume which is to be transformed, we have, in Planck units, that the density of black holes of mass m coming from fluctuations is of the order of

$$\rho(m) \approx \frac{1}{\pi^3} \exp(-\Delta F/T), \tag{11.6}$$

where ρ is here expressed in number density per Planck volume. Plotting ρ as a function of T, (see for example Fig.11.2) we see that ρ peaks at a given temperature which is of order T_P for a black hole mass of order m_P. If we imagine that the universe started in a hot Big Bang and gradually cooled, looking at Fig.11.2, we see that at very high temperatures the amount of black holes of a given mass created from fluctuations is relatively small. Then as the universe starts to cool, the number of black holes increases until it reaches a maximum value at $T_{Max}(m)$ (see Fig.11.3) at which point, when the universe cools further,

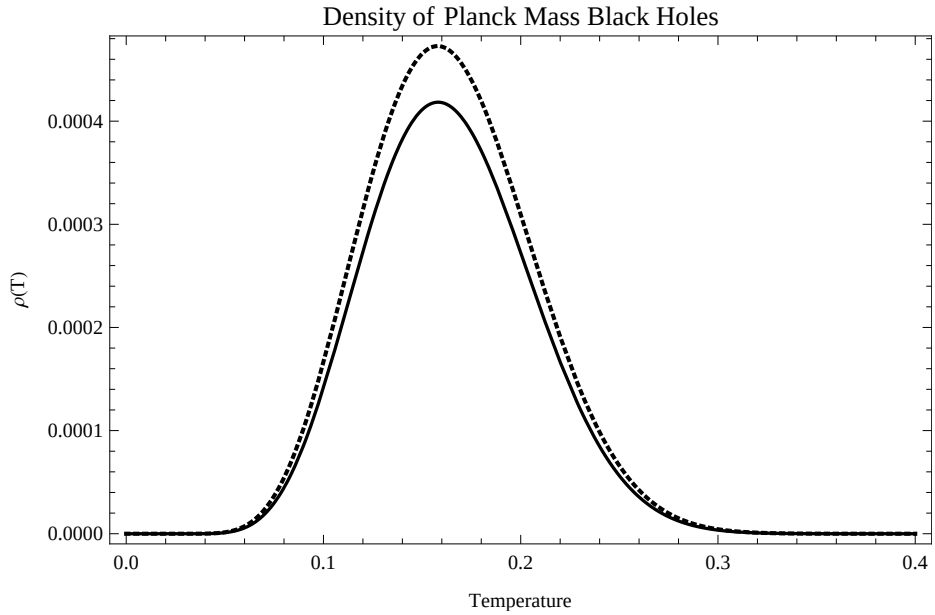

Figure 11.2: $\rho(T)$, the LQBHs density created due to fluctuations for $m = 1$, and $a_0 = 0.5$ in Planck units (the value 0.5 here is chosen to amplify the difference with the classical Schwarzschild black hole). The dashed line represents the classical density for $a_0 = 0$.

no more black holes of mass m are created and the existing black holes start to evaporate. By varying Eq.(11.6) with respect to T, we find that $T_{Max}(m)$ the temperature for which the maximum amount of black holes are formed is

$$T_{Max}(m) = \begin{cases} \frac{\sqrt{3}5^{1/4}\left(m\left(3a_0^2+16m^4\right)\right)^{1/4}}{2^{9/8}\left({a_0}^{3/2}\left(a_0^2+16m^4\right)\kappa\right)^{1/4}\pi^{3/4}} & \text{if } m \leq \sqrt{a_0}/2, \\ \frac{\sqrt{3}m5^{1/4}\left(3a_0^2+16m^4\right)^{1/4}}{\left(a_0^2+16m^4\right)^{5/8}\kappa^{1/4}\pi^{3/4}} & \text{if } m \geq \sqrt{a_0}/2. \end{cases} \tag{11.7}$$

Combining Eq.(11.6) and Eq.(11.7), we can obtain the maximal primordial density of black holes ρ_{max}. Fig.11.4 is a graph of this quantity in Planck units and for $\beta = 4$. One more subtlety however must be considered before the number of black holes produced can be calculated. Formula Eq.(11.6) is only valid if the universe can reach local equilibrium. If the time scale for the expansion of the universe is much shorter than the time scale for

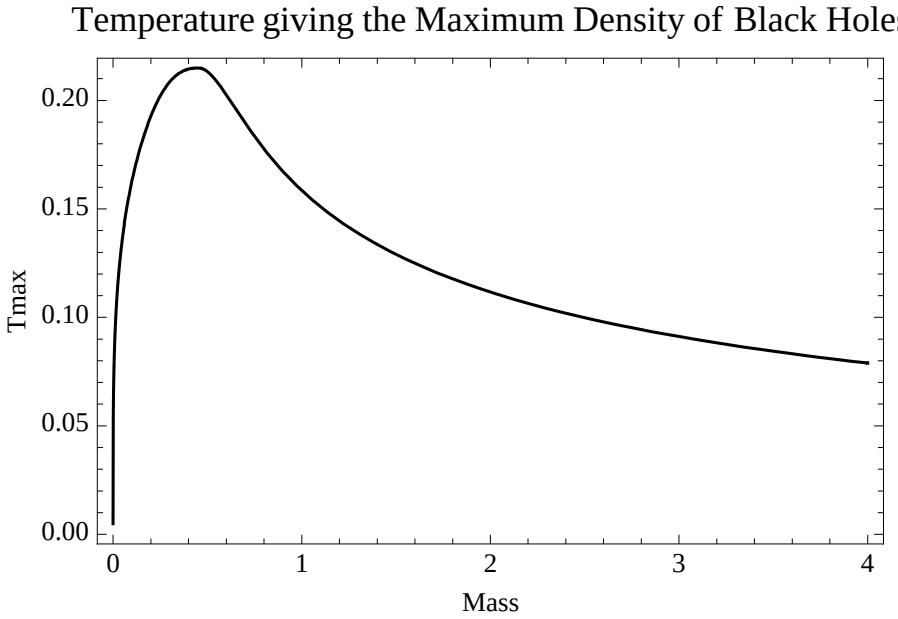

Figure 11.3: The temperature T_{Max} (Eq.(11.7)) at which the density of black holes created through fluctuations is maximised as a function of the mass of the black holes in Planck units. Observe that the temperature is of the order of the Planck temperature T_P in the given mass range. Here we used $\beta = 4$.

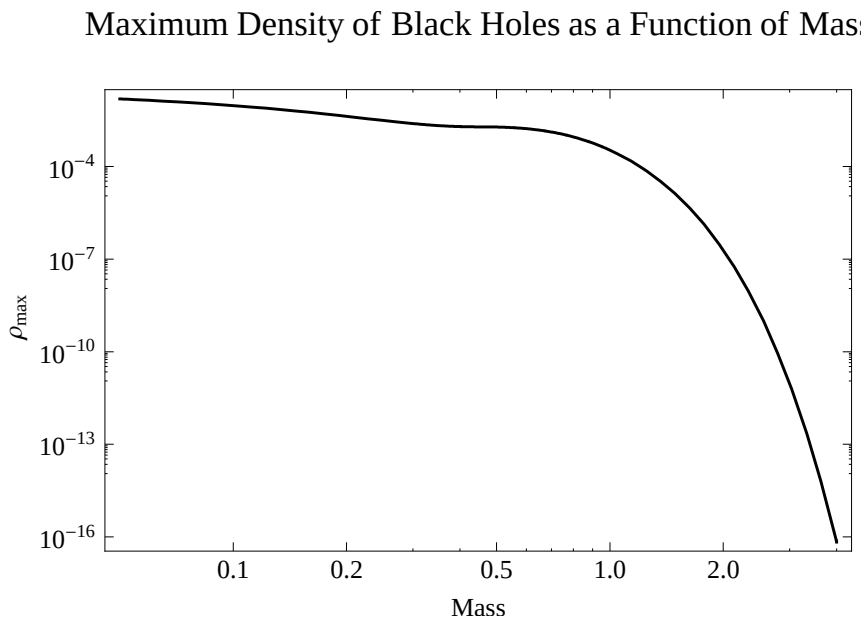

Figure 11.4: The maximal value of $\rho(m,T) \approx \exp(-\Delta F/T)/\pi^3$ as a function of the mass m. The value of the temperature T at which the maximal value of ρ is attained is plotted in Fig.11.3. Both the mass m and the temperature are in Planck units. Here we used $\beta = 4$.

collisions between the particles, the universe expands before equilibrium can take place and so Eq.(11.6), which requires equilibrium, is not valid. It can be shown [77], that local equilibrium is reached for temperatures

$$T \ll 10^{15}\text{GeV} - 10^{17}\text{GeV}. \tag{11.8}$$

This comes from equating the reaction time of matter $t_c \approx 1/\sigma n v$ with the typical expansion time of the universe $t_H \approx 1/T^2$ in the radiation dominated era, where $\sigma \approx \alpha^2/T^2$ is the effective crossection, $n \approx T^3$ is the number density for ultrarelativistic species, $v \approx 1$ is the typical speed of the particles and α is the dimensionless running coupling constant. This means that before the universe cooled down to temperatures below 10^{15}GeV, the universe expanded too quickly to have time to create black holes from fluctuations in the matter density. The fact that the universe must first cool down to below 10^{15}GeV before black holes can be created means that black holes of mass m will not be created at temperature $T_{Max}(m)$ of Eq.(11.7) but rather at temperature $T_{cr}(m) = \min\{T_{Max}(m), T_{eq}\}$ where $T_{eq} \lesssim 10^{15}$GeV is the temperature below which local equilibrium can be achieved and thus black holes can be created. As can be seen in Fig.11.5, this means that for a significant range of black hole masses, from about $10^{-17}\, m_P$ to $10^{8}\, m_P$ the maximal density will be created when the universe reaches temperature T_{eq}. As it turns out, this range will encompass the quasi-totality of black holes responsible for dark matter or any other physical phenomenon considered in what follows. The fact that black holes are created only once the universe

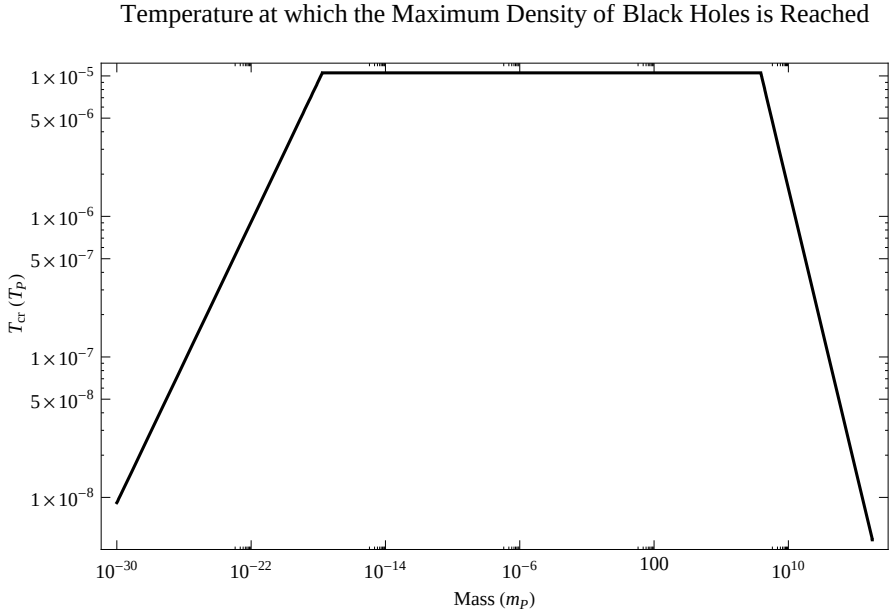

Figure 11.5: The temperature T_{cr} at which the density of black holes created through fluctuations is maximised as a function of the mass of the black holes in Planck units where we take into consideration the fact that for temperature higher than $T_{eq} \lesssim 10^{15}$GeV black holes do not have time to form because of the rapid expansion. Here we used $\beta = 4$ and $T_{eq} = 13\% \times 10^{15}$GeV. We note that for the physically relevant range $10^{-17}\, m_P \leq m \leq 10^{8}\, m_P$, $T_{cr}(m) = T_{eq}$; this is the case for all T_{eq} between 1% and 100 % of 10^{15}GeV.

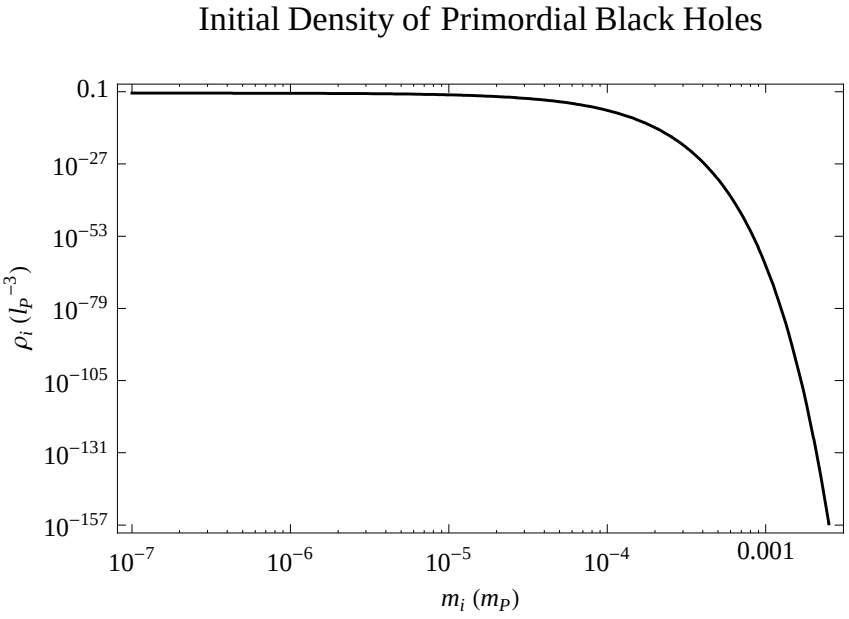

Figure 11.6: The initial density of primordial black holes as given by Eq.(11.9) as a function of the initial mass of the black hole. Both the mass m and the temperature are in Planck units. Here we used $\beta = 4$ and $T_{eq} = 13\% \times 10^{15}$GeV. The choice of T_{eq} is significant here because the density is very sensitive to T_{eq}.

has cooled down to T_{eq} entails that the initial density of black holes is

$$\rho_i(m) \approx \frac{1}{\pi^3} \exp(-\Delta F(m)/T_{cr}(m)), \tag{11.9}$$

(where the dependencies on the black hole mass m are explicitly written) and not of the density plotted in Fig.11.4. Graphing Eq.(11.9), we see in Fig.11.6 that only black holes with an initial mass of less then $10^{-2}\, m_P$ are created in any significant numbers.

We are thus presented with the following picture: as the temperature cools from the Big Bang, and the expansion of the universe starts to slow down, fluctuations of the matter start producing Ultra-light black holes of a hundreth of a Planck mass and less, as can be seen from Fig.11.6. Once this initial density of black holes is formed and the universe

starts cooling further, these primordial black holes will start to evaporate since they will be hotter than the surrounding matter.

11.0.2 Evaporation of Ultra-light LQBHs

Once the black holes are formed, the only way they can disappear is through evaporation. When the mass, m, of a black hole satisfies $m \geq \sqrt{a_0}/2$, the LQBHs evaporate like a Schwarzschild black hole would:

$$\frac{dm}{dt} = \frac{\pi^2}{60} A(m) T^4 - \frac{\pi^2}{60} A(m) (T_{BH}(m))^4, \tag{11.10}$$

where $\pi^2/60$ is Stefan-Boltzmann's constant in Planck units, $A(m)$ is the area of the LQBH horizon, T is the temperature of the radiation in the universe and $T_{BH}(m)$ is the temperature of the LQBH. So the first term in the last equation represents the radiation absorbed by the black hole while the second term is the radiation emitted by the black hole. Things take on a new twist however when the mass falls below $\sqrt{a_0}/2$, which will happen within 1000 years of the Big Bang for black holes created with an initial mass of less than $100\, m_P$. As illustrated in Fig.9.2a the black hole horizon, as well as the space surrounding it, is separated from the rest of the universe by a wormhole of Planckian diameter. The wormhole as well the chunk of space surrounding the horizon form very slowly and gradually as can be seen from (8.8,8.9). So we can divide space in three parts: 1) the inside of the black hole, 2) a relatively small (compared to the rest of the universe) bag of space in between the black hole horizon and the mouth of the wormhole and 3) (infinite) flat space outside of the mouth of the wormhole. Theoretically, these three subsystems could be at three different

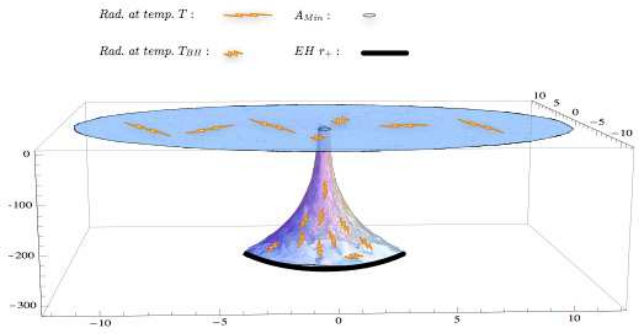

Figure 11.7: The black hole horizon and its accompanying patch of space are in thermal equilibrium at temperature T_{BH}. The rest of the universe has radiation in thermal equilibrium at temperature T. The two can interact radiatively through a Planckian surface of area $A_{\rm Min}$.

temperatures. However, because the size of the horizon of the black hole is greater than the size of the mouth of the worm-hole ($4\pi(2m)^2 + a_0^2/(2m)^2 > 4\pi(2a_0)$) and becomes ever more so as the black hole gets smaller, the bag of space between the horizon and the mouth of the wormhole will thermalise faster with the black hole than with flat space. Since the bag also starts out with a very small volume and this volume changes only slowly, the thermalisation of the bag with the black hole happens rather rapidly (on on Hubble time scales). Hence, for cosmological purposes, we can suppose that the black hole and the bag of radiation between the horizon and the mouth of the wormhole are in thermal equilibrium at the temperature of the black hole, T_{BH}, and that the combined system interacts via thermal radiation with the outside flat space through the Planck-sized mouth of the wormhole which has area $A_{\rm Min}$. We shall label the temperature of the radiation in the flat space (the CMB) T. This situation is illustrated in Fig.11.7. The volume of the bag of space

between the horizon and the mouth of the wormhole is

$$\begin{aligned} V_{bag} &= \int_{r=2m}^{\sqrt{a_0}} 4\pi g_{\theta\theta}\sqrt{g_{rr}}dr \\ &\approx \frac{8a_0^{3/2}\sqrt{a_0 - 4\sqrt{a_0}\,m}\left(a_0 + 2\sqrt{a_0}\,m + 6m^2\right)\pi}{15m^3}, \end{aligned} \tag{11.11}$$

if δ_b is of the order of unity or less (which is the natural choice). This is an approximation, the equation is precise up to a factor of $1 < \chi(m) < 2^{\frac{3}{2}}$. As it turns out though, the worm-hole radiation term is not at all significant for the value and precision considered here. However, for completeness, we will include it. The energy density of thermal radiation at temperature T is $\pi^2 T^4/15$. Thus the energy of the combined black hole and bag of space in thermal equilibrium with it between the horizon and the mouth of the worm-hole is $m + \pi^2\, V_{bag}\, T_{BH}^4/15$. Writing the conservation of energy considering that the two systems (LQBH+ bag and flat space) interact via black body radiation through the mouth of the worm-hole, we get:

$$\begin{aligned} &\frac{d}{dt}\left[m + \left(V_{bag}(m)\,\frac{\pi^2}{15}(T_{BH}(m))^4\right)\right] \\ &\quad = \frac{\pi^2}{60}A_{\rm Min}T(t)^4 - \frac{\pi^2\kappa}{60}A_{\rm Min}(T_{BH}(m))^4, \end{aligned} \tag{11.12}$$

where possible curvature corrections have been neglected. We have used that the power of the thermal radiation (in Planck units) emitted by a black body is of surface area A and temperature T obeys the Stefan-Bolzmann law:

$$P = \frac{\pi^2\kappa}{60}A\,T^4, \tag{11.13}$$

where κ depends on the number of particles that can be radiated. $\kappa = 1$ if only electromagnetic radiation is emitted and $\kappa = 36.5$ if all the particles of the Standard Model (including the Higgs) can be radiated. As we will be dealing with extremely hot temperatures at which all the Standard Model particles are relativistic and thus all particles can be emitted, we will be using $\kappa = 36.5$ in what follows though in fact it will make no difference whether we use $\kappa = 1$ or $\kappa = 36.5$. Using (11.1, 11.11) and approximating $T(t) \approx T_{CMB}(t_0/t)^{2/3}$, where T_{CMB} is the temperature of the cosmic microwave background today and t_0 is the age of the universe we obtain Eq.(11.14). We can make this simplification because this is the equation for the temperature of radiation in a matter dominated universe, and the length of time for which the universe was not matter dominated is negligible in standard cosmology for our purposes. This allows us to calculate the masses of the ultra-light black holes today numerically. We find that, all black holes that initially started with mass $m_i = 0.001\, m_P$ are de facto stable: the difference between the initial mass m_i and the mass of the black hole today m_0 satisfies

$$\frac{m_i - m_0}{m_i} \approx 10^{-14}, \tag{11.14}$$

where we have taken $\beta = 4$ (but the result is not sensitive to the exact value of β) and for smaller initial masses the difference is even smaller. In Fig.11.8 are represented different value of the mass m_0 of a LQBH today as a function of it's initial mass m_i.

If, for example, we consider a LQBH of mass $m_0 = 0.000635\, m_P$, by Wien's Law they

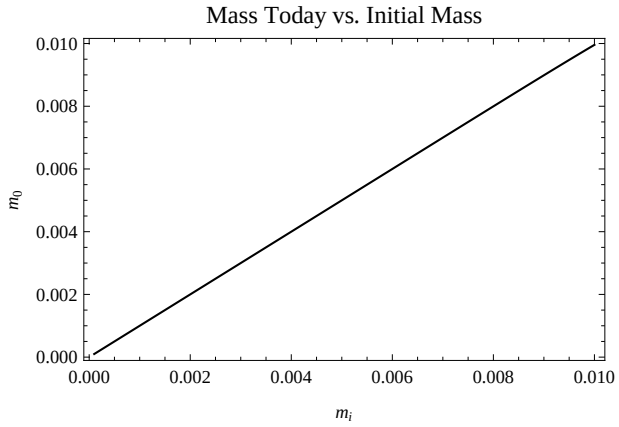

Figure 11.8: The mass today m_0 of a black hole created with mass m_i during the Big Bang. Both masses are in Planck units. m_0 is obtained from m_i through Eq.(11.12) ($\beta = 4$).

radiate with maximum intensity at

$$E_\gamma = 2\pi\, m_P \left(\frac{\omega_b}{l_P T_P} \frac{1}{T_{BH}(m)} \right)^{-1} \approx 1.46 \times 10^{19} \mathrm{eV}. \tag{11.15}$$

Where $\omega_b = 2.897768551 \times 10^{-3}\,\mathrm{mK}$, m_P is the Planck mass in eV's and T_P is the Planck temperature in Kelvins. This means that the ultra-light black holes would not have had time, in the life-time of the universe, to thermalise with the CMB. This does not stop them from being very stable in any case as the calculated value of m_0 above shows. The mass m_0 in eV is $m_0 \approx 7.75 \times 10^{24}\,\mathrm{eV}$ and the temperature in degrees Kelvin is $T(m_0) \approx 3.44 \times 10^{22}\,\mathrm{K}$.

11.0.3 Number of e-folds Elapsed Since LQBHs Creation to Account for Dark Matter

For all values of the initial black hole mass m_i, we know, thanks to Eq.(11.12) what the black hole's current mass is. We also know what the initial concentration of each type of

black hole was from Eq.(11.9). In addition, we know that the current matter density for dark matter is approximately $0.22\rho_{crit}$. If we now suppose that currently all dark matter is actually composed of ultra-light black holes, we have that

$$\int_0^\infty \frac{(a(t_i))^3 m_0(m_i)\rho_{max}(m_i)}{(a(t_0))^3} dm_i = 0.22\rho_{crit}, \tag{11.16}$$

where $a(t_0)$ is the scale factor of the Universe at present (t_0), $a(t_i)$ is the scale factor of the universe when the primordial black holes were created (t_i) and so $\frac{(a(t_i))^3\rho_i(m_i)}{(a(t_0))^3}$ is the current number density of black holes of mass $m_0(m_i)$. Since the scale factor does not depend on m_i, we can rearrange this equation to find out the number of e-folds N_e that the universe is required to have expanded since the creation of the primordial black holes for the light black holes to form the totality of dark matter:

$$N_e := \ln\frac{a(t_o)}{a(t_i)} = \frac{1}{3}\ln\left(\frac{\int_0^\infty\ m_0(m_i)\rho_i(m_i)dm_i}{0.22\rho_{crit}}\right), \tag{11.17}$$

and

$$\frac{a_o}{a_i} := \frac{a(t_o)}{a(t_i)} = \left(\frac{\int_0^\infty\ m_0(m_i)\rho_i(m_i)dm_i}{0.22\rho_{crit}}\right)^{\frac{1}{3}}. \tag{11.18}$$

The integral in Eq.(11.17), is evaluated to give $1.58\times10^{-12}\,m_P\,l_P^{-3}$. This implies a number of e-folds between the creation of the black holes and the present day of

$$N_e \approx 85 \quad \text{and} \quad \frac{a_0}{a_i} \approx 10^{37}, \tag{11.19}$$

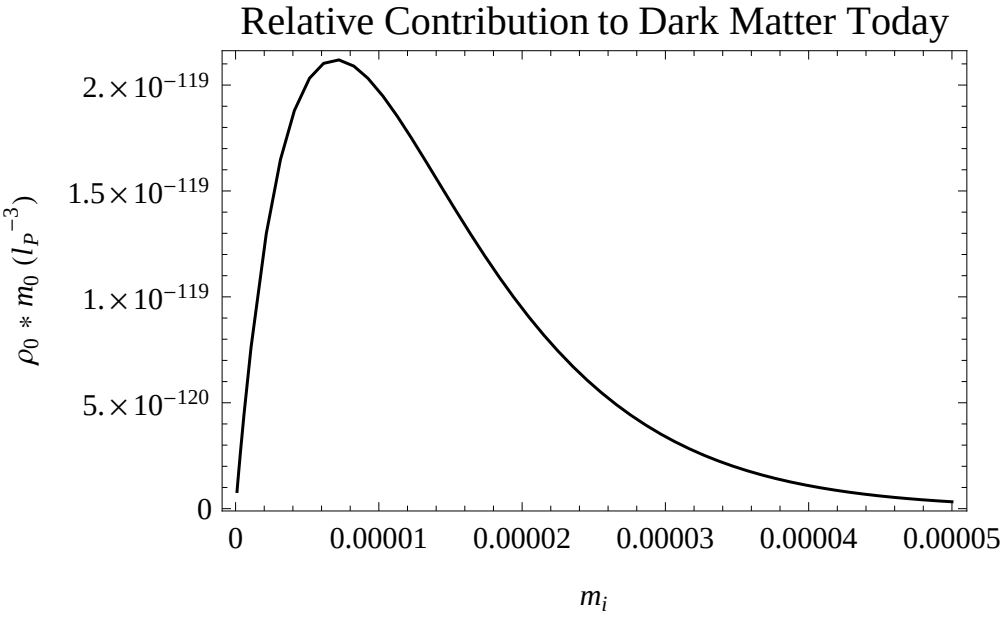

Figure 11.9: This graph shows the current mass density of black holes as a function of their initial mass m_i. $\rho_0(m_0)$ is the current number density of black holes of mass m_0, so $\rho_0 = \rho_i\,(a_i^3/a_0^3)$. Because, for all practical purposes, $m_0 = m_i$, the area under the curve is the present matter density due to LQBH. If that density is equal to $0.22\rho_{crit}$, the LQBH will account for all dark matter. From this graph, we see that at present times, LQBH mass density is entirely dominated by black holes which had an initial mass of about $10^{-5}m_P$. In this graph we have used $\beta = 4$ (the graph is not very sensitive to this choice) and $T_{eq} = 13\% \times 10^{15}$GeV (the numerical values of the graph vertical axis are sensitive to this value but location of the peak and the general shape of the graph are not).

where we have used $T_{eq} = 1.3 \times 10^{14}$GeV and $\beta = 4$ though these last two results are very robust under changes of T_{eq} and β.

Thus, if we want all dark matter to be explained by ultra-light black holes, then the universe must have expanded by a scale factor of 10^{37} between the creation of the black holes and the present day to achieve an ultra-light black-hole mass density of approximately $0.22\rho_{crit}$, the estimated dark matter density. Since the end of inflation, the universe has expanded by a scale factor of about 10^{26}. This implies that the ultra-light black holes have to be created towards the end of the period of inflation which means that inflation should be going on when the universe is at temperature of the order of 10^{14}GeV-10^{15}GeV.

This is indeed close to the range of temperatures at which inflation is predicted to happen in the simplest models of inflation (10^{14}GeV-10^{16}GeV). But because this model requires a radiation dominated universe, a double stage inflation would probably be needed. It is also possible that inflaton fluctuation could provide the same results but as it is not known what the inflaton is, it is more difficult to investigate.

So if black holes make up the majority of dark matter we have the following picture. Primordial black holes were created during an inflationary period when the universe had a temperature in the 10^{14}GeV-10^{15}GeV range. Since their creation the Universe has expanded by 85 e-folds. From Fig.11.9 we see that the majority of the black holes making up the dark matter would have been created with an initial mass of around $10^{-5}m_P$; Eq.(11.12) then implies that their mass has changed by less than 1 part in 10^{-14} since their creation making these black holes very stable. That is the case (due to the Planck-sized area of the mouth of the worm-hole) even though the radiation they emit is still very hot. From Wien's law we have that the maximum intensity of their radiation is for particles of energy of about 10^{13}eV.

Chapter 12

Ultra High Energy Cosmic Rays

As their Hawking radiation might be the only way for us to detect ultra-light LQBH, in this chapter, which is a modification of the equivalent section in [76], we investigate whether the Ultra High Energy Cosmic Rays (UHECR) might be the Hawking radiation of the ultra light LQBH composing dark matter.

Hot ultra-light black holes are very interesting phenomenologically because there is a chance we could detect their presence, through their radiation, if they are in sufficient quantities. The mass of ultra-light LQBHs today is $m_0 \approx 10^{24}\mathrm{eV}$. Therefore, the black holes forming the dark matter in our galaxy emit UHECR we could see. The question is: how much is emitted?

In fact, Greisen Zatsepin and Kuzmin proved that cosmic rays which have travelled over $50\,\mathrm{Mpc}$ will have an energy less than $6 \times 10^{19}\mathrm{eV}$ (called the GZK cutoff) because they will have dissipated their energy by interacting with the cosmic microwave background [38]. However, collaborations like HiRes or Auger [1] have observed cosmic rays with energies higher than the GZK cutoff, ultra high energy cosmic rays (UHECR). The logi-

cal conclusion is then that within a $50\,\mathrm{Mpc}$ radius from us, there is a source of UHECR. The problem is that we do not see any sources for these UHECR within a $50\,\mathrm{Mpc}$ radius[1]. The ultra-light LQBHs which we suggest could be dark matter do however emit UHECR. Could it be that these black holes not only constitute dark matter but are also the source for UHECR? This is not such a new idea, it has already been proposed that dark matter could be the source for the observed UHECR [16].

Let us compare the predicted emissions of UHECR from LQBHs with the observed quantity of UHECR. Detectors of UHECR, like Auger or HiRes, cover a certain surface area A_D and register events of UHECRs hitting their detector. Let us suppose that the source for UHECR is indeed the dark matter. It is believed that dark matter forms an halo (a ball) around the Milky Way of roughly the size of the Milky Way, let R_{MW} be the radius of the Milky Way. We suppose the dark matter is centred in the halo of the Milky Way. R_{MW} is then roughly $50000\,\mathrm{ly}$ (light-years). For the purpose of the following calculations, we can suppose that the Earth is on the outer edge of the Milky Way (in fact it is $30000\,\mathrm{ly}$ from the centre). If we then suppose that all the UHECRs we observe come from the matter halo of the Milky Way, and if the production rate (in particle of UHECR per metre cubed per second) of UHECR is σ ($[\sigma] = \mathrm{particles\ s^{-1}m^{-3}}$), then the halo produces $\frac{4\pi}{3}R_{MW}^3\sigma$ particles of UHECR per second. Since the Milky Way is in equilibrium, that means that $\frac{4\pi}{3}R_{MW}^3\sigma$ particles of UHECR per second cross the 2-sphere of area $4\pi R_{MW}^2$ enveloping the Milky Way and its halo. Thus, with a detector of area A_D on this 2-sphere, the detector should

[1]The Auger collaboration has found a correlation between the provenance of UHECR and nearby Active Galactic Nuclei (AGN). However, it is not know how AGN could produce UHECR. On the other hand, AGN are strongly correlated to dark matter distribution.

have a rate of detection of UHECR events of

$$R_E = \frac{A_D}{4\pi R_{MW}^2}\frac{4\pi}{3}R_{MW}^3\sigma = \frac{A_D R_{MW}\sigma}{3}. \tag{12.1}$$

Therefore we should have that

$$\sigma = \frac{3R_E}{A_D R_{MW}}. \tag{12.2}$$

Let us use Auger's data [1], for Auger we have that $A_D = 3000\,\mathrm{km}^2$ and $R_E = 3$ events per year. This gives us an observed σ of

$$\sigma_{obs} \approx 10^{-37}\,\frac{\text{UHECR particles}}{\text{s m}^3}. \tag{12.3}$$

We must compare this value with the predicted production of UHECR by LQBHs. Using Planck's Law, Eq.(11.1) and the fact that the bag is in equilibrium with the black hole and the pair radiates through the worm-hole mouth of area $A_{\mathrm{Min}} = 8\pi a_0$ we have that (in Planck units), the rate of emission of particles of energy ν by an ultra-light black hole is

$$R_{BH}(\nu, m_0) = \frac{2A_{\mathrm{Min}}}{\pi}\frac{\nu^2}{e^{\frac{\nu}{T_{BH}(m_0)}} - 1}. \tag{12.4}$$

This implies that the collective rate of emission of particles of energy ν by all primordial ultra light black holes, on average in the universe, is

$$R_{BH}(\nu) = \int_{m_0=0}^{\sqrt{a_0}/2} \rho_0(m_0)\frac{2A_{\mathrm{Min}}}{\pi}\frac{\nu^2}{e^{\frac{\nu}{T_{BH}(m_0)}} - 1}dm_0, \tag{12.5}$$

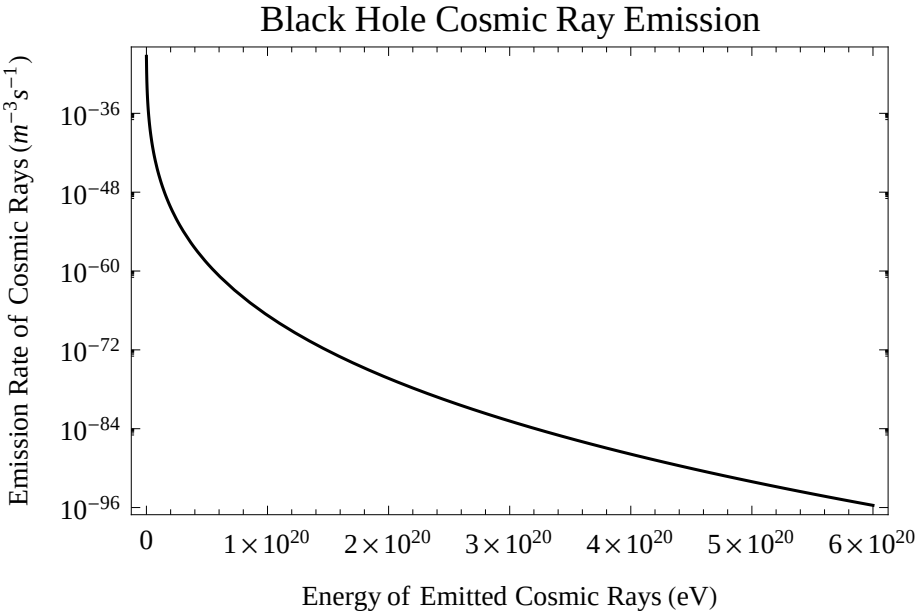

Figure 12.1: The average emission rate of particles by primordial ultra light black holes in the universe given by Eq.(12.5) assuming $\beta = 4$ and $T_{eq} = 1.3 \times 10^{14}$GeV.

where $\rho_0(m_0) = \rho_i(m_0)(a_i^3/a_0^3)$ is the present day number density of black holes of mass m_0. Eq.(12.5) is plotted in Fig.12.1. However, the local dark matter density is much larger than the average dark matter density in the universe. Hence there should be more radiation emitted in our local neighbourhood than on average in the universe. The dark matter density of the Milky Way halo, determined by the rotation curves, is calculated to be $\rho_{MWDM} = 0.3\,\mathrm{GeVcm}^{-3}$[23]. If we suppose that the distribution of ultra-light black holes in the Milky Way is the same as in the universe as a whole, we then have that

$$\rho_{MWBH}(m_0) = \frac{\rho_{MWDM}\,\rho_i(m_0)}{\int_{m=0}^{\infty}\rho_i(m)\,m\,dm}, \tag{12.6}$$

where $\rho_{MWDM}(m_0)$ is the number density of black holes of mass m_0 in the Milky Way at present. In this case, analogously to Eq.(12.5), we have that locally, the collective rate of

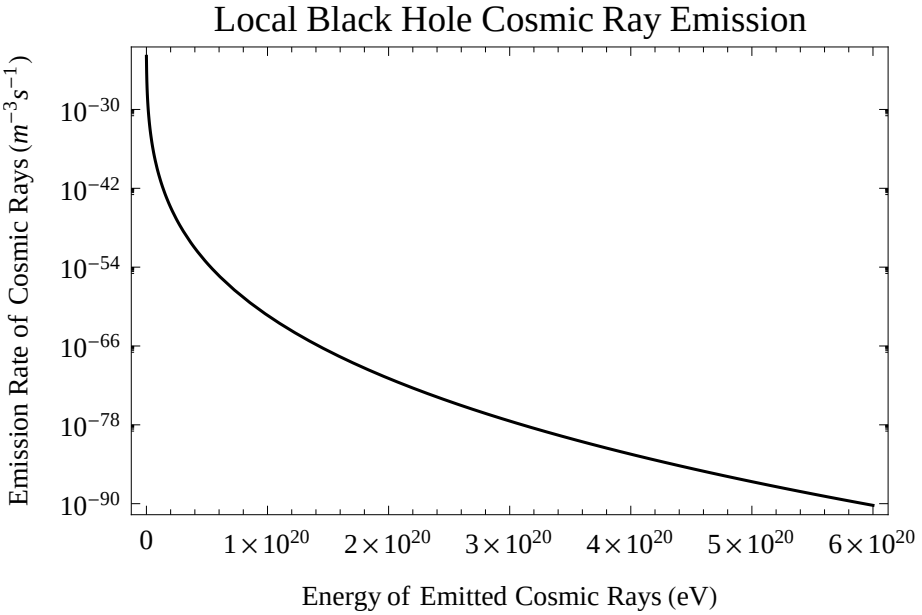

Figure 12.2: The local emission rate of particles by primordial ultra light black holes in the Milky Way given by Eq.(12.7) assuming $\beta = 4$ and $T_{eq} = 1.3 \times 10^{14}$GeV.

emission of particles of energy ν by all local primordial ultra light black holes is

$$R_{LocalBH}(\nu) = \int_{m_0=0}^{\sqrt{a_0}/2} \rho_{MWBH}(m_0) \frac{2A_{\rm Min}}{\pi} \times \frac{\nu^2}{e^{\frac{\nu}{T_{BH}(m_0)}} - 1} dm_0, \tag{12.7}$$

which is plotted in Fig.12.2. This implies a theoretical production rate of UHECR photons in the Milky Way of

$$\sigma_{th} = \int_{m_0=0}^{\infty} \int_{6\times10^{19}\,\mathrm{eV}}^{m_0} \frac{2A_{\rm Min}\,\rho_{MWBH}(m_0)\,\nu^2}{\pi(e^{\frac{\nu}{T_{BH}(m_0)}} - 1)} d\nu. \tag{12.8}$$

As it turns out, the result of σ_{th} is very robust for parameters except for T_{eq} on which σ_{th} is very sensitive. In order to agree with Eq.(12.3), we must have $T_{eq} \approx 13\% \times 10^{15}$GeV.

This is in great accordance with Eq.(11.8). If $T_{eq} \gg 13\% \times 10^{15}$GeV, then ultra light black holes cannot form the majority of dark matter, because if they did, they would emit much more ultra high energy cosmic rays than we observe. If $T_{eq} \ll 13\% \times 10^{15}$GeV, then it is still possible that ultra light black holes form the majority of dark matter but they cannot be the source of the ultra high energy cosmic rays that we observe because they will not radiate enough. Only if $T_{eq} \approx 13\% \times 10^{15}$GeV is it possible that dark matter consist mostly of ultra light black holes and that those black holes are simultaneously the source for the observed ultra high energy cosmic rays. Interestingly, it turns out that $T_{eq} \approx 13\% \times 10^{15}$GeV is consistent with the theory [77]. Furthermore, seeing as, appart from their mass and the fact that they radiate very slightly, the characteristics of the ultra-light LQBH are similar to traditional WIMPS, their effect on star formation and fusion models should be similar to WIMPS.

Chapter 13

Summary

In the previous chapters, we studied the new Reissner-Nordström-like metric obtained in the paper [74]. We recall the LQBH metric

$$ds^2 = -\frac{(r-r_+)(r-r_-)(r+r_\star)^2}{r^4+a_0^2}dt^2 + \frac{dr^2}{\frac{(r-r_+)(r-r_-)r^4}{(r+r_\star))^2(r^4+a_0^2)}} + \Big(\frac{a_0^2}{r^2}+r^2\Big)d\Omega^{(2)}. \tag{13.1}$$

The metric has two horizons that we have denoted r_+ and r_-; r_+ is the Schwarzschild event horizon and r_- is an inner horizon tuned by the polymeric parameter δ_b. The solution has many similarities with the Reissner-Nordström metric but without curvature singularities anywhere. In particular the region $r = 0$ corresponds to another asymptotically flat region. No massive particle can reach this region in a finite proper time. A careful analysis shows that the metric has a *Schwarzschild core* in $r \approx 0$ of mass $M \propto a_0/m$. We have studied the black hole thermodynamics : temperature, entropy and the evaporation process. The main results are the following. The temperature $T(m)$ goes to zero for $m \approx 0$

and reduces to the Bekenstein-Hawking temperature for large values of the mass. The black hole entropy in terms of the event horizon area is $S = \frac{A^2 - A_{\rm Min}^2}{4\sqrt{|A^2 - A_{\rm Min}^2|}}$.

We have investigated a model for collapse and evaporation of a black hole that is entirely singularity-free. The spacetime does not have an event horizon, but two trapping horizons. By generalising the previously derived static metric to a dynamical one by use of the Vaidya metric we found that the gravitational stress-energy tensor builds up a negative contribution that violates the positive energy condition and prevents the formation of a singularity. We divided spacetime into six different regions described by different metrics, and constructed the causal diagram for the complete evaporation. The value of the scenario studied here is that it provides a concrete, calculable, model for how quantum gravitational effects alter the black hole spacetime.

The evaporation process needs an infinite time in our semiclassical analysis but the difference with the classical result is evident only at the Planck scale. The fact that the black holes can never fully evaporate provides a possible resolution of the information loss paradox. Furthermore, we showed that because of the temperature profile of the LQBH, the fact that the temperature decreases for very light black holes, a black hole in thermal environment will never totally evaporate but will thermalise with the background. The CMB is such a background that can stabilise the ultra-light black holes. Since the horizon of an ultra-light LQBH is hidden behind a wormhole with a Planck size cross section, cold and light black holes could act as very weakly interacting dark matter. However the universe is not old enough for black holes created during the Big Bang to have cooled down to 2.7 K; they would still be excessively hot.

We know that in the very early universe ultra-light black holes cannot be created be-

cause the universe expands at rate which is much faster than the rate of collisions between particles. Particles of the Standard Model start colliding together at a rate faster than expansion of the universe when the temperature has cooled lower than 10^{15}GeV-10^{17}GeV. If we suppose that the temperature T_{eq} at which local equilibrium of the matter is achieved and thus black holes can be formed from fluctuations of the matter is 13% of 10^{15}GeV then ultra-light black holes can explain both dark matter and cosmic rays with energies above the GZK cut off.

Once the universe has cooled to 1.3×10^{14}GeV, ultra-light black holes, the overwhelming majority of which have a mass inferior to $5 \times 10^{-5} m_P$, would be created from matter fluctuations. These black holes are still very hot and radiate, but because they are hidden behind a Planck-sized wormhole, they do so very slowly and on average would lose less than 1 part in 10^{14} of their mass since their creation. For all practical purposes they are stable. If the universe has expanded by a scale factor of 10^{37} since their creation the mass of all these ultra-light black holes would exactly equal the mass of dark matter and they could explain the entirety of dark matter.

Since the universe has expanded by a scale factor of about 10^{28} since the end of inflation, and that it expanded by a scale factor of at least 10^{28} during inflation, the fact that universe has expanded by a scale factor of 10^{37} since the birth of the black holes would mean that the black holes would have been created during inflation. This in turn would mean that inflation would still be underway when the universe had temperature of 1.3×10^{14}Gev. This is very close to the simplest models of inflation which situates inflation at energy scales of 10^{15}GeV-10^{16}GeV.

In turn, if the black holes were created when the universe was at a temperature of

1.3×10^{14}GeV, then the amount of cosmic rays with energies higher than the GZK cut off that they would emit would correspond exactly to the amount of such radiation observed. Because they interact with the CMB, cosmic rays cannot travel more than 50 Mpc before seeing their energy fall below the GZK cut off: 6×10^{19}eV. However we do see particles with energies above the GZK cut off but we do not see any sources for such energetic particles within 50 Mpc from us. These energetic particles, dubbed ultra high energy cosmic rays are thus a mystery for the moment.

Hence in conclusion, ultra-light LQG black holes have the potential to resolve two outstanding problems in physics: "what is dark matter and where do the ultra high energy cosmic rays come from?" It is also noteworthy that much of these results do not actually depend on exact details of the black holes. The essential feature is that the temperature of the black holes goes to zero when their mass goes to zero, the results being very generic. It is thus likely that the same effect could be observed with non-commutative black holes and asymptotic safety gravity black holes [78] [21], both of which exhibit zero temperature at zero mass or for a remnant mass. The same analysis we think could be applied to the new Hořava-Lifshitz quantum gravity [51].

Part IV

Conclusion

Chapter 14

Conclusion

14.1 Summary

In this thesis, after having reviewed Quantum Graphity, Loop Quantum Graphity, the Lieb-Robinson bound and simplified models of Loop Quantum Gravity, we derived two new Lieb-Robinson bounds, one that takes into the relative strengths of the interactions which is important to understand the functional dependence of the speed of information propagation on the interaction strengths and is important in order to get a tight bound. The other extends the Lieb-Robinson bound to a larger class of systems where the local operators of the Hamiltonian need not be bounded, only their commutators need be.

When then proceeded to investigate the phenomenology of Loop Quantum Black holes and found that they had extremely interesting behaviour when they were lighter than the Planck mass. First their horizons becomes hidden behind a Planck-sized wormhole. Their heat capacity becomes positive, and they become quasi-stable, taking an infinite amount of time to evaporate. We found that ultra light primordial black holes of typical mass

$\approx 10^{-5} m_P$ could be responsible for most of the dark matter. Furthermore, their emission spectrum suggests that the black holes making up the dark matter halo of our galaxy could be the source of ultra high energy, supra-GZK cutoff radiation.

14.2 Outlook

Now that we have developed powerful tools to investigate the emergence of gravity in condensed-matter like systems, it is time to use them. We are already working on investigating critical phases of the emergence in both Quantum Graphity and other systems.

Now that we have outlined some of the phenomenological consequences of the Loop Quantum Black holes, it is time to make these predictions more precise in order to really compare to experiment. We are currently calculating the exact proportions of each species of ultra high energy particles emitted by the black hole in order to compare with Auger, HiRes and other observatories to see how well our models compare to experiment. So far the calculations look promising. We are also working on obtaining the Loop Quantum black hole metric for spinning black holes.

PART V

APPENDICES

Appendix A

Multiple Interactions Calculations

In Eq.(4.37) the end points of the chain are separated by a graph distance of $\sum_{k=1}^{n-1} D_{a(i_k)}^{a(i_k)\to a(i_{k+1})}$. Hence if $d(P,Q) > \sum_{k=1}^{n-1} D_{a(i_k)}^{a(i_k)\to a(i_{k+1})}$ the chain cannot link P to Q, where $a(i_k) \in \{1, 2, \ldots, m\}$ labels the operator type of i_k and $h(i_k) \in \{h_1, h_2, \ldots, h_m\}$ gives the coupling constant of operator i_k. We can thus legitimately multiply every term by $\exp\Big(\lambda\big(\sum_{k=1}^{n-1} D_{a(i_k)}^{a(i_k)\to a(i_{k+1})} - d(P,Q)\big)\Big)$ and drop the endpoint condition. This gives us:

$$\|K_{a\ b}^{i_1\ j}(t)\| \leq$$

$$M\sum_{n=0}^{\infty}\frac{|\ t\ |^n}{n!}\Big(\sum_{i_2\in Z_{i_1}} 2h(i_2)\ldots\sum_{i_{n+1}\in Z_{i_n}} 2h(i_{n+1})\Big)\exp\Big(\lambda\big(\sum_{k=1}^{n-1} D_{a(i_k)}^{a(i_k)\to a(i_{k+1})} - d(P,Q)\big)\Big)$$

$$= Me^{-\lambda d(P,Q)}\sum_{n=0}^{\infty}\frac{|\ 2t\ |^n}{n!}\Big(\sum_{i_2\in Z_{i_1}} h(i_2)e^{\lambda D_{a(i_1)}^{a(i_1)\to a(i_2)}}\ldots\sum_{i_{n+1}\in Z_{i_n}} h(i_{n+1})e^{\lambda D_{a(i_n)}^{a(i_n)\to a(i_{n+1})}}\Big). \tag{A.1}$$

The equivalent equation for commutator bounded systems is:

$$\|K_{a\ b}^{i_1\ j}(t)\| \leq$$

$$M\sum_{n=0}^{\infty}\frac{|\ t\ |^n}{n!}\Big(\sum_{i_2\in Z_{i_1}}2h(i_2)K_{a(i_1)a(i_2)}\cdots\sum_{i_{n+1}\in Z_{i_n}}2K_{a(i_n)a(i_{n+1})}h(i_{n+1})\Big)\exp\Big(\lambda\big(\sum_{k=1}^{n-1}D_{a(i_k)}^{a(i_k)\to a(i_{k+1})}-d(P,Q)\big)\Big)$$

$$=Me^{-\lambda d(P,Q)}\sum_{n=0}^{\infty}\frac{|\ 2t\ |^n}{n!}\Big(\sum_{i_2\in Z_{i_1}}K_{a(i_1)a(i_2)}h(i_2)e^{\lambda D_{a(i_1)}^{a(i_1)\to a(i_2)}}\cdots\sum_{i_{n+1}\in Z_{i_n}}K_{a(i_n)a(i_{n+1})}h(i_{n+1})e^{\lambda D_{a(i_n)}^{a(i_n)\to a(i_{n+1})}}\Big). \tag{A.2}$$

For $(l_1,l_2)\in\{1,\ldots,m\}^2$, $l_1\neq l_2$ and $\lambda>0$ we define

$$N_{l_1l_2}(\lambda)\equiv n_{l_1\to l_2}h_{l_2}e^{\lambda D_{l_1}^{l_1\to l_2}}\text{ for bounded systems}$$

$$N_{l_1l_2}(\lambda)\equiv n_{l_1\to l_2}K_{l_1l_2}h_{l_2}e^{\lambda D_{l_1}^{l_1\to l_2}}\text{ for commutator-bounded systems}$$

$$N_{l_1l_1}(\lambda)\equiv 0, \tag{A.3}$$

We will proceed for bounded systems but note that the commutator bounded derivation is virtually identical. Now, from an operator of type 1, there are $n_{1\to l}$ ways to choose an operator of type l as the next in the chain and there are $m-1$ possibilities for $l\in\{2,\ldots,m\}$, and similarly for the other operator types. So, if we consider the embedded sums

$$\sum_{i_2\in Z_{i_1}}h(i_2)e^{\lambda D_{a(i_1)}^{a(i_1)\to a(i_2)}}\cdots\sum_{i_{n+1}\in Z_{i_n}}h(i_{n+1})e^{\lambda D_{a(i_n)}^{a(i_n)\to a(i_{n+1})}}, \tag{A.4}$$

we see that each of individual sum of the type

$$\sum_{i_{k+1}\in Z_{i_k}} h(i_{k+1}) e^{\lambda D_{a(i_k)}^{a(i_k)\to a(i_{k+1})}} \tag{A.5}$$

can be written as

$$\sum_{l\neq a(i_k)} n_{a(i_k)}^{a(i_k)\to l} h_l e^{\lambda D_{a(i_k)}^{a(i_k)\to l}} = \sum_{l\neq a(i_k)} N_{a(i_k)\to l}(\lambda). \tag{A.6}$$

This means for fixed n we can write

$$\begin{aligned}\sum_{i_2\in Z_{i_1}} h(i_2) e^{\lambda D_{a(i_1)}^{a(i_1)\to a(i_2)}} \dots \sum_{i_{n+1}\in Z_{i_n}} h(i_{n+1}) e^{\lambda D_{a(i_n)}^{a(i_n)\to a(i_{n+1})}} \\ = \sum_{a_2\neq a(i_1)} N_{a(i_1)a_2}(\lambda) \dots \sum_{a_{n+1}\neq a_n} N_{a_n a_{n+1}}(\lambda).\end{aligned} \tag{A.7}$$

of Eq.(A.1) where the a_l's represent interaction types. We thus have that Eq.(A.7) has $(m-1)^n$ terms, each of which has the form

$$N_{a_1a_2}(\lambda) N_{a_2a_3}(\lambda) N_{a_3a_4}(\lambda) \dots N_{a_n a_{n+1}}(\lambda). \tag{A.8}$$

Let us call a *linking sequence of N's of length q* a finite sequence of $N_{ij}(\lambda)$'s $N_{a_1b_1}(\lambda)$, $N_{a_2b_2}(\lambda)$,..., $N_{a_q b_{q+1}}(\lambda)$ such that $a_{l+1} = b_l$. Considering that there are only m interactions, we have that the set of transition factors $\{N_{ab}(\lambda) | 1 \leq a \leq m, 1 \leq b \leq m, a \neq b\}$ contains $m(m-1)$ elements, thus any sequence of $m(m-1)+1$ N's will necessarily have at least one repetition. Hence there are a finite number of linking sequences of N's such that all N's in the sequence are different, and they are of length $q \leq m(m-1)$. Let us call a linking sequence

of N's such that all N's in the sequence are different and such that $a_1 = b_{q+1}$ an *elementary cycle*. To each elementary cycle $N_{a_1a_2}(\lambda), N_{a_2a_3}(\lambda), \ldots, N_{a_qa_1}(\lambda)$ we associate two numbers:

$$k_{a_1a_2\ldots a_q} \equiv \sqrt[q]{\prod_{l=1}^{q} h_{a_l} n_{a_l \to a_{l+1}}}$$
$$\xi_{a_1a_2\ldots a_q} \equiv \frac{\sum_{l=1}^{q} D_{a_l}^{a_l \to a_{l+1}}}{q} \tag{A.9}$$

where we have made the identification $a_1 = a_{q+1}$. We then have that

$$N_{a_1a_2}(\lambda)N_{a_2a_3}(\lambda)\ldots N_{a_qa_1}(\lambda) = (k_{a_1a_2\ldots a_q} e^{\lambda \xi_{a_1a_2\ldots a_q}})^q. \tag{A.10}$$

Now Eq.(A.8) is the product of a linking sequence of N's of length n. In the first $m(m-1)+1$ N's of the product there must be, as previously mentioned, at least two identical N's, let us call it $N_{b_1b_2}$, now. Because we are dealing with the product of a linking sequence of N's, the subsequence of N's starting with the first $N_{b_1b_2}$ and ending with N just before the second $N_{b_1b_2}$ is an elementary cycle of the type $N_{b_1b_2}, N_{b_2b_3}, \ldots, N_{b_qb_1}$ and if we remove it from the full sequence, the remaining sequence is still a linking sequence of length $n - q$. So we can now write Eq.(A.8) as

$$(k_{b_1b_2\ldots b_q} e^{\lambda \xi_{b_1b_2\ldots b_q}})^q N_{c_1c_2}(\lambda)\ldots N_{c_{n-q}c_{n+1-q}}(\lambda), \tag{A.11}$$

where $N_{c_1c_2}, \ldots, N_{c_{n-q}c_{n+1-q}}(\lambda)$ is linking sequence of N's. This process can be reiterated until at most $m(m-1)$ N's are left.

$$
\begin{aligned}
& N_{13}\underbrace{N_{32}N_{24}N_{43}}_{(k_{324}e^{\lambda\xi_{324}})^3}N_{32}\ \underbrace{N_{24}N_{42}}_{(k_{24}e^{\lambda\xi_{24}})^2}\ N_{24}N_{43}N_{32}N_{21}N_{13}N_{34} \\
=&(k_{324}e^{\lambda\xi_{324}})^3(k_{24}e^{\lambda\xi_{24}})^2 N_{13}\underbrace{N_{32}N_{24}N_{43}}_{(k_{324}e^{\lambda\xi_{324}})^3}N_{32}N_{21}N_{13}N_{34} \\
=&\ (k_{324}e^{\lambda\xi_{324}})^6(k_{24}e^{\lambda\xi_{24}})^2\underbrace{N_{13}N_{32}N_{21}}_{(k_{132}e^{\lambda\xi_{132}})^3}N_{13}N_{34} \\
=&\ (k_{324}e^{\lambda\xi_{324}})^6(k_{24}e^{\lambda\xi_{24}})^2(k_{132}e^{\lambda\xi_{132}})^3 N_{13}N_{34}.
\end{aligned}
\tag{A.12}
$$

Example of the rewriting of a term of the form in Eq.(A.8) as a product of the elementary cycles defined in Eq.(A.9). The dependence on λ is not written explicitly in the above for simplicity.

So if we now define

$$
L(\lambda) \equiv \max_{2\le r\le m(m-1)}\ \max_{(a_1,a_2,\ldots,a_r)\in\{1,\ldots,m\}^r}\left\{k_{a_1\ldots a_r}e^{\lambda\xi_{a_1a_r}}|1\le p<q\le r,(a_p,a_{p+1})\neq(a_q,a_{q+1})\right\} \tag{A.13}
$$

$$
G(\lambda) \equiv \max_{(l_1,l_2,l_3,l_4)\in\{1,\ldots,m\}^4}\left\{\frac{N_{l_1l_2}(\lambda)}{N_{l_3l_4}(\lambda)}|N_{l_3l_4}(\lambda)\neq 0\right\} < \infty \tag{A.14}
$$

we conclude from the previous argument that

$$N_{a_1a_2}(\lambda)N_{a_2a_3}(\lambda)N_{a_3a_4}(\lambda)\dots N_{a_na_{n+1}}(\lambda) \leq G(\lambda)^{m(m-1)}(L(\lambda))^n. \tag{A.15}$$

Since there are $(m-1)^n$ such term in Eq.(A.7) this in turn gives us that

$$\sum_{i_2\in Z_{i_1}} h(i_2)e^{\lambda D^{a(i_1)\to a(i_2)}_{a(i_1)}} \dots \sum_{i_{n+1}\in Z_{i_n}} h(i_{n+1})e^{\lambda D^{a(i_n)\to a(i_{n+1})}_{a(i_n)}} \leq G(\lambda)^{m(m-1)}\left((m-1)L(\lambda)\right)^n. \tag{A.16}$$

Inserting this last inequality in Eq.(A.1), we obtain

$$\begin{aligned}\|K_a{}^{i_1}{}_b{}^{j}(t)\| &\leq \tilde{M}(\lambda)e^{-\lambda d(P,Q)}\sum_{n=0}^{\infty}\frac{|\ 2t\ |^n}{n!}\big((m-1)L(\lambda)\big)^n \\ &= \tilde{M}(\lambda)\exp\Big(\lambda\big(\frac{2(m-1)L(\lambda)}{\lambda}\ |\ t\ | -d(P,Q)\big)\Big),\end{aligned} \tag{A.17}$$

where $\tilde{M}(\lambda) = M(G(\lambda))^{M(m-1)}$. This last inequality implies a Lieb-Robinson speed of $\frac{2(m-1)L(\lambda)}{\lambda}$ for any positive λ. To obtain the tightest bound we take the infimum over λ

$$v_{LR} = \inf_{\lambda>0}\frac{2(m-1)L(\lambda)}{\lambda}. \tag{A.18}$$

Appendix B

Effective Energy Momentum Tensor

Here we give the Einstein tensor for the metric of the collapsing and evaporating black hole of chapter 10.

The effective energy momentum tensor is defined by $\widetilde{T}^{\mu}_{\nu} = G^{\mu}_{\nu}/8\pi$. The components of the Einstein tensor in coordinate (v, r, θ, φ) are:

$$
\begin{aligned}
&G^{v}_{\ v} = \frac{r^2}{(a_0^2 + r^4)^3 (r + r_*)^3} \times \\
&[2a_0^2 r^4 (r + r_*)(6r^2 + 7r_- r_+ - 7r(r_- + r_+) - 2rr_* \\
&-r_*^2) - a_0^4(-r_- r_+ r_* + r_*^3 + 2r^2(r_- + r_+ + 2r_*) \\
&+3r(-r_- r_+ + r_*^2)) - r^8(-r_- r_+ r_* + r_*^3 \\
&+r(r_- r_+ + 2(r_- + r_+) r_* + 3r_*^2))] \, ,
\end{aligned}
$$

$$
\begin{aligned}
G^r_{\ r} &= -\frac{r^2}{(a_0^2+r^4)^3(r+r_*)^3} \times \\
&[2a_0^2 r^4(r+r_*)(-r_-r_+ + r_*^2 + r(r_- + r_+ + 2r_*)) \\
&+a_0^4(4r^3 - 2r^2(r_- + r_+ - 2r_*) - r_-r_+r_* + r_*^3 \\
&+r(r_-r_+ + 3r_*^2)) + r^8(4r^2 r_* + 3r_-r_+r_* + r_*^3 \\
&+r(r_-r_+ - 2(r_- + r_+)r_* + 3r_*^2))] \ , \\
\\
G^\theta_{\ \theta} &= \frac{r^3}{(a_0^2+r^4)^3(r+r_*)^4} \times \\
&[r^7(r^2 r_-r_+ + r(2r^2 + 6r_-r_+ - 3r(r_- + r_+))r_* \\
&+(r-2r_-)(r-2r_+)r_*^2) + 2a_0^2 r^4(r^2(r_- + r_+) \\
&+(r_- + r_+)r_*^2 + r(r_- - r_*)(-r_+ + r_*)) \\
&+a_0^4(4r^3 - 2r^2(r_- + r_+ - 3r_*) + 2r_-r_+r_* \\
&+r(r_-r_+ - 3(r_- + r_+)r_* + r_*^2))] \ .
\end{aligned}
\tag{B.1}
$$

BIBLIOGRAPHY

[1] R. Abbasi *et al.* [HiRes Collaboration], *Observation of the GZK cutoff by the HiRes experiment*, Phys. Rev. Lett. 100 (2008) 101101 [astro-ph/0703099]; J. Abraham *et al.* [Pierre Auger Collaboration], *Observation of the suppression of the flux of cosmic rays above* $4 \times 10^{19} eV$, Phys. Rev. Lett. **101** (2008) 061101 [arXiv:0806.4302].

[2] S. Ansoldi, P. Nicolini, A. Smailagic and E. Spallucci, "Noncommutative geometry inspired charged black holes," Phys. Lett. B **645**, 261 (2007). [arXiv:gr-qc/0612035].

[3] M. Arzano, *Black hole entropy, log corrections and quantum ergosphere* Phys.Lett.B634 (2006) 536-540, [gr-qc/0512071]; M. Arzano, A.J.M. Medved, E. C. Vagenas, *Hawking radiation as tunneling through the quantum horizon* JHEP 0509 (2005) 037, [hep-th/0505266]; R. Banerjee, B. Ranjan Majhi, *Quantum Tunneling and Back Reaction*, Phys. Lett. B 662 (2008) 62-65, [arXiv:0801.0200]; R. Banerjee, B. Ranjan Majhi *Quantum Tunneling Beyond Semiclassical Approximation* JHEP 0806 (2008) 095, [arXiv:0805.2220] R. Banerjee, B. Ranjan Majhi, *Quantum Tunneling and Trace Anomaly* [arXiv:0808.3688]; B. Ranjan Majhi, *Fermion Tunneling Beyond Semiclassical Approximation*, [arXiv:0809.1508].

[4] A. Ashtekar, "New Variables for Classical and Quantum Gravity". Phys. Rev. Lett. **57** (18): 22442247 (1986).

[5] A. Ashtekar, " New Hamiltonian formulation of general relativity", Phys. Rev. D **36** 1587-1602.

[6] A. Ashtekar, "Loop Quantum Cosmology: An Overview," Gen. Rel. Grav. **41** (2009) 707 [arXiv:0812.0177 [gr-qc]].

G. A. Mena Marugan, "A Brief Introduction to Loop Quantum Cosmology," AIP Conf. Proc. **1130** (2009) 89 [arXiv:0907.5160 [gr-qc]].

[7] A. Ashtekar & M. Bojowald, " Black hole evaporation : A paradigm" Class. Quant. Grav. 22 (2005) 3349-3362, [gr-qc/0504029].

[8] A. Ashtekar and M. Bojowald, " Quantum geometry and Schwarzschild singularity" Class. Quant. Grav. 23 (2006) 391-411, [gr-qc/0509075]; L. Modesto, *Loop quantum black hole*, Class. Quant. Grav. 23 (2006) 5587-5602, [gr-qc/0509078].

[9] A. Ashtekar and B. Krishnan, Phys. Rev. Lett. **89**, 261101 (2002); Phys. Rev. **D68**, 104030 (2003).

[10] A. Ashtekar, M. Bojowald and J. Lewandowski, " Mathematica structure of loop quantum cosmology", Adv. Theor. Math. Phys. 7 (2003) 233-268, [gr-qc/0304074].

[11] A. Aurilia, R. Balbinot and E. Spallucci, "Quantum bubble dynamics in the presence of gravity," Phys. Lett. B **262**, 222 (1991).

[12] E. Ayón-Beato and A. Garciá, Phys. Rev. Lett. **80**, 5056 (1998).

[13] R. Balbinot and É. Poisson, "Stability of the Schwarzschild-de Sitter model," Phys. Rev. D **41**, 395 (1990).

[14] C. Barcelo, S. Liberati, S. Sonego and M. Visser, "Fate of gravitational collapse in semi-classical gravity," Phys. Rev. D **77**, 044032 (2008) [arXiv:0712.1130 [gr-qc]].

[15] J. Bardeen, Proc. GR5, Tiflis, USSR (1968).

[16] V. Berezinsky, M. Kachelriess and A. Vilenkin, " Ultra-high energy cosmic rays without GZK cutoff", Phys. Rev. Lett. 79 (1997) 4302 [astro-ph/9708217].

[17] G. P. Berman, G. D. Doolen, D. D. Holm, V. I. Tsifrinovich, "Quantum computer on a class of one-dimensional Ising systems" Physics Letters A. 193: 444–450 (1994).

[18] C. G. Bohmer, K.Vandersloot, *Loop quantum dynamics of the Schwarzschild Interior*, [arXiv:0709.2129]; Dah-Wei Chiou, *Phenomenological Loop Quantum Geometry of the Schwarzschild Black Hole*, arXiv:0807.0665.

[19] M. Bojowald, *Loop quantum cosmology*, Living Rev. Rel. 8:11, 2005, [gr-qc/0601085]; M. Bojowald, *Absence of singularity in loop quantum cosmology* Phys. Rev. Lett. 86:5227-5230, 2001, [gr-qc/0102069].

[20] L. Bombelli & R. J. Torrence *Perfect fluids and Ashtekar variables, with application to Kantowski-Sachs models* Class. Quant. Grav. **7** (1990) 1747-1745.

[21] A. Bonanno, M. Reuter, *Renormalization group improved black hole space-times*, Phys. Rev. D 62 (2000) 043008, [hep-th/0002196]; A. Bonanno, M. Reuter *Spacetime structure of an evaporating black hole in quantum gravity*, Phys. Rev. D 73 (2006) 083005, [hep-th/0602159].

[22] A. Borde, Phys. Rev. **D55**, 7615 (1997).

[23] J. L. Bourjaily, *Determining the actual local density of dark matter particles*, Eur. Phys. J. C 40N6 (2005) 23 [astro-ph/0410470].

[24] S. Bravyi, M. B. Hastings and F. Verstraete, "Lieb-Robinson Bounds and the Generation of Correlations and Topological Quantum Order," Phys. Rev. Lett. **97** (2006) 050401 [arXiv:quant-ph/0603121v1].

[25] P. Coleman, A. J. Schofield, "Quantum criticality," Nature 433: 226229 (2005).

[26] F. Conrady, L. Freidel, *Quantum geometry from phase space reduction*, [arXiv:0902.0351]; J. W. Barrett, R. J. Dowdall, W. J. Fairbairn, H. Gomes, F. Hellmann, *Asymptotic analysis of the EPRL four-simplex amplitude*, [arXiv:0902.1170]; F. Conrady, L. Freidel, *Path integral representation of spin foam models of 4d gravity*, Class. Quant. Grav.25, 245010, 2008, [arXiv:0806.4640]; F. Conrady, L. Freidel, *On the semiclassical limit of 4d spin foam models*, Phys. Rev. D78, 104023, 2008, [arXiv:0809.2280]; J. Engle, E. Livine, R. Pereira, C. Rovelli, *LQG vertex with finite Immirzi parameter*, Nucl. Phys. B799 (2008) 136-149, [arXiv:0711.0146]; J. Engle, R. Pereira, C. Rovelli, *Flipped spinfoam vertex and loop gravity* Nucl. Phys. B798 (2008) 251-290, [arXiv:0708.1236]; J. Engle, R. Pereira, C. Rovelli, *The Loop-quantum-gravity vertex-amplitude*, Phys. Rev. Lett. 99 (2007) 161301, [arXiv:0705.2388]; E. Alesci, C. Rovelli, *The Complete LQG propagator I. Difficulties with the Barrett-Crane vertex*, Phys. Rev. D76 (2007) 104012, [arXiv:0708.0883]; S. Speziale, *Background-free propagation in loop quantum gravity* [arXiv:0810.1978]; E. Bianchi, L. Modesto, C. Rovelli, S. Speziale *Graviton propagator in loop quantum gravity*, Class. Quant. Grav. 23 (2006) 6989-7028, [gr-qc/0604044]; L. Modesto, C. Rovelli *Particle scattering in loop quantum gravity* in Phys. Rev. Lett. 95 (2005) 191301, [gr-qc/0502036];

E. Bianchi, L. Modesto, *The Perturbative Regge-calculus regime of loop quantum gravity*, Nucl. Phys. B 796 (2008) 581-621, [arXiv:0709.2051]; E. Bianchi, A. Satz, *Semiclassical regime of Regge calculus and spin foams*, [arXiv:0808.1107].

[27] M., Cramer and J., Eisert, "Correlations and spectral gap in harmonic quantum systems on generic lattices," New J. Phys. 8, 71 (2006) [arXiv:quant-ph/0509167].

[28] M. Cramer, A. Serafini, J. Eisert, arXiv:0803.0890v2.

[29] P. A. M. Dirac, Lectures on Quantum Mechanics, Belfer Graduate School of Science, Yeshiva University Press, New York, 1964.

[30] I. Dymnikova, Gen. Rel. Grav. **24**, 235 (1992); Int. J. Mod. Phys. **D5**, 529 (1996); Class. Quantum Grav. **19**, 725 (2002); Int. J. Mod. Phys. **D12**, 1015 (2003).

[31] J. Eisert, D. Gross, arXiv:0808.3581v3

[32] J. Eisert and T. J. Osborne, "General Entanglement Scaling Laws from Time Evolution," Phys. Rev. Lett. **97** (2006) 150404 [arXiv:quant-phys/0603114].

[33] J. Eisert, M.B. Plenio, J. Hartley, and S. Bose, Phys. Rev. Lett. **93**, 190402 (2004).

[34] A. Fabbri and J. Navarro-Salas, *Modeling Black Hole Evaporation*, Imperial College Press (2005).

[35] M. J. Feigenbaum, "The Theory of Relativity - Galileo's Child," [arXiv:0806.1234].

[36] R. Gambini, J. Pullin, Black holes in loop quantum gravity: The Complete spacetime, Phys. Rev. Lett.101:161301, 2008, [arXiv:0805.1187]; M. Campiglia, R. Gambini,

J. Pullin, *Loop quantization of spherically symmetric midi-superspaces : the interior problem*, AIP Conf. Proc. 977:52-63, 2008, [arXiv:0712.0817]; M. Campiglia, R. Gambini, J. Pullin, Loop quantization of spherically symmetric midi-superspaces Class. Quant. Grav. 24:3649-3672, 2007, [gr-qc/0703135].

[37] A. Gogolin, A. Nersesyan, AM Tsvelik, *Bosonization and Strongly Correlated Systems*, Cambridge University Press, (1998).

[38] K. Greisen, *End To The Cosmic Ray Spectrum?*, Phys. Rev. Lett. 16, 748 (1966); G. T. Zatsepin and V. A. Kuzmin, *Upper limit of the spectrum of cosmic rays*, JETP Lett. 4, 78 (1966) [Pisma Zh. Eksp. Teor. Fiz. 4, 114 (1966)].

[39] Z.-C. Gu, and X.-G. Wen, arXiv:gr-qc/0606100v1

[40] V. P. Frolov, M. A. Markov and V. F. Mukhanov, "THROUGH A BLACK HOLE INTO A NEW UNIVERSE?," Phys. Lett. B **216**, 272 (1989).

[41] V. P. Frolov, M. A. Markov and V. F. Mukhanov, "BLACK HOLES AS POSSIBLE SOURCES OF CLOSED AND SEMICLOSED WORLDS," Phys. Rev. D **41**, 383 (1990).

[42] A. Hamma, F. Markopoulou, I. Prémont-Schwarz and S. Severini, "Lieb-Robinson bounds and the speed of light from topological order," Phys. Rev. Lett. **102** (2009) 017204 [arXiv:0808.2495 [quant-ph]].

[43] M. B. Hastings, Phys. Rev. B. **69**, 104431 (2004)

[44] M. B. Hastings, Phys. Rev. Lett. **93**, 140402 (2004)

[45] M.B. Hastings, and T. Koma, Comm. Math. Phys. **265**, 781 (2006).

[46] S.W. Hawking, G.F.R. Ellis *The large scale structure of space-time* Cambridge University Press, 1973.

[47] S. A. Hayward, Phys. Rev. **D49**, 6467 (1994); Class. Quantum Grav. **15**, 3147 (1998); Phys. Rev. **70**, 104027 (2004); Phys. Rev. Lett. **93**, 251101 (2004).

[48] S. A. Hayward, "Formation and evaporation of regular black holes," Phys. Rev. Lett. **96**, 031103 (2006) [arXiv:gr-qc/0506126].

[49] J. A. Hertz, "Quantum critical phenomena," Phys. Rev. B. , Volume 14, Issue 3, August 1, 1976, pp.1165-1184.

[50] W. A. Hiscock, Phys. Rev. **D23**, 2813; 2823 (1981).

[51] P. Hořava, *Quantum Gravity at a Lifshitz Point*, Phys. Rev. D 79, 084008, 2009, [arXiv:0901.3775]; Gianluca Calcagni, *Cosmology of the Lifshitz universe*, [arXiv:0904.0829]; Y. S. Myung, Y. W. Kim, *Thermodynamics of Hořava-Lifshitz black holes* [arXiv:0905.0179]; R. G. Cai, L. M. Cao, N. Ohta, *Thermodynamics of Black Holes in Hořava-Lifshitz Gravity*, [arXiv:0905.0751]; Y. S. Myung, *Thermodynamics of black holes in the deformed Hořava-Lifshitz gravity*, [arXiv:0905.0957].

[52] M. Horodecki, J. Oppenheim, A. Winter, "Quantum information can be negative" Nature 436:673-676 (2005), [arXiv:quant-ph/0505062v1].

[53] S. Hossenfelder, L. Modesto and I. Prémont-Schwarz, "A model for non-singular black hole collapse and evaporation," [arXiv:0912.1823 [gr-qc]].

[54] S. Hossenfelder and L. Smolin, "Conservative solutions to the black hole information problem," [arXiv:0901.3156]; A. Ashtekar, V. Taveras, M. Varadarajan, *Information is*

Not Lost in the Evaporation of 2-dimensional Black Holes, Phys. Rev. Lett. 100, 211302, 2008, [arXiv:0801.1811].

[55] V. Husain and R. B. Mann, "Thermodynamics and phases in quantum gravity," Class. Quant. Grav. **26** (2009) 075010 [arXiv:0812.0399 [gr-qc]].

[56] R. Kantowski and R. K. Sachs, J. Math. Phys. 7 (3) (1966); L. Bombelli & R. J. Torrence *Perfect fluids and Ashtekar variables, with application to Kantowski-Sachs models*, Class. Quant. Grav. 7 (1990) 1747-1745.

[57] J. I. Kapusta, *Nucleation Rate for Black Holes* Phys. Rev. D **30** (1984) 831.

[58] A. Kempf, "Information-theoretic natural ultraviolet cutoff for spacetime," Phys. Rev. Lett. **103**, 231301 (2009) [arXiv:0908.3061 [gr-qc]].

[59] A. Kempf, R. Portugal, "Group velocity of discrete-time quantum walks," Phys. Rev. A **79**, 052317 (2009) [arXiv:0901.4237v1 [quant-ph]].

[60] A.Y. Kitaev Annals Phys. **303**, 2 (2003).

[61] J. B. Kogut, "An introduction to lattice gauge theory and spin systems," Rev. Mod. Phys. 51 (1979) 659.

[62] J. B. Kogut and L. Susskind, "Hamiltonian Formulation Of Wilson's Lattice Gauge Theories," Phys. Rev. D **11**, 395 (1975).

[63] T. Konopka, "Statistical Mechanics of Graphity Models," Phys. Rev. D **78** (2008) 044032 [arXiv:0805.2283 [hep-th]].

[64] T. Konopka, F. Markopoulou and L. Smolin, arXiv:hep-th/0611197.

[65] T. Konopka, F. Markopoulou and S. Severini, "Quantum Graphity: a model of emergent locality," Phys. Rev. D **77** (2008) 104029 [arXiv:0801.0861 [hep-th]].

[66] K. V. Kuchar, *Geometrodynamics of Schwarzschild Black Hole*, Phys. Rev. D50 (19994) 3961-3981, [gr-qc/9403003]; T. Thiemann, *Reduced models for quantum gravity*, Lect. Notes Phys. 434 (1994) 289-318, [gr-qc/9910010]; H.A. Kastrup, T. Thiemann, *Spherically symmetric gravity as a completely integrable system*, Nucl. Phys. B 425 (1994) 665-686, [gr-qc/9401032]; T. Thiemann, H.A. Kastrup, *Canonical quantization of spherically symmetric gravity in Ashtekar's selfdual representation* Nucl. Phys. B 399 (1993) 211-258, [gr-qc/9310012].

[67] R. B. Laughlin, G. G. Lonzarich, P. Monthoux, and D. Pines, "The quantum criticality conundrum," Adv. Phys. 50, 361-365. (2001).

[68] E. H. Lieb, and D. W. Robinson, Comm. Math. Phys. **28**, 251 (1972).

[69] M. Mars, M. M. Martín-Prats and J. M. M. Senovilla, Class. Quantum Grav. **13**, L51 (1996).

[70] M. R. Mbonye and D. Kazanas, Phys. Rev. **D72**, 024016 (2005).

[71] K. A. Meissner, "Black hole entropy in loop quantum gravity," Class. Quant. Grav. 21 (2004) 5245 [gr-qc/0407052].

[72] L. Modesto, *Disappearance of the black hole singularity in loop quantum gravity*, Phys. Rev. D 70 (2004) 124009, [gr-qc/0407097]; L. Modesto, *The kantowski-Sachs space-time in loop quantum gravity*, International Int. J. Theor. Phys. 45 (2006) 2235-2246, [gr-qc/0411032]; L. Modesto, *Loop quantum gravity and black hole singularity*, proceedings

of 17th SIGRAV Conference, Turin, Italy, 4-7 Sep 2006, [hep-th/0701239]; L. Modesto, *Gravitational collapse in loop quantum gravity*, Int. J. Theor. Phys.47 (2008) 357-373, [gr-qc/0610074]; L. Modesto, *Quantum gravitational collapse*, [gr-qc/0504043].

[73] L. Modesto, *Black hole interior from loop quantum gravity*, Advances in High Energy Physics Volume 2008 (2008), Article ID 459290 [gr-qc/06011043]; L. Modesto, *Evaporating loop quantum black hole*, [gr-qc/0612084].

[74] L. Modesto, *Space-Time Structure of Loop Quantum Black Hole*, arXiv:0811.2196.

[75] L. Modesto, *Fractal Structure of Loop Quantum Gravity*, [arXiv:0812.2214]; L. Modesto, *Fractal Quantum Space-Time*, [arXiv:0905.1665]; F. Caravelli, L. Modesto, *Fractal Dimension in 3d Spin-Foams*, [arXiv:0905.2170].

[76] L. Modesto and I. Prémont-Schwarz, "Self-dual Black Holes in LQG: Theory and Phenomenology," Phys. Rev. D **80**, 064041 (2009) [arXiv:0905.3170 [hep-th]].

[77] V. Mukhanov, *Physical Foundations of Cosmology*,(Cambridge University Press, Cambridge, 2005), pp. 74-75.

[78] Yun Soo Myung, Yong-Wan Kim, Young-Jai Park, *Thermodynamics of regular black hole*, [arXiv:0708.3145]; Yun Soo Myung, Yong-Wan Kim, Young-Jai Park, *Quantum Cooling Evaporation Process in Regular Black Holes* Phys. Lett. B (2007) 656:221-225, [gr-qc/0702145]; P. Nicolini, *Noncommutative Black Holes, The Final Appeal To Quantum Gravity: A Review*, [arXiv:0807.1939]; R. Banerjee, B. Ranjan Majhi, S. Samanta, *Noncommutative Black Hole Thermodynamics*, Phys. Rev. D77 (2008) 124035,

[arXiv:0801.3583]; Banerjee, Bibhas Ranjan Majhi, Sujoy Kumar Modak, *Area Law in Noncommutative Schwarzschild Black Hole*, [arXiv:0802.2176].

[79] P. Nicolini, "A model of radiating black hole in noncommutative geometry," J. Phys. A **38**, L631 (2005). [arXiv:hep-th/0507266].

[80] P. Nicolini, "Noncommutative Black Holes, The Final Appeal To Quantum Gravity: A Review," Int. J. Mod. Phys. A **24**, 1229 (2009). [arXiv:0807.1939 [hep-th]].

[81] P. Nicolini and E. Spallucci, "Noncommutative geometry inspired wormholes and dirty black holes," [arXiv:0902.4654 [gr-qc]].

[82] B. Nachtergaele, Y. Ogata, and R. Sims, J. Stat. Phys. **124**, 1 (2006) [arXiv:math-ph/0603064v1].

[83] B. Nachtergaele, H. Raz, B. Schlein, and R. Sims, Comm. Math. Phys. **286**, 1073-1098 (2009)

[84] B. Nachtergaele and R. Sims, Comm. Math. Phys. **265**, 119 (2006).

[85] B. Nachtergaele, and R. Sims, Comm. Math. Phys. **276**, 437-472 (2007).

[86] B. Nachtergaele, and R. Sims, [arXiv:0712.3318].

[87] D. Oriti, *Group field theory as the microscopic description of the quantum spacetime fluid: A New perspective on the continuum in quantum gravity* [arXiv:0710.3276].

[88] T.J. Osborne, Phys. Rev. Lett. **97**, 157202 (2006)

[89] T.J. Osborne, Phys. Rev. A **75**, 032321 (2007)

[90] Pierre Auger Collaboration, "Correlation of the Highest-Energy Cosmic Rays with Nearby Extragalactic Objects", Science, Vol. 318. no. 5852, pp. 938-943 (2007), [arXiv:0711.2256v1 [astro-ph]].

[91] A.S.T. Pires, L.S. Lima, M.E. Gouvea, "The phase diagram and critical properties of the two-dimensional anisotropic XY model" J. Phys.: Condens. Matter 20: 015208 (2008).

[92] M.B. Plenio, J. Hartley, and J. Eisert, New J. Phys. **6**, 36 (2004).

[93] I. Prémont-Schwarz ,A. Hamma, I. Klich and F. Markopoulou, "Lieb-Robinson bounds for commutator-bounded operators ," Phys. Rev. A **81**, 040102(R) (2010) .[arXiv:0912.4544 [quant-ph]].

[94] I. Prémont-Schwarz ,J. Hnybida, "Lieb-Robinson bounds with dependence on interaction strengths," [arXiv:1002.4190v1 [math-ph]].

[95] I. Prémont-Schwarz , "Emergence of spacetime: how to construct quantum black holes and exotic universes in the lab," article in preparation.

[96] C. Rovelli and L. Smolin, *Loop Space Representation Of Quantum General Relativity*, Nucl. Phys. B 331 (1990) 80; C. Rovelli, "Area is the length of Ashtekar's triad field," *Phys. Rev.* **D47** (1993) 1703–1705. C. Rovelli and L. Smolin, *Discreteness of area and volume in quantum gravity*, Nucl. Phys. B 442 (1995) 593; E. Bianchi, *The Length operator in Loop Quantum Gravity*, Nucl. Phys. B 807 (2009) 591-624, [arXiv:0806.4710].

[97] C. Rovelli, *Quantum Gravity*, (Cambridge University Press, Cambridge, 2004); A. Ashtekar, *Background independent quantum gravity: A Status report*, Class. Quant. Grav.

21, R53 (2004), gr-qc/0404018; T. Thiemann, *Loop quantum gravity: an inside view*, hep-th/0608210; T. Thiemann, *Introduction to Modern Canonical Quantum General Relativity*, gr -qc/0110034; *Lectures on Loop Quantum Gravity*, Lect. Notes Phys. 631, 41-135 (2003), gr-qc/0210094.

[98] S. Sachdev, *Quantum Phase Transitions*, Cambridge University Press, Cambridge U.K. (1999).

[99] H. Sahlmann, "Loop quantum gravity - a short review," [arXiv:1001.4188 [gr-qc]].

[100] T. Schneider, J. M. Singer, "D-XY Critical Behavior in Cuprate Superconductors," Physica C: Superconductivity Volumes 341-348, Part 1, November 2000, Pages 87-91 [arXiv:cond-mat/0001258].

[101] N. Schuch, J .I. Cirac, M.M. Wolf, "Quantum states on Harmonic lattices," Commun. Math. Phys. 267, 65 (2006) [arXiv:quant-ph/0509166v2]

[102] M. Simpson and R. Penrose, " Internal instability in Reissner-Nordström black hole", Int. J. Theor. Phys. 7 (1973) 183-197.

[103] E. Spallucci, A. Smailagic and P. Nicolini, "Pair creation by higher dimensional, regular, charged, micro black holes," Phys. Lett. B **670**, 449 (2009). [arXiv:0801.3519 [hep-th]].

[104] R. B. Stinchcombe, "Ising model in a transverse field : I. Basic theory," J. Phys. C: Solid State Phys. 6: 2459-2483 (1973).

[105] P. C. Vaidya, Proc. Indian Acad. Sci. **A33**, 264 (1951).

[106] X.-G. Wen, *Quantum Field Theory of Many-Body Systems*, (Oxford Univ. Press, Oxford, 2004); Phys. Rev. B **40**, 7387 (1989); Int. J. Mod. Phys. B **4**, 239 (1990); Adv. Phys. **44**, 405 (1995).

[107] X.-G. Wen and Q. Niu, Phys. Rev. B **41**, 9377 (1990).

[108] X.-G. Wen, Phys. Rev. D **68**, 065003 (2003).

[109] X. Zhang and Y. Ling, "Inflationary universe in loop quantum cosmology," JCAP 0708 (2007) 012 [gr-qc/0705.2656].